MODEL POLYIMIDE FILMS: SYNTHESIS, CHARACTERIZATION, AND DEPOSITION BY RESONANT INFRARED LASER ABLATION

BY

NICOLE LEIGH DYGERT

Dissertation

Submitted to the Faculty of the

Graduate School of Vanderbilt University

in partial fulfillment of the requirements

for the degree of

DOCTOR OF PHILOSOPHY

in

Interdisciplinary Materials Science

December, 2008

Nashville, TN

Approved:

Richard F. Haglund, Jr.

E. Duco Jansen

Eva M. Harth

G. Kane Jennings

Kenneth E. Schriver

To my parents for seeing me *there and back again*

ACKNOWLEDGEMENTS

This dissertation would not have been possible without the generous funding support from: the National Science Foundation (NSF) Integrative Graduate Research Experience and Training (IGERT) program (2004-2006), Naval Research Laboratory (N00173-05-P-0059), the free electron laser is supported by the Medical FEL Program of the Department of Defense (F49620-01-1-0429).

I thank my dissertation committee for their assistance and support throughout the completion of this research especially my research advisor, Dr. Haglund. The free-electron laser staff has been instrumental in accomplishing the research contained herein. For providing me with a greater understanding of various research topics and for invaluable assistance with experiments, I thank: Mark Mackanos, Dr. Schriver, and John Kozub (plume shadowgraphy); Tony Gies (GPC and mass spectrometry); Theo Dingemans (PEI synthesis); Joe Pickel (MALLS and TGA-MS).

My time at the University of Delft taught me many things, perhaps most importantly that I do not enjoy continuously pluvial weather and should thus avoid Seattle and other such locales. A monumental thank you goes to Theo Dingemans for mentoring me in organic synthesis and for making me feel like a part of the family. Thanks to my fellow graduate students in the Haglund group, the fourth floor office, and in the Materials Science department for making my life more entertaining. Thanks to Stephen Johnson for help in numerous FEL endeavors.

Finally thank you to my family and friends whose continued empathy and support was essential in completing this dissertation. I give a big thank you to my husband Phil and my two cats, Skeeter and Indy, for enduring more than a month of bad moods. I owe

an enormous debt of gratitude to my parents for always believing in me. Finally thank goodness for the 80's that taught me "when the going gets tough the tough get going".

TABLE OF CONTENTS

LIST OF FIGURES

LIST OF TABLES

LIST OF ABBREVIATIONS

BPDA	3,3′,4,4′-biphenyltetracarboxylic dianhydride
BTDA	benzophenone 3,3'4,4'-tetracarboxylic dianhydride
DMF	dimethyl formamide
FTIR	Fourier transform infrared spectroscopy
GPC	gel permeation chromatography
IR	infrared
MALLS	multi-angle laser light scattering
MAPLE	matrix assisted pulsed laser evaporation
MS	mass spectrometry
NMP	N-methyl pyrrolidinone
ODA	4,4' oxidianiline
P0	4,4' oxidianiline
P0-P3 BTDA	polyamic acid of P0-P3 diamine copolymerized with BTDA in a solvent
P1	1,4bis(4-aminophenoxy)benzene
P2	bis[4-(4-aminophenoxy)phenyl]ether
P3	1,4bis[4(4-aminophenoxy)phenoxy]benzene
PAA	polyamic acid
PAI	polyamide imide specifically for our experiments poly(trimellitic anhydride chloride) copolymerized with 4,4'-methylene dianiline
PC	polycarbonate
PEG	polyethylene glycol
PEI	polyether imide
PET	polyethylene terephthalate
PI	polyimide
PLE	pulsed laser evaporation
PMDA	pyromellitic dianhydride
PMDA-ODA	polyamic acid of PMDA copolymerized with ODA in a solvent
PS	polystyrene
PTFE	polytetrafluoroethylene
PVC	polyvinyl chloride
PVF	polyvinyl fluoride
QELS	quasi-elastic light scattering
RIR-LA	resonant infrared laser ablation
SEC	size exlusion chromatography (same as GPC)
TGA	thermogravimetric analysis
UV	ultraviolet
XPS	x-ray photoelectron spectroscopy

CHAPTER I

INTRODUCTION

Nicole Leigh Dygert

Interdisciplinary Materials Science

Vanderbilt University

Nashville, TN 37235

1.1 Background and Motivation

Advances in polymer synthesis have allowed for the creation of organic materials capable of replacing steel, emitting light, and insulating spacecraft from high re-entry temperatures.[1,2] Today there is also a great deal of interest in utilizing lasers to process and characterize polymeric materials.[3-6] For instance Dyer et al recently used a 157 nm F_2 laser to ablate three different polymers: glycidyl azide, trianzene, and polyimide.[3] The laser was used to determine the dependence of ion generation on fluence, illustrating its usefulness as a spectroscopic tool.[3] Sohn and co-workers used a 785 nm femtosecond laser in order to create microscopic holes and patterns in a polypropylene film.[4] The holes make the film breathable, allowing for the exchange of gases.[4] Polymers and lasers are also combined to form state-of-the-art devices; Ko et al fabricated multi-layer passive and active electronic components on a flexible polymer substrate.[5] Low-temperature laser processing was used to sinter and shape gold nanoparticles on the surface of the polymer.[5] Lasers are also being used to process natural polymeric materials. Doraiswamy used an ArF (193 nm) laser to transfer a natural mussel protein using matrix assisted pulsed laser evaporation (MAPLE).[6] Thus there is a wide array of applications combining lasers and polymers, for deposition of thin films, patterning of polymeric substrates, and detailed spectroscopic studies.

Lasers have a long history of use in materials processing; one of the first applications of the laser was using its energy in order to facilitate flash pyrolysis of ceramics, metals and oxides.[7-9] In 1965, Smith and Turner used a ruby laser to deposit thin films of SbS_3, As_2S_3, ZnTe, MoO_3, and other materials.[9] Groh and Haas independently deposited inorganic materials such as SiO, SiO_2, and other oxides using a

CO_2 laser tuned to 10.6 μm.[7,8] Schwarz et al noticed that a continuous wave laser produced incongruent evaporation of the material, while pulsed lasers were able to achieve congruent evaporation and stoichiometric depositions.[10]

It would take until 1982 for work on the laser ablation of synthetic polymers to begin.[11-16] Laser deposition of polymers was first attempted in 1985, by Sirajuddin and Reddy using a continuous 60 W CO_2 laser at 10.6 μm to deposit a pyroelectric film of poly(vinyl fluoride) (PVF).[17] Fourier transform infrared spectroscopy (FTIR) showed that the laser deposited film of PVF closely resembled the starting material; however the molecular weight was decreased from 10,000 Da to 3450 Da as determined by gel permeation chromatography (GPC).[17] Hansen and Robitaille further advanced the field by depositing the first polymer films by pulsed laser evaporation (PLE); they deposited thin films of polyimide (PI), polyethylene terephthalate (PET), polycarbonate (PC), poly(methyl methacrylate) (PMMA), and Nylon 6,6 with varying degrees of success using several UV wavelengths and one near IR wavelength.[16] Table 1.1 shows the polymer film qualities obtained by Hansen and Robitaille at the different wavelengths. Hansen et al showed similar before and after FTIR spectra for PLE PC, but there was one extra peak in the PLE PC spectrum.[16] For PI x-ray photoelectron spectroscopy (XPS) was used to compare the original material to the PLE PI; the Hansen and Robitaille results showed only 2% difference in the carbon, oxygen, and nitrogen ratios.[16] In contrast, earlier work on the ablation of PI by UV radiation by Srinivasan and co-workers showed the only condensable plume product to be elemental carbon.[18] Srinivasan showed that the surface of the ablated PI had a 50% lower ratio of oxygen to carbon compared to unablated PI by XPS.[18]

Table 1.1: From Hansen and Robitaille, quality of UV pulsed laser evaporation of various polymers[16]

TABLE I. Compilation of the absorption coefficient, observed morphology and (if measured) refractive index (RI) of the PLE deposit, and measured deposition pulse energy threshold (10 ns pulses focused to ~0.1 cm^2) for the indicated polymers at several wavelengths. Literature values for the RI's of the bulk materials are given at left.

		Evaporation wavelength			
Polymer	RI	193 nm	248 nm	355 nm	1064 nm
Poly (tetrafluoro-ethylene)	1.376[a]	1×10^2 cm^{-1} [b] no deposit >7 mJ	c no deposit >29 mJ	c ···	c no deposit >100 mJ
Polyethylene	1.49[a]	5×10^2 cm^{-1} [b] no deposit >5 mJ	c d	c ···	c ···
Poly (methylmeth-acrylate)	1.49[a]	1.4×10^4 cm^{-1} [e] smooth film <5 mJ	1×10^3 cm^{-1} [e] particles f	c ···	c particles 150 mJ
Nylon 6,6	1.53[a]	4×10^4 cm^{-1} [g] smooth film 1.51, <5 mJ	$<7\times10^3$ cm^{-1} [g] smooth film 1.52[h]	c ···	c no deposit >80 mJ
Polycarbonate	1.585[a]	5×10^4 cm^{-1} [g] smooth film 1.79, <5 mJ	$>6\times10^3$ cm^{-1} [g] smooth film 1.63, <5 mJ	c part./film 15–30 mJ	c part./film 30 mJ
Poly (ethylene terephthalate)	1.576[a]	2×10^5 cm^{-1} [i] smooth film 1.71, <3 mJ	1×10^5 cm^{-1} [i] smooth film 1.61, <7 mJ	c ···	c part./film 25–50 mJ
Polyimide	1.695[j]	4×10^5 cm^{-1} [k] smooth film 2.01, <3 mJ	2×10^5 cm^{-1} [k] smooth film 1.89, <3 mJ	2×10^4 cm^{-1} [k] film <9 mJ	c particles <30 mJ

[a] Reference 20.
[b] Reference 16.
[c] Absorption coefficient assumed to be negligible ($<10^2$ cm^{-1}).
[d] At 266 nm threshold >13 mJ, no deposit.
[e] Reference 17.
[f] Very slow deposition at 5 mJ, transition to rapid growth near 40 mJ.
[g] Estimated.
[h] Threshold is 10–30 mJ, highly dependent on target translation rate.
[i] Reference 18.
[j] Reference 21.
[k] Reference 19.

The polymer properties and synthetic method play an important role in the development of new processing techniques. The first all-synthetic polymer was made by Leo Baekeland by combining phenol and formaldehyde to create Bakelite in 1907.[1,2] Table 1.2 shows the commercialization of some of the more common polymers. Bakelite is a thermoset polymer; thermosets are cross-linked into a three-dimensional network structure and cannot be melted or dissolved, but only swollen in suitable solvents to form gels. Chronologically the next set of polymers polyvinyl chloride, polystyrene, poly(methyl methacrylate) are thermoplastics; these polymers may be melted and dissolved while leaving the chemical composition unaltered. The 1920's saw the first major development for polymer theory. Before the 1920's polymers were considered to be akin to colloids being composed of small particles held together by physical

association. Staudinger proposed his *Macromolecular Hypothesis* in 1920 stating that polymers were composed of bonded repeating units forming a long chain with high molecular weight.[1,2] Experiments on proteins by Fischer and on cellulose by Mark and Meyer confirmed Staudinger's hypothesis.[1] In the 1930's Carothers put the *Macromolecular Hypothesis* to practical use by combining bifunctional monomers to form long, linear chains. Carothers helped to create polyesters, nylon, and neoprene at DuPont.[2]

Table 1.2: Commercial debut of common polymers[2,19]

Year	Polymer	Producer
1909	Poly(phenol–*co*–formaldehyde)	General Bakelite Corporation
1927	Poly(vinyl chloride)	B.F. Goodrich
1929	Poly(styrene–*stat*–butadiene)	I.G. Farben
1930	Polystyrene	I.G. Farben/Dow
1936	Poly(methyl methacrylate)	Rohm and Haas
1936	Nylon 66 (Polyamide 66)	DuPont
1936	Neoprene (chloroprene)	DuPont
1939	Polyethylene	ICI
1943	Poly(dimethylsiloxane)	Dow Corning
1954	Poly(ethylene terephthalate)	ICI
1960	Poly(*p*-phenylene terephthalamide)[a]	DuPont
1982	Polyetherimide	GEC

In the 1950's polymer chemists at DuPont were working on a new thermosetting polymer, polyimide. The material had to be processed in two stages: first a diamine and dianhydride were combined in a polar aprotic solvent to create a processable polyamic acid. Then the polyamic acid (PAA) was coated onto a substrate and heated to undergo cyclodehydration and form the polyimide. They called it Kapton® and it began to be mass produced in 1955.[20] Polyimides found uses for applications in the semiconductor and automobile industries due to their excellent properties: low dielectric constant, low coefficient of thermal expansion, good mechanical strength, and high thermo-oxidative stability.

Initial work on laser processing of polyimides focused on the patterning of semiconductor substrates using UV radiation.[13,14,18,21-23] Eventually, interest in directly depositing films of polyimide was stimulated, beginning with the work of Hansen et al.[16] The UV light tended to unravel the polymer chains, degrading the molecular weight and subsequently the tensile strength.[24] Other researchers began exploring the possibility of exciting vibrational, infrared modes to transfer and pattern polyimides.[25-28] The majority of research in the infrared was done with CO_2 lasers. The CO_2 laser is the original workhorse of the laser machining industry offering affordable high-power output and large area machining. However the CO_2 laser only offers a few wavelengths between 9 and 11 μm, the main two modes are 9.6 and 10.6 μm. The modes of the CO_2 laser are fairly far into the mid-infrared and in this range there are few strongly absorbing polymer vibrational modes.

At Vanderbilt we are fortunate to have access to a mid-infrared tunable free electron laser (FEL).[29,30] The FEL allows us to tune to any infrared mode between 2-10 μm. Only one other research group has investigated polyimide processing with an FEL. Kelley used the FEL at the Thomas Jefferson Laboratory National Accelerator Facility to ablate Kapton® films at 3.10 and 5.80 μm; the second wavelength corresponds to the strong imide carbonyl stretch bond.[25] Kelley showed that there was no apparent carburization with a single pulse having sufficient energy to generate a fully formed hole; however, with an increasing number of pulses the carbon deposits increased.[25] Our own results contradicted this, illustrating that both glass supported and free-standing films showed signs of carburization at fluences high enough to puncture a hole in the film using the carbonyl resonance.[31,32] Other authors have found poor surface quality when

ablating PI films in the infrared. For instance Zeng et al showed that CO_2 (9.3 μm) laser ablation of a 125 μm thick Kapton® film had poor surface quality after ablation due to thermalization of the surrounding areas.[27] The research thus far indicates that it may be difficult to transfer fully cured PI films with IR radiation. The XPS results of Zeng's[27] experiment supported Ortelli's[26] proposed decomposition path described for UV-laser irradiation; the polyimide decomposes thermally in distinct steps beginning with the imide ring, then the aromatic system, and finally the carbonyl groups. Thus, another technique was needed to transfer the polyimide without degrading its properties.

1.2 Specific Goals

The hypothesis of this dissertation is that high performance polymers may be transferred intact using resonant infrared laser ablation (RIR-LA). The purpose of this novel deposition technique is to allow precise patterning of the polymers onto the substrate in order to avoid additional wet processing steps. The specific goals of the project were to: (1) determine if thermoset polymers could be transferred using infrared laser ablation without degradation; (2) analyze the characteristics of the resulting RIR-LA films; and (3) investigate the mechanism behind the ablative transfer. Prior work in our research group showed that neat thermoplastic polymers, such as polyethylene glycol (PEG), polyethylene terephthalate (PET), and polystyrene (PS) could be successfully transferred using tunable infrared radiation from the FEL.[33-35] The term ablation is used for our technique in lieu of evaporation, because evaporation implies simple boiling while ablation encompasses multiple material removal mechanisms. Thus we set out to transfer thermosetting and other high performance polymers by RIR-LA.

To accomplish the first goal the infrared laser transfer of the polyimide, Kapton®, was investigated. All of the prior work on polyimides used the fully cured polyimide as the target material. The transferred films showed signs of thermal damage and reduction in molecular weight.[27,36] After a brief look at the ablation of the fully cured films, we transitioned into transferring the PAA precursor solution. Building on the work previously done with matrix assisted pulsed laser evaporation (MAPLE), which illustrated that polymers could remain thermally intact after ablation if dissolved in the correct solvent, we undertook experiments to transfer PAA, a precursor to PI. In our experiments we worked with significantly higher concentrations (1-20%) than previously employed in the UV-MAPLE technique pioneered at the Naval Research Laboratory (1-5%).[37] After that, additional imide polymers were transferred including the polyamide imides and the polyether imides. The polyamide imides (PAI) offered a partially cross-linked polymeric structure. PAI remains soluble after a curing cycle due to its retained amide linkages. Due to greater mobility the cure temperature is considerably lower for PAI (150 °C) than PI (250 °C). Finally poly ether imides (PEI) were synthesized at the Technical University of Delft under the direction of Dr. Theo Dingemans (Associate Professor of Chemistry and Aerospace Engineering). PEIs offered an interesting homologous series of materials to study. The diamine monomer series (abbreviated P0-P3) increases by one aromatic ring, starting with two rings in P0 and working up to five rings in P3 (see structure below in figure 1.1). The diamine monomers were combined with a dianhydride monomer (BTDA) to form a polymeric series. PEIs are of commercial interest because some combinations of diamine and dianhydride monomers generate ordered liquid crystalline structures.[38]

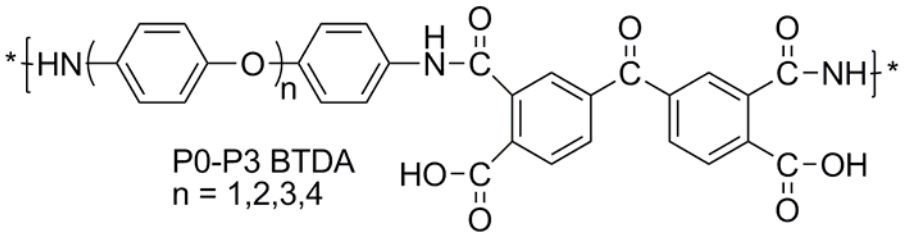

Figure 1.1: Structure of P0-P3 BTDA

For the second goal, the RIR-LA films were characterized using a broad range of techniques. The preservation of chemical structure was investigated using Fourier transform infrared spectroscopy (FTIR). The changes in the FTIR spectrum of PI with temperature have been well documented,[39] making it an ideal starting material. The physical appearance of the films was examined with optical microscopy. We were looking for smooth, pinhole free films, without large surface particulate. The surface roughness profile and the film thickness were determined by profilometry. Multi-angle laser light scattering (MALLS) and gel permeation chromatography (GPC) were used in order to compute the molecular weight before and after the RIR-LA ablation process. A reduction in the polymer molecular weight would indicate that the transferred polymer is being degraded either by photofragmentation or thermal decomposition during the laser ablation process. The decomposition temperatures of traditional solution cast films were compared to those of RIR-LA polymer films using thermogravimetric analysis with an attached mass spectrometer. A discrepancy in the decomposition products would implicate compositional differences between the solution cast polymers films and the RIR-LA polymer films.

The third goal of investigating the ablation mechanism was partially accomplished by using pump-probe shadowgraphy to examine the plume dynamics. Additional mechanistic information was gleaned from quartz crystal microbalance (QCM) studies where the rate of ablation was determined for various combinations of polymers (PI, PAI, PEI) and resonant wavelengths. QCM measurements of PEI allowed for the elucidation of the effect of the diamine chain length on the RIR-LA transfer rates. Due to the heat-induced transformation of the PAA precursor into the polyimide, the laser transfer of the polymers also acted as a "molecular thermometer". If an elevated temperature was reached in the plume, then imide peaks should appear in the FTIR spectra.

1.3 Significant Contribution

The research contained in this thesis represents a significant contribution to the field of laser ablation of high performance polymers. It represents the first attempt to transfer the precursor solution of PI using infrared laser ablation. In addition to offering a unique way to transfer thermosetting and high performance polymers, an important piece of the mechanistic puzzle of laser ablation was uncovered. Previous research indicates that extremely high temperatures are reached during UV laser ablation,[22,40] high enough to decompose the polymer leaving only fragments or a lower molecular weight material. We have shown by the unaltered FTIR spectra of both PI and PAI that these polymers do not "feel" the high temperature of the ablation plume. FTIR only determines that the chemical composition is unaltered; it cannot resolve changes in molecular weight. The preservation of the chemical structure is attributed to the matrix creating a solvation shell

and shielding the polymer from the high temperatures. This has been shown for UV-MAPLE transfer with small percentages of polymer (< 5%) for wavelengths resonant with the matrix.[37,41,42] In our experiments we have deposited intact polymer films from precursor solutions containing up to 20 weight percent polymer. We have demonstrated that either the matrix or the polymer itself may be excited without thermal damage to the collected material. The molecular weight studies of the RIR-LA polymer films show a smaller molecular weight reduction compared to IR or UV laser ablation of cured PI films.[18,43] The technique opens up new avenues for laser ablation intact of polymers.

1.4 Overview

The body of the dissertation has been divided into four independent chapters that have either been submitted, or are in the process of being prepared for submission, to peer-reviewed journals. First Chapter II presents some background information about the experiments. Chapter III is a manuscript published in the Journal of Physics Conference Series entitled "resonant infrared pulsed laser deposition of a polyimide precursor", this chapter covers the initial work on Kapton® film and then on the PAA precursor. Chapter III also details the early results of the plume shadowgraphy experiments. Chapter IV is a paper published in Applied Physics A entitled "deposition of a polyimide precursor by resonant infrared laser ablation"; detailed FTIR studies are presented along with evidence for molecular weight preservation. Chapter V discusses the expansion of the RIR-LA technique to other members of the polyimide family, polyamide imide (PAI) and polyether imide (PEI); it presents FTIR data on the intact local structure of the RIR-LA polymer films. Chapter V also characterizes the thickness and roughness of the produced

RIR-LA films. Chapter VI covers QCM results for PI, PAI, and PEI and elucidates some of the mechanisms at work in the infrared ablation process. Chapter VII examines the molecular weight of the RIR-LA films using MALLS. TGA is used to determine the decompositional differences between solution-cast and RIR-LA. Conclusions are presented in Chapter VIII.

1.5 References

[1] F. Rodriguez, *Principles of Polymer Systems*, 4th ed. (Taylor & Francis, Philadelphia, 1996).

[2] L. H. Sperling, *Introduction to Physical Polymer Science*, 3rd ed. (Wiley-Interscience, New York, 2001).

[3] P. E. Dyer, M. Pervolaraki, C. D. Walton, T. Lippert, M. Kuhnke, and A. Wokaun, Appl. Phys. A **90,** 403-9 (2008).

[4] I.-B. Sohn, Y.-C. Noh, S.-C. Choi, D.-K. Ko, J. Lee, and Y.-J. Choi, Appl. Surf. Sci. **254,** 4919-24 (2008).

[5] S. H. Ko, J. Chung, H. Pan, C. P. Grigoropoulos, and D. Poulikakos, Sensors & Actuators A **134,** 161-8 (2007).

[6] A. Doraiswamy, R. J. Narayan, R. Cristescu, I. N. Mihailescu, and D. B. Chrisey, Mat. Sci. & Eng. C **27,** 409-13 (2007).

[7] G. Groh, J. Appl. Phys. **39,** 5804-5 (1968).

[8] G. Hass and J. B. Ramsay, Appl. Opt. **8,** 1115-8 (1969).

[9] H. M. Smith and A. F. Turner, Appl. Opt. **4,** 147-8 (1965).

[10] H. Schwarz and H. A. Tourtellotte, J. Vac. Sci. Technol. **6,** 373-8 (1969).

[11] R. Srinivasan and W. Mayne-Banton, Appl. Phys. Lett. **41,** 576-8 (1982).

[12] H. H. G. Jellinek and R. Srinivasan, J. Phys. Chem. **88,** 3048-51 (1984).

[13] R. Srinivasan, M. A. Smrtic, and S. V. Babu, J. Appl. Phys. **59,** 3861-7 (1986).

[14] R. Srinivasan, B. Braren, D. E. Seeger, and R. W. Dreyfus, Macromolecules **19,** 916-21 (1986).

[15] J. H. Brannon, J. R. Lankard, A. I. Baise, F. Burns, and J. Kaufman, J. Appl. Phys.

58, 2036-43 (1985).

[16] S. G. Hansen and T. E. Robitaille, Appl. Phys. Lett. **52,** 81-3 (1987).

[17] M. Sirajuddin and P. J. Reddy, Thin Solid Films **124,** 139-54 (1985).

[18] R. Srinivasan, B. Braren, and R. W. Dreyfus, J. Appl. Phys. **61,** 372-6 (1987).

[19] L. A. Utracki, *Polymer Alloy and Blends* (Hanser, New York, 1990).

[20] T. Takekoshi, in *Polyimides: Fundamentals and Applications*; *Vol. 1*, 1st ed., edited by M. K. Ghosh and K. L. Mittal (Marcel Dekker, New York, 1996), p. 7-49.

[21] R. Srinivasan and B. Braren, Chem. Rev. **89,** 1303-16 (1989).

[22] D. P. Brunco, M. O. Thompson, C. E. Otis, and P. M. Goodman, J. Appl. Phys. **72,** 4344-50 (1992).

[23] D. Bauerle, M. Himmelbauer, and E. Areholz, J. Photochem. and Photobio. A **106,** 27-30 (1997).

[24] G. Blanchet, J. Appl. Phys. **80,** 4082-89 (1996).

[25] M. J. Kelley, Mat. Res. Soc. Symp. **617,** 1-6 (2000).

[26] E. E. Ortelli, F. Geiger, T. Lippert, and A. Workaun, Appl. Spect. **55,** 412-9 (2001).

[27] D. W. Zeng, K. C. Yung, and C. S. Xie, Surf. Coat. and Tech. **153,** 210-6 (2002).

[28] T. Y. S. Tou, W.O; Wong, K.H, Applied Surface Science **248,** 281-285 (2005).

[29] C. A. Brau, *Free-Electron Lasers*, Vol. 22 (Academic Press, Boston, 1990).

[30] C. A. Brau, Nucl. Instr. Meth. A **318,** 38-41 (1992).

[31] N. L. Dygert, K. E. Schriver, and R. F. Haglund, Jr, J. of Physics Conference Series **59,** 651-6 (2007).

[32] N. L. Dygert, K. E. Schriver, and R. F. Haglund, Jr., Proc. SPIE **6107,** 212-20 (2006).

[33] M. R. Papantonakis and R. F. Haglund, Jr., Appl. Phys. A **79,** 1687-94 (2004).

[34] D. M. Bubb, J. S. Horwitz, J. H. Callahan, R. A. McGill, E. J. Houser, D. B. Chrisey, M. R. Papantonakis, R. F. Haglund, M. C. Galicia, and A. Vertes, J. Vac. Sci. Technol. A **19,** 2698-2702 (2001).

[35] D. M. Bubb, M. R. Papantonakis, B. Toftmann, J. S. Horwitz, R. A. McGill, D. B. Chrisey, and R. F. Haglund, J. Appl. Phys. **91,** 9809-9814 (2002).

[36] R. Srinivasan, R. R. Hall, W. D. Loehle, W. D. Wilson, and D. C. Albee, J. Appl. Phys. **78,** 4881-7 (1995).

[37] D. B. Chrisey, A. Pique, R. A. McGill, J. S. Horwitz, B. R. Ringeisen, D. M. Bubb, and P. K. Wu, Chem. Rev. **103,** 553-76 (2003).

[38] T. J. Dingemans, E. Mendes, J. J. Hinkley, E. S. Weiser, and T. L. StClair, Macromolecules **41,** 2474-84 (2008).

[39] M. Anthamatten, S. A. Letts, K. Day, R. C. Cook, A. P. Gies, T. P. Hamilton, and W. K. Nonidez, J. Poly Sci A **42,** 5999-6010 (2004).

[40] P. E. Dyer and R. Srinivasan, Appl. Phys. Lett. **48,** 445-7 (1986).

[41] D. M. Bubb, B. R. Ringeisen, J. H. Callahan, M. Galicia, A. Vertes, J. S. Horwitz, R. A. McGill, E. J. Houser, P. K. Wu, A. Pique, and D. B. Chrisey, Appl. Phys. A **73,** 121-123 (2001).

[42] P. K. Wu, B. R. Ringeisen, J. Callahan, M. Brooks, D. M. Bubb, H. D. Wu, A. Pique, B. Spargo, R. A. McGill, and D. B. Chrisey, Thin Solid Films **398,** 607-614 (2001).

[43] J. H. Brannon and J. R. Lankard, Appl. Phys. Lett. **48,** 1226-28 (1986).

CHAPTER II

EXPERIMENTAL BACKGROUND

Nicole Leigh Dygert

Interdisciplinary Materials Science

Vanderbilt University

Nashville, TN 37235

2.1 Polymers

Polymers are differentiated from other organic compounds by their high molecular weight and molecular weight distribution. This high molecular weight is what gives them their mechanical properties, while they are chemically indistinguishable from their lower molecular weight counterparts. The organization of the atoms comprising the polymer structure is considered the chain conformation. The chain may experience rotation about a bond but the chain conformation cannot be altered without breaking and reforming bonds. The chains also experience a secondary bonding force, the Van der Waals force, between the chains. The chains may be highly ordered, generating crystalline or semi-crystalline polymers, or they may be amorphous. The solvent and other additives have a large effect on the behavior and properties of the polymer. For example, the solvent N-methyl pyrrolidinone (NMP) is considered a plasticizer and chain extender; it helps the polymer attain a higher molecular weight while maintaining the ability to flow.

There are two main classes of polymers, thermoplastics and thermosets. Thermoplastics soften and flow upon the application of pressure and heat. Most thermoplastics can be re-molded several times without undergoing chemical degradation.[1] Thermosets, once heated, react irreversibly so that subsequent application of heat and pressure do not cause them to soften and flow. Polymers using only a single monomer are termed homopolymers, while those comprising more than one monomer are copolymers. All of the polymers described in the forthcoming chapters are copolymers.

2.2 Polyimide Synthesis

A two-step process (see figure 2.1) is commonly used to synthesize polyimides. In the first step a solution of diamine in a polar aprotic solvent is prepared and a dianhydride is added. Nucleophilic attack of the amino group of the carbonyl carbon of the anhydride group occurs, followed by the opening of the anhydride ring to form the polyamic acid (PAA), see figure 2.2.

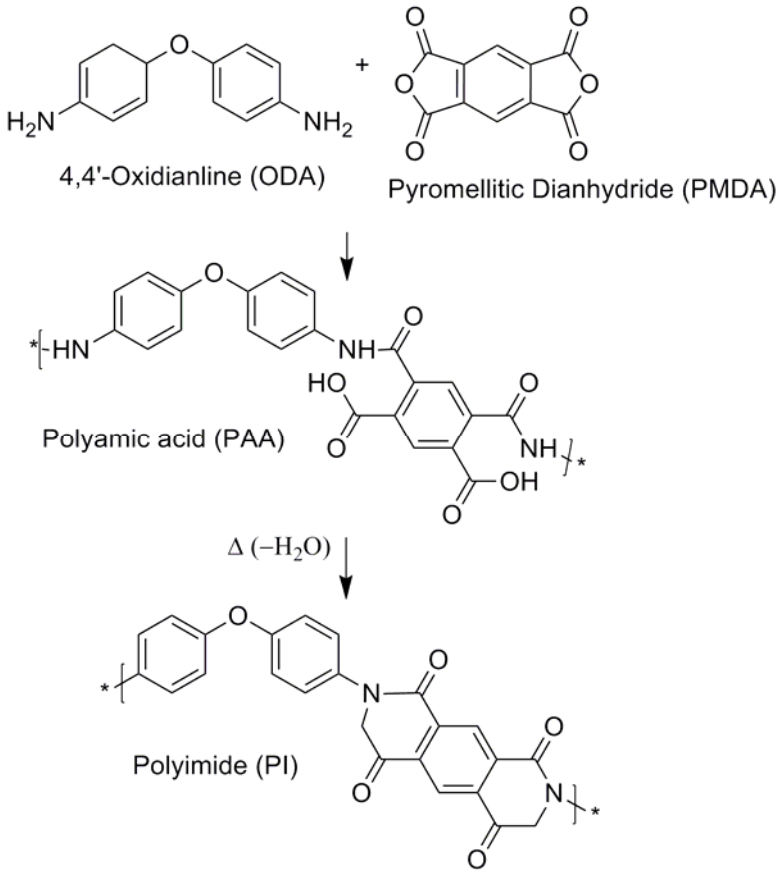

Figure 2.1: Synthetic Route to Polyimide

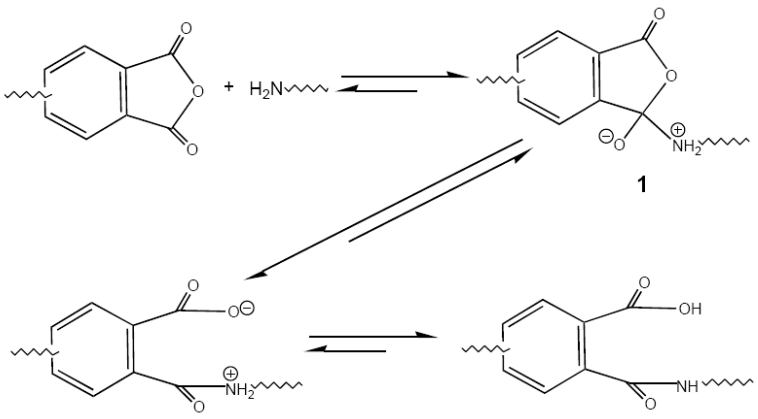

Figure 2.2: Nucleophilic acyl substitution

The formation of the PAA is usually complete within 24 hours at ambient temperatures. The reaction rate is dependent on the solvent, with the rate being faster for more basic and more polar solvents.[2] PAA is known to undergo hydrolysis even at ambient temperatures, so the reaction should be performed under a blanket of inert gas. The water causes degradation (see figure 2.3) in the molecular weight of the polymer, thus the PAA must be refrigerated to slow the hydrolysis reaction.

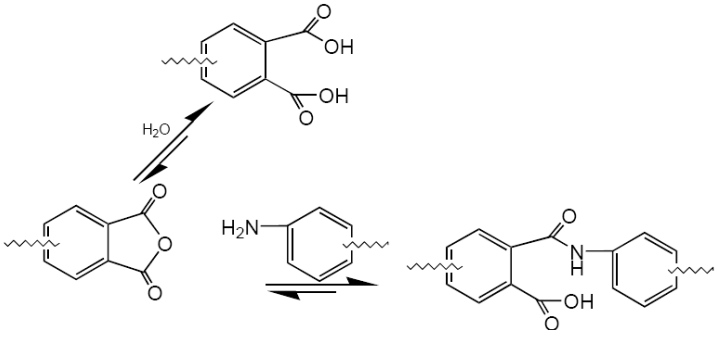

Figure 2.3: Hydrolysis of Polyamic acid

The second step requires a thermal (see figure 2.4) cure or chemical dehydration (see figure 2.5) to form the polyimide through cyclodehydration. The quality of the PI film formed after curing is affected by the degree of imidization, uniformity of the surface, and the interactions of the PAA with the solvent. Solvent PAA interactions have been studied by several authors.[3,4] The solvent forms a complex through hydrogen bonding of the NMP carbonyl to the hydrogen on the amide and carboxylic groups. The existence of a 4:1 NMP di(amic) I acid complex was shown by Brekner and co-workers using thermogravimetric analysis.[4] Due to the electronegativity of the oxygen atom the NMP is more strongly bound to the carboxylic acid group. The carboxylic NMP helps to prevent the reverse reaction that would otherwise degrade the PAA chain and regenerate the original monomers.[5,6] Incapacitating the reverse reaction is especially important in step growth polycondensation polymerizations, such as polyimide, as it is critical to have a significantly faster forward reaction in order to achieve high molecular weights. Zhan and co-workers showed that the degree of imidization also depends on the solvent content of the film; specifically, they showed that prior removal of the solvent leads to lower curing temperatures and higher quality films.[3] This effect is also due to the hydrogen bonding of the NMP which can hinder the removal of water and, the closure of the five-member lactam ring in the PAA.

The synthesis of polyamide imide and polyether imide are similar in mechanism to synthesis of polyimide and will not be explicitly discussed. For a discussion on polyamide imide synthesis see Imai and for polyether imides refer to Dingemans.[7,8]

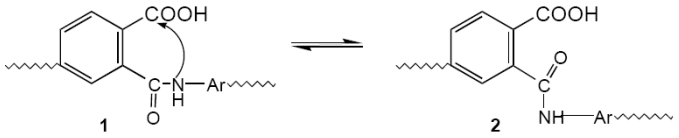

Figure 2.4: Thermal cyclodehydration

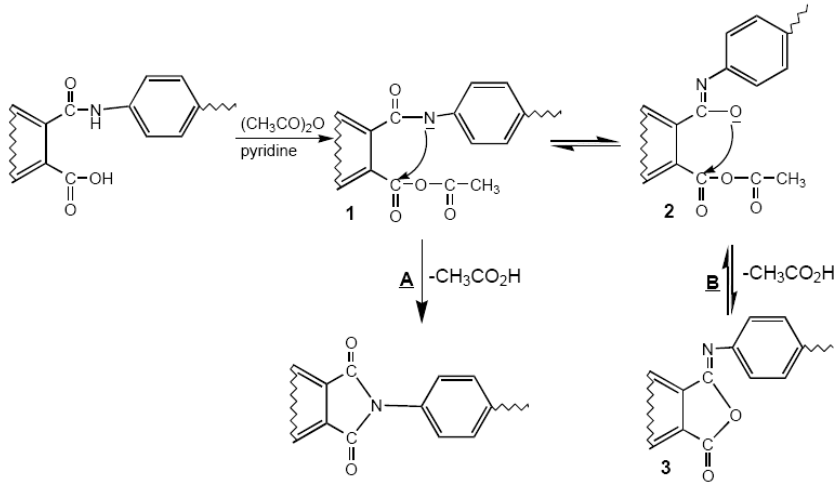

Figure 2.5: Chemical Dehydration

2.3 Polymer molecular weight

Unlike organic molecules, the molecular weight of a polymer is not unique and polymers may be synthesized with a distribution of molecular weights. The molecular weight achieved is determined by the synthetic method and any subsequent chemical reactions. Therefore a quoted polymer molecular weight is an average molecular weight. The four common molecular weight averages are: weight average (from light-scattering), number average (colligative properties), Z-average (ultracentrifuge measurements), and viscosity average (dilute viscosity measurements). The definitions for the number and weight-average molecular weight are shown below (eqs 2.1 and 2.2).[1] If both are

known the weight average molecular weight (M_w) may be divided by the number average molecular weight (M_n) to give the polydispersity index (PDI) (eq. 2.3).[1] The weight-average molecular weight should always be larger than the number average molecular weight and polydispersities of 1.5-2.0 are common.[9]

$$M_n = \frac{\sum_i M_i N_i}{\sum_i N_i} \qquad (2.1)$$

$$M_w = \frac{\sum_i N_i M_i^2}{\sum_i N_i M_i} \qquad (2.2)$$

N_i is the number of molecules of molecular weight M_i

$$PDI = \frac{M_w}{M_n} \qquad (2.3)$$

2.4 Light Scattering

The principal method used to determine the weight-average molecular weight is light scattering. The application of light scattering theory to polymers begins with the work of Einstein and Smoluchowski who examined fluctuations in the refractive indices of liquids.[10] The simplified equations used in light scattering experiments today were developed by Debye and Zimm.[11-13] The result of their labor was an equation that relates the observed light scattering intensity to the osmotic pressure, π:

$$\frac{Hc}{R(\theta)} = \frac{1}{RT}\left(\frac{\partial \pi}{\partial c}\right)_T \qquad (2.1)$$

where R(θ) is the Rayleigh ratio and is equal to $(I_\theta w^2)/(I_0 V_s)$ where I_θ is the light intensity at angle θ scatter from a volume V_s, when the distance from the source is w and the incident light intensity is I_0.[9] Other terms are defined: R is the universal gas constant, T

is temperature in K, and c is the concentration in g/cm^3. The optical constant H appearing on the left hand side of the equation is given by:

$$H = \frac{2\pi_1^2 n_0^2 (dn/dc)^2}{N_A \lambda^4} \tag{2.2}$$

where π_1 represents the constant with a value of 3.1416 and not the osmotic pressure π, n_0 is the refractive index at a wavelength λ, N_A is Avogadro's number, and the dn/dc is the differential change in refractive index with concentration.[9] The value of dn/dc must be determined for each solvent-polymer pairing.

The basic equation for the determination of molecular weight and size of polymers using scattering is derived from the above equation (2.1) combined with the osmotic pressure equation. Osmotic pressure is a colligative property; these properties depend on the number of molecules present in a solution and not on the chemical composition. Equation 2.3 shows the relationship of osmotic pressure and molecular weight:

$$\lim_{c \to 0} \frac{\pi}{c} = \frac{RT}{M_n} \tag{2.3}$$

where π is the osmotic pressure, c is concentration, R is the universal gas constant, T is temperature, and M_n is the number average molecular weight.[9] Interactions between the solute and the solvent at finite concentrations result in the virial coefficients A_2 and higher order terms. The equation incorporating the virial coefficients is:

$$\frac{\pi}{c} = RT\left(\frac{1}{M_n} + A_2 c + A_3 c + \ldots\right) \tag{2.4}$$

The second virial coefficient, A_2, represents the interaction of one polymer molecule and the solvent, while higher virial coefficients incorporate multiple polymer solvent

interactions.[9] The first virial coefficient A_1 is equal to $(1/M_n)$. For dilute solutions, with approximately 1% solute concentration the slope is linear allowing for the elimination of higher order virial coefficients (A_3…). The second virial coefficient is dependant on both the temperature and the solvent.

Combining equations 2.1 and 2.4 generates the basic equation for molecular weight and size determination for light scattering.

$$\frac{Hc}{R(\theta) - R(solvent)} = \frac{1}{M_w P(\theta)} + 2A_2 c \tag{2.5}$$

In the above equation M_w is the weight average molecular weight and $P(\theta)$ is the scattering form factor.[9] The 2 in front of the second virial coefficient comes from the differentiation of equation 2.4. The form factor, $P(\theta)$, describes angular scattering arising from the conformation of a single chain. $P(\theta)$ is a function of the z-averages size, shape, and conformation of the polymer molecule. As the angle θ approaches zero the structure factor becomes independent of shape; this region is known as the Guinier region.[9] In the Guinier region the form factor $P(\theta)$ is a measure of the radius of gyration, R_g. For a random coil the polymer form factor is given by

$$P(\theta) = \frac{2}{R_g^4 K^4}\left\{R_g^2 K^2 - \left[1 - \exp(-R_g^2 K^2)\right]\right\} \tag{2.6}$$

The expanded form of equation 2.6 is below:

$$P(\theta) = 1 - \frac{K^2 R_g^2}{3} + \ldots \tag{2.7}$$

where

$$K = \frac{4\pi_1}{\lambda}\sin\left(\frac{\theta}{2}\right) \tag{2.8}$$

The radius of gyration is a slightly misleading term, the quantity R_g^2 is defined as the mean square distance away from the center of gravity, $R_g^2 = \left(\frac{1}{N}\right)\sum_{i=1}^{N} r_i^2$, for N scattering points of distance r_i.[9] It is also sometimes referred to as the root mean square radius (RMS) and may alternatively be defined as follows: $\left\langle R_g \right\rangle = \sqrt{\left[\frac{\sum_i m_i r_i^2}{\sum_i m_i}\right]}$ where m_i represents a point mass.

Zimm derived the key equations for the limits of zero angle and zero concentration respectively and used them to relate measured light scattering intensity to the M_w and R_g. The equations may be written:

$$\left(\frac{Hc}{R(\theta)}\right)_{\theta=0} = \frac{1}{M_w} + 2A_2c + \ldots \tag{2.9}$$

$$\left(\frac{Hc}{R(\theta)}\right)_{c=0} = \frac{1}{M_w}\left[1 + \frac{1}{3}\left(\frac{4\pi_1}{\lambda'}\right)^2 R_g^2 \sin^2\frac{\theta}{2} + \ldots\right] \tag{2.10}$$

where λ' is the wavelength of light in solution (λ_0/n_0).[9] By combining equations 2.9 and 2.10 a Zimm plot may be created. Figure x shows an example of plotting equations 2.9 and 2.10 in order to extract the M_w and R_g. Some common units for the light scattering terms are shown in table 2.1.

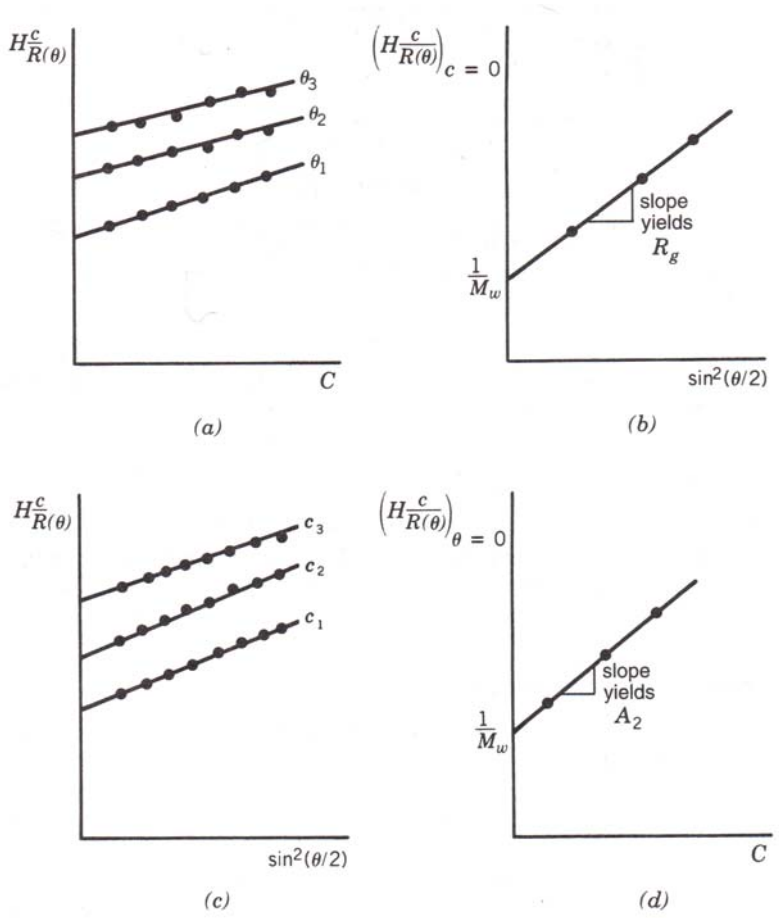

Figure 2.6 a-d: a) shows a plot of H[c/R(θ)] versus concentration for several angles extrapolated to c = 0, b) is a replot of the intercepts of (a) versus $\sin^2(\theta/2)$, c) same data from (a) replotted against $\sin^2(\theta/2)$ first, and d) the intercepts of (c) are plotted against concentration from Sperling[9]

Table 2.1: Light scattering units table from Sperling[9]

$H = \frac{\text{mol} \cdot \text{cm}^2}{\text{g}^2}$	$A_2 = \frac{\text{mol} \cdot \text{cm}^3}{\text{g}^2}$
$c = \frac{\text{g}}{\text{cm}^3}$	$R(\theta) = \text{cm}^{-1}$
	$\theta = \text{degrees}$
	$(\frac{\sin^2 \theta}{2}$ for 90° is 0.500, unitless)
$M_w = \frac{\text{g}}{\text{mol}}$	

The Zimm plot allows for the calculation of M_w, R_g, and A_2 on a single figure. An example of a Zimm plot is shown below in figure 2.7.

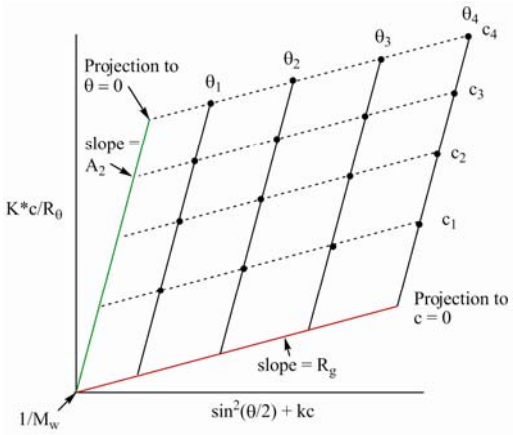

Figure 2.7: Example of a Zimm construction

Today most light scattering instruments come with built-in software packages to run through the calculations. The multi-angle laser light scattering (MALLS) instrument we used (DAWN HELEOS, Wyatt Technologies, Santa Barbara, CA) came with the software package ASTRA. Since the instrument is measuring detector voltages, which are proportional to light scattering intensities, a calibration factor must be used. The calibration is calculated by first measuring a known strong scatterer, such as toluene, where the Rayleigh ratio, $R(\theta)$ is already known.[14] The calibration constant corrects the measured $R(\theta)$ values to match with the known $R(\theta)$. Corrections are also made for reflections arising from different cell geometries. The calibration constant is determined only for the 90 ° detector and is independent of the sample to be studied. The detectors at other angles have their own unique geometrical factors and sensitivity. To normalize the other detectors an isotropic scatterer is introduced into the pure sample solvent.[14] An isotropic scatterer is one that scatters equally in all directions and $R(\theta)$ is independent of θ. In our experiments 30,000 narrow molecular weight distribution polystyrene with an

approximate radius of 3 nm was dissolved in NMP for the normalization procedure. When multiplied by its normalization coefficient each detector will give the same R(θ) as the 90 ° detector. Then the experimental data is collected and an appropriate fit method is chosen.

We collected light scattering data for all of the solutions and then used two different formalisms to solve for the molecular weight. First the Zimm method was used which has been discussed earlier in this section. An example of an obtained ASTRA Zimm plot is shown below in figure 2.8 for a PMDA-ODA standard. Then the Debye method was applied where the molecular weight is determined for each concentration. The molecular weight data from each concentration are then averaged and the standard deviation is computed as the error. An example of the Debye plot from ASTRA is shown below in figure 2.9 for 3.45 μm RIR-LA PMDA-ODA.

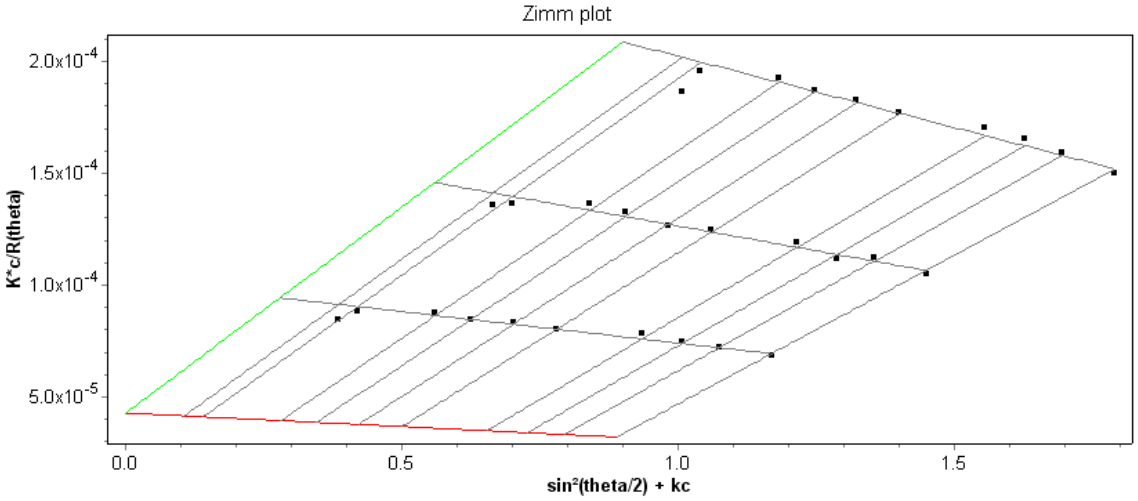

Molar mass (Mw): (2.321±0.136)e+4 g/mol
2nd virial coefficient: (8.048±0.199)e-3 mol mL/g²

Figure 2.8: Zimm plot from ASTRA program of PMDA-ODA standard.

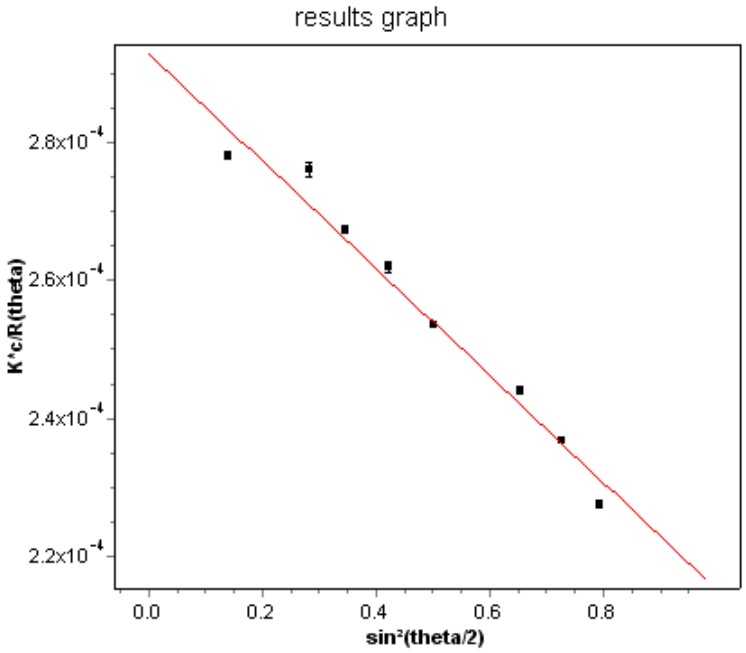

Molar Mass: (7.523 ± 0.084) e+3 g/mol

Figure 2.9: Debye plot output by ASTRA from
3.45 μm RIR-LA PMDA-ODA

Dynamic light scattering is also known as quasi-elastic laser light scattering (QELS). The random motion of solute particles in a solvent is called Brownian motion. In an experiment, light is scattered from the moving particles and the light experiences constructive and destructive interference depending on the relative positions of the particles; the scattered intensity is dependent on time. A QELS measurement uses a fast photon counter to measure the time dependent fluctuations in the scattered light. QELS is used to determine the hydrodynamic radius of the polymer through the correlation function. The equation for the hydrodynamic radius is $D = \frac{k_B T}{6\pi\eta R_H}$ where D is the diffusion coefficient (determined by the correlation function), k_B is the Boltzmann constant, T is the temperature, η is the solution viscosity, and $6\pi\eta R_H$ is the frictional

coefficient of a hard sphere in a viscous medium.[14] The hydrodynamic radius is the radius of a hypothetical hard sphere that diffuses with the same speed as the particle under examination. A graphic from the Malvern website illustrating the different radii for lysozyme is shown in figure 2.10.[15] The R_g and R_H have been previously defined, R_R is the radius established by rotating the molecule about its geometric center, and R_M is the equivalent radius of a sphere with the same mass and volume as the particle.

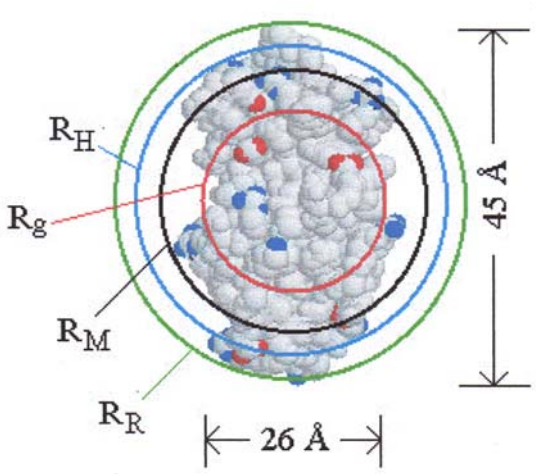

Figure 2.10: Different radii measurements for lysozyme from reference[15]

From our data we found that there was too much scatter associated with the QELS measurement to allow the determination of the hydrodynamic radius. This is probably caused by the strong solvent interactions discussed earlier. We tried adding a 1% LiBr salt solution to the polymer solution but did not see any improvement in the consistency of the radii. In figure 2.11 the output of ASTRA for QELS shows both the correlation function used to determine the diffusion coefficient and the residual correlation function.

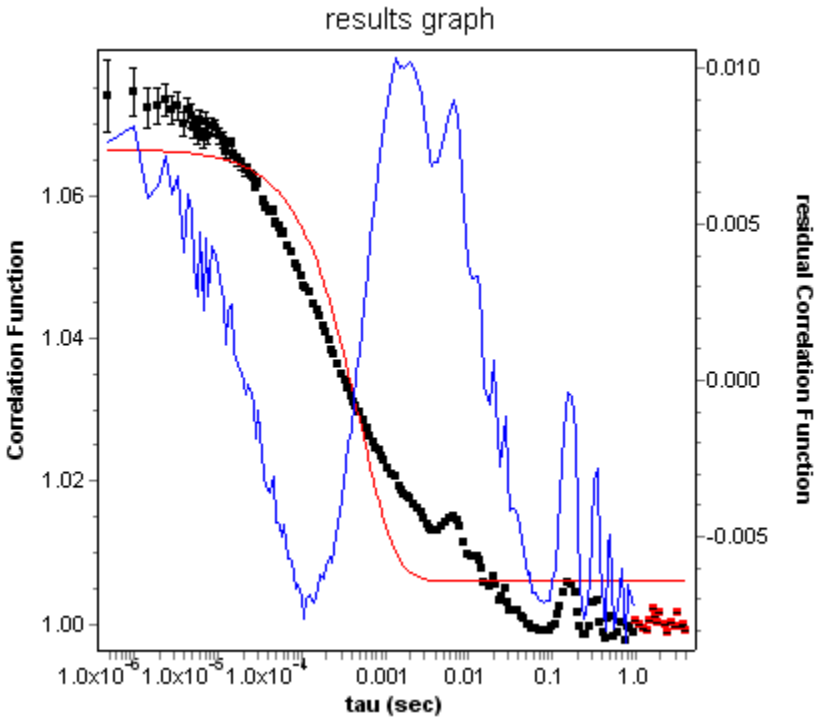

R_H: 111.9 ± 13.3 nm
D: (2.18 ± 0.26) e^{-8} cm²/sec

Figure 2.11: QELS output for 3.45 μm RIR-LA PMDA-ODA

2.5 References

1 F. Rodriguez, *Principles of Polymer Systems*, 4th ed. (Taylor & Francis, Philadelphia, 1996).

2 T. Takekoshi, in *Polyimides: Fundamentals and Applications*; *Vol. 1*, 1st ed., edited by M. K. Ghosh and K. L. Mittal (Marcel Dekker, New York, 1996), p. 7-49.

3 Y. K. Xu, M. S. Zhan, and K. Wang, Journal of Polymer Science Part B-Polymer Physics **42,** 2490-2501 (2004).

4 M. J. Brekner and C. Feger, J. of Poly. Sci A **25,** 2005-20 (1987).

5 M. M. Koton, V. V. Kudryatsev, N. A. Adrova, K. K. Kalnin'sh, A. M. Dubnova, and V. M. Svetlichnyi, Polymer Science (USSR) **16,** 2411 (1973).

6 A. N. Pravednikov, I. Y. Kardesh, N. P. Glukhoyedov, and A. Y. Ardashnikov, Polymer Science (USSR) **15,** 399 (1973).

[7] Y. Imai, in *Polyimides: Fundamentals and Applications*, edited by M. K. Ghosh and K. L. Mittal (Marcel Dekker Inc., New York, 1996), p. 49-70.

[8] T. J. Dingemans, E. Mendes, J. J. Hinkley, E. S. Weiser, and T. L. StClair, Macromolecules **41,** 2474-84 (2008).

[9] L. H. Sperling, *Introduction to Physical Polymer Science*, 3rd ed. (Wiley-Interscience, New York, 2001).

[10] P. J. Wyatt, Analytica Chimica Acta **272,** 1-40 (1993).

[11] P. Debye, J. Phys. Coll. Chem. **51,** 18 (1947).

[12] B. Zimm, J. Chem. Phys. **16,** 1093 (1948).

[13] B. Zimm, J. Chem. Phys. **16,** 1099-1116 (1948).

[14] W. T. Corporation, (Wyatt Technology Corporation, 2007).

[15] M. Instruments; *Vol. 2008* (Malvern Instruments, 2008).

CHAPTER III

RESONANT INFRARED PULSED LASER DEPOSITION OF A POLYIMIDE PRECURSOR

Nicole L. Dygert [1], Kenneth E. Schriver [2,3], and Richard F. Haglund, Jr. [2,3]

1- Department of Interdisciplinary Materials Science

2- Department of Physics and Astronomy

3- W. M. Keck Foundation Free Electron Laser Center

Vanderbilt University, Nashville, TN 37235

This manuscript was published in *Journal of Physics: Conference Series* **59** (2007) 651-6

3.1 Overview

Neat thermoplastic polymers have been previously transferred intact by resonant infrared radiation.[1-3] In this chapter we begin investigating the possibility of transferring thermosetting polymers using infrared radiation. Polyimide was chosen as an ideal material, it was readily available as a commercial cured film and in its precursor solution form polyamic acid (PAA). The PAA may be transformed to polyimide by either a thermal cure (>200 °C) or chemical dehydration. Polyimides find numerous commercial applications due to their excellent thermoxidative stability. We examined the possibility of transferring a film of cured polyimide and a dropcast film of the PAA precursor solution by resonant infrared pulsed laser deposition (RIR-PLD). The precursor PAA required half of the energy needed to see visible ablation in the cured polyimide. Then the PAA was ablated first at ambient conditions and then as a liquid nitrogen frozen target under vacuum while collecting the ablated material on glass slides. The PAA was deposited in droplet-like morphologies when ablation occurred in air, and in string-like moieties in the case of ablation in vacuum. In the as-deposited condition, the PAA was easily removed by washing with NMP; however, once cured thermally for thirty minutes, the PAA hardened, indicating the expected thermosetting property. This implies that the necessary thermal cure temperatures are either not reached in the plume or that there is not enough time for sufficient heat to transfer to the polymeric precursor to induce curing. The major component of the PAA is the solvent N-methylpyrrolidinone (NMP) (85 wt%). We used plume shadowgraphy to compare the ablation behaviour of the pure solvent to the PAA. There is a large viscosity difference between the water-like NMP and the honey-like PAA. Plume shadowgraphy showed clear contrasts in the ablation

mechanism between ablation of the solvent alone and the ablation of the PAA, even at low concentrations. The shockwave velocities of the ejected PAA were measured at various wavelengths to determine the effect of the resonant wavelength on ablation trajectories. A wavelength dependence in plume velocity was observed, with the solvent resonant mode behaving differently than the polymer resonant modes.

3.2 Introduction

Polymer thin films are now widely used in sophisticated optical, electronic, and medical technologies ranging from micro-electro-mechanical systems (MEMS) to polymer light-emitting diodes and drug-delivery coatings. In these applications, particularly where multiple thin coatings are necessary to realize the functionality, or where parallel processing to deposit multiple coatings, for example, on sensor arrays, or multi-layer PLEDs, it would be desirable to have a solvent-free, vapor-phase coating technique that would circumvent the difficulties associated with solvent compatibility and precise thickness control that are inherent in such liquid-phase deposition processes as spin-coating or dip-coating. We have previously demonstrated that ablation of polymers and other organic materials by infrared (IR) lasers that are resonant with a vibrational mode in the target has been the subject of several recent papers.[4] With resonant infrared ablation, localized anharmonic vibrational modes are directly excited, generating the energy density and nuclear motion required for vaporization by mechanisms that are still subjects of active investigation.

In this paper, we demonstrate preliminary results indicating successful deposition of polyimide precursor, without initiating the curing of this thermosetting polymer during

the ablation process. In addition to illustrating the low-temperature property of resonant infrared pulsed laser deposition, this demonstration also exhibits a possible new route for deposition that is compatible with subsequent patterning of substrates and expanded uses of polyimide in the electronics industry.

3.2.1 Polyimides

Since their commercial introduction by DuPont in the 1960s, polyimide films have been used as wire insulation, substrates for printed circuit boards, and solar panel cells. Powell and Lopez discussed the possibilities of PIs replacing polycarbonates as the standard for gas-filled windows (*Hohlraums*) and filters for x-ray astronomy.[5] Polyimides are synthesized by a two-step process (see figure 3.1). First, a dianhydride and diamine are combined in a polar solvent to form the poly (amic acid) precursor (PAA); we used pyromellitic dianhydride (PMDA) and 4,4'-oxidianiline (ODA), dissolved in the solvent N-methylpyrrolidinone (NMP). Our precursor solution of 15 wt% PAA in NMP was obtained from Sigma Aldrich. The choice of solvent affects the degree of cross linking and polymer chain length. NMP promotes longer chains prior to the cross linking step by increasing melt flow. The second step requires a thermal cure to induce cyclodehydration. Generally the PAA is cured around 250 °C to ensure complete conversion to polyimide (PI). To prevent trapping of water vapor, the film must be thin and uniform. Patterning of the PI is challenging because thermosetting polymers are not readily removed, except possibly by UV laser ablation, after curing.

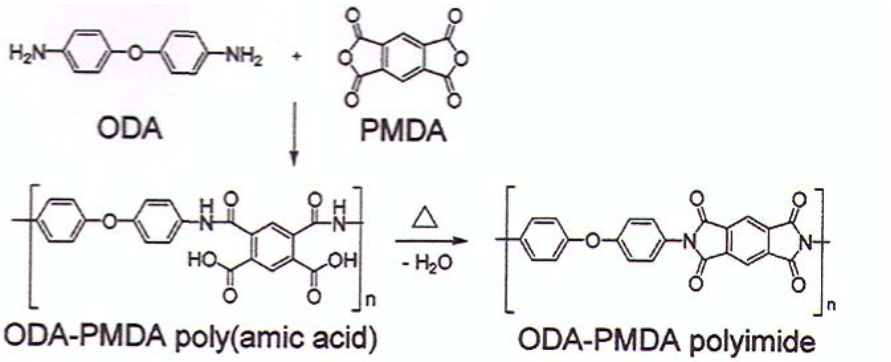

Figure 3.1: Synthetic Route to Polyimide from ref. [6]

3.3 Experimental Procedure

3.3.1 Free electron laser

The ablation laser used in our experiments was an rf-linac driven free-electron laser (FEL)[7], wavelength tunable from 2 to 10 μm. The accelerator in the FEL is powered by an S-band klystron at 2.865 GHz that produces 4 μs macropulses at a repetition rate of 30 Hz. Within each macropulse, the small acceptance angle of the rf accelerator produces some 10^4 micropulses of approximately 1 ps duration. The optical bandwidth of the pulses is typically 1 % of the center frequency (FWHM) with a micropulse energy of several μJ, yielding a peak unfocused irradiance of order 10^7 W/cm^2. The fluence for the experiments reported here is that of the macropulse.

3.3.2 Materials

We first investigated laser ablation of commercially obtained amber-colored Kapton® tape approximately 63 μm thick with silicon adhesive on one side, at 5.9 μm wavelength corresponding to strong absorption in the C=O stretch mode. A film of the

15% PAA was formed by applying a thin layer to a glass slide and drying under moderate vacuum for 20 minutes.

3.3.3 Vacuum chamber

For vacuum PLD experiments, the FEL beam was introduced into the vacuum chamber by way of a BaF_2 entrance window and focused onto the target by a 50 cm focal length BaF_2 lens. Using a pyroelectric joulemeter, we measured the transmission through the lens and entrance window to be approximately 0.8. The base pressure of our deposition chamber for the experiments in vacuum was 10^{-5} torr or less. The beam was rastered across the surface of the target at a frequency of 15 Hz while the target was rotated at 2 Hz to maintain a relatively even ablation across the surface of the frozen target.

3.3.4 Laser deposition process

Resonant infrared pulsed laser deposition (RIR-PLD) was used to transfer PAA under vacuum at ambient temperatures onto glass substrates. In RIR-PLD, it is typical for the polymer to remain in the electronic ground state during ablation, thus minimizing photochemical damage. Previous studies have shown that RIR-PLD is generally associated with temperature rises of only a few tens of degrees and with deposition rates substantially higher than those typical of UV PLD of inorganics. A solid target was made by freezing the PAA in liquid nitrogen for use in the chamber. An ablation wavelength of 3.45μm was chosen to resonate with a strong absorption in the NMP, so that the NMP provided matrix-assisted ablation of intact PAA molecules. Material was deposited at

fluences above 0.5 J/cm^2. The same wavelength was also used to transfer the precursor PAA in air. Additional RIR-PLD experiments were performed at the polymer resonant wavelength both under vacuum and in air.

3.3.5 Plume Shadowgraphy

The temporal evolution of the ablation plume was recorded by triggering a nitrogen laser-pumped Rhodamine 6G dye laser to illuminate the plume in shadowgraph mode, while a digital camera captured the image. The parameters of wavelength (6.67, 5.9, 4.8 and 3.45 μm), fluence (1-2 J/cm^2) and polymer concentration (0, 1, 5, 10, 15 wt % PAA) were varied. Shock-wave velocities for different wavelengths (figure 3.4) were obtained by measuring the shock front with a machinist ruler, with an error of order ±0.1mm. Temporal jitter in the risetime of the FEL pulse causes only ns uncertainties in the time scale. A knife-edge measurement was used to obtain the laser spot size.

3.4 Discussion

3.4.1 Kapton® experiments

After drying the vacuum PAA film was transparent in color, contrasting the amber colored Kapton® tape. The supported Kapton® tape showed definable ablation above 3 J/cm^2, while the vacuum PAA film ablated with only 1.5 J/cm^2. Indicating greater ease of transferring the precursor compared to the cured PI. Transferring the liquid polymer precursor in air resulted in a pale yellow as-deposited material; it was readily removed by a solvent wipe with NMP. This simple experiment reveals that the

PAA is transferred without an excessive temperature rise, allowing it to remain in the uncured state. After heating to 150 °C on a laboratory hotplate for 30 minutes the deposited film could not be removed with an NMP wipe, although at that temperature it is likely that the film was not fully imidized. Moreover, as-deposited material did not change colour as would be expected if cross-linking and imidization had occurred; this also indicates little or no electronic excitation during ablation, since the characteristic amber colour of Kapton® and other PI films is due to electron transfer from diamine to dianhydride. Here, the colour change of the PAA from a transparent film at ambient temperatures to amber was seen only after heating.

3.4.2 Optical Microscopy

Atmospheric and vacuum RIR-PLD showed a mixture of string and droplet geometries when examined under the optical microscope. Atmospheric ablation at 3.45 μm (figure 3.2) produced droplet geometries, particularly with increasing fluence and a reduced target-to-substrate distance. Under vacuum at the same wavelength (figure 3.3), the deposited material formed a network of strings with some small droplets interspersed. The droplets appear to result from expulsion of the solvent matrix, either by itself or with the solvent encapsulating some of the PAA. The droplet geometries dried into visually smoother films compared to the string morphologies. A smooth, uniform film is the ideal for most industrial applications. Further experiments will be required to determine which films possess the best overall qualities such as strength, uniformity, hardness, *etc*. PAA has also been transferred at 5.9 μm (not pictured), with similar material geometries. Holding all other parameters (target to substrate distance, fluence, and PAA

concentration) constant, the 3.45 μm and the 5.9 μm wavelength do not produce the same film geometry, suggesting that there is a fundamental difference in the ablation mechanism between the polymer-resonant and the solvent-resonant wavelengths. More conclusive studies are needed to determine the precise effects of the resonant wavelength on film parameters.

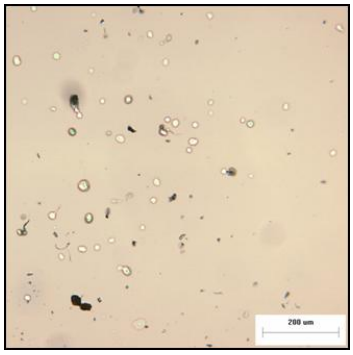

Figure 3.2: Atmospheric RIR-PLD

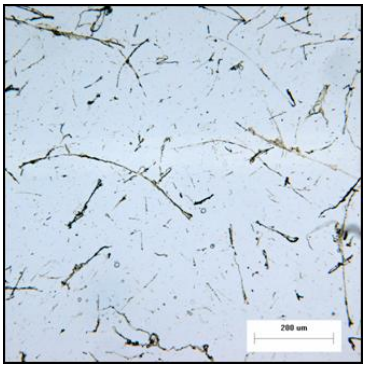

Figure 3.3: Vacuum RIR-PLD

3.4.3 Plume Shadowgraphy

FTIR spectra of PAA in NMP showed a strong absorption at 5.9 μm (carbonyl stretch), 3.45 μm to the (OH and CH stretches), 6.67 μm (aromatic ring mode), and 4.8 μm (non-resonant). NMP also has a strong resonance at 3.45 μm (alkane stretch); given the strong solvent interaction, 3.45 μm appeared to be an ideal solvent excitation wavelength. The spectra of PAA in NMP *vs.* pure NMP show nearly identical peak areas for 3.45μm, while for 5.9 μm the polymer peak area is approximately 20 times larger than the NMP peak area. Figure 3.4 shows how the velocity shock front varied temporally with changing FEL wavelength. The polymer resonant wavelengths (5.9 and 6.67 μm) generate a more rapidly expanding shockwave with peak velocities around 400 m/s. At

the solvent resonance (3.45 µm) the shockwave expansion is delayed and only reaches a maximum velocity of approximately 300 m/s. The different wavelengths share a common velocity profile as shown below.

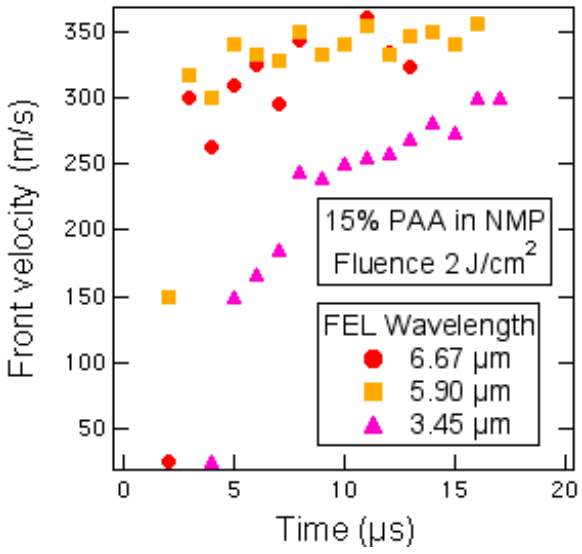

Figure 3.4: Shock front velocity measured as a function of time from the plume shadowgraph data. Note that the polymer resonant wavelengths produce ablation starting at about 2 µs after the FEL pulse, and the velocities reach a saturation value early in the plume expansion phase. When irradiated at 3.45 µm, solvent resonant, the PAA-NMP mixture shows a slower onset, at about 4 µs, and a lower shock-front velocity throughout the plume expansion phase.

Ablation of the solvent alone (0 % PAA) at 5.9 µm showed a vapor cloud initially, as time progresses an increasing amount of liquid is ejected (figure 3.5). In contrast the 15 % PAA showed some initial liquid disturbance dying down to a vapor plume with a few liquid ejecta remaining. At times on the order of milliseconds a "smoke" persisted from the polymer, hypothesized to be from reactions with the air.

Another notable difference is the greater dispersion of the polymer plume compared to the solvent plume. The increased dispersion could be a result of the more rapid shockwave movement illustrated above. Changing the concentration and hence the viscosity of the liquid caused only minor differences at the same wavelength. Raising the fluence resulted in a more violent expulsion of material, but minimally increased the propagation of the shockwave.

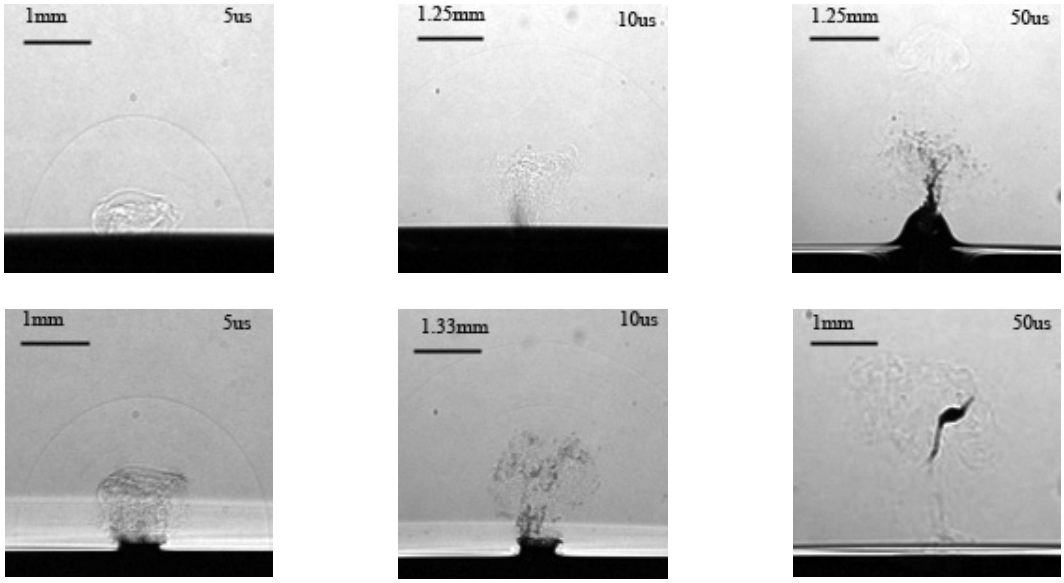

Figure 3.5: Shadowgraphs taken at 5, 10 and 15 μs after the initiation of FEL ablation at 5.90 μm for solutions of NMP (top row) and 15% PAA in NMP (bottom row). The distance scales were derived from calibration measurements made with a machinist ruler.

3.5 Conclusions

Although a number of thermoplastic polymers have been vaporized and deposited intact in previous experiments, the application of the RIR-PLD process to thermosetting polymers represents a qualitatively new and important demonstration of this process. Because these polymers set by cross-linking at temperatures around 250 °C, the

successful deposition of uncured PAA illustrates the low-temperature character of RIR-PLD. Moreover, these preliminary experiments suggest that it should be possible to combine RIR-PLD deposition with post-deposition laser curing and patterning — a result potentially very desirable in many MEMS and microelectronics or microphotonics applications.

The excitation of the solvent NMP to facilitate the transfer of the polymer conceptually resembles matrix-assisted laser desorption-ionization (MALDI) mass spectrometry. However, the crucial difference is that the major product of the ablation is the neutral polymer species as opposed to ionic species. Similarities also exist between the process and ultra-violet matrix-assisted pulsed laser evaporation (UV-MAPLE) investigated by the Naval Research Laboratory (NRL) group.[8] Once again the processes differ in several key respects: the energy for the PAA/NMP process is deposited into vibrational modes rather than the electronic modes activated by UV-MAPLE, the material from the PAA is ejected in a volumetric expansion as opposed to a surface ablation process, and the PI precursor is transferred without curing, unlike UV ablation where the transferred material is often fragmented.

The current experiments show a different ablation characteristic than the prior studies of IR laser ablation in Kapton® films. For example, the measurement of CO_2 laser ablation of Kapton® films showed shockwaves that had expansion velocities an order of magnitude larger than those observed here.[9] A higher degree of thermal damage to the material was also shown in the Kapton® film experiments. Working with the precursor solution to the PI gives a unique opportunity to minimize the thermal damage with RIR-PLD, while simultaneously maximizing the potential applications. While there

are a number of unanswered questions in regards to the ablation mechanisms involved, the low temperature nature of the RIR-PLD and its potential for future work are evident.

3.6 Acknowledgements

We thank Dr. Michael Papantonakis of the Naval Research Laboratory and Professor Duco Jansen and Dr. Mark Mackanos of Vanderbilt for assistance with experimental apparatus. These experiments were partially supported by the Naval Research Laboratory (N00173-05-P-0059); the free-electron laser is supported by the Medical FEL Program of the Department of Defense (F49620-01-1-0429). NLD is supported by a National Science Foundation IGERT fellowship (DMR-0333392).

3.7 References

1 D. M. Bubb, J. S. Horwitz, J. H. Callahan, R. A. McGill, E. J. Houser, D. B. Chrisey, M. R. Papantonakis, R. F. Haglund, M. C. Galicia, and A. Vertes, J. Vac. Sci. Technol. A **19,** 2698 (2001).

2 D. M. Bubb, M. R. Papantonakis, B. Toftmann, J. S. Horwitz, R. A. McGill, D. B. Chrisey, and R. F. Haglund, J. Appl. Phys. **91,** 9809 (2002).

3 M. R. a. H. Papantonakis, R.F, Applied Physics A-Materials Science & Processing **79,** 1687 (2004).

4 R. F. Haglund, Jr, D. M. Bubb, D. R. Ermer, J. S. Horwitz, E. J. Houser, G. K. Hubler, B. Ivanov, M. R. Papantonakis, B. R. Ringeisen, and K. E. Schriver, *Laser precision micromanufacturing*, Vol. 5063 (2003).

5 F. R. Powell and H. H. F. T.-. Lopez, Fusion Technology **31,** 497 (1997).

6 A. P. Gies, W. K. Nonidez, M. Anthamatten, and R. C. Cook, Macromolecules **37,** 5923 (2004).

7 G. S. Edwards, D. Evertson, W. Gabella, R. Grant, T. L. King, J. Kozub, M. Mendenhall, J. Shen, R. Shores, S. Storms, and R. H. Traeger, IEEE J. Sel. Top. Quantum Electron. **2,** 810 (1996).

[8] D. B. Chrisey, A. Pique, R. A. McGill, J. S. Horwitz, B. R. Ringeisen, D. M. Bubb, and P. K. Wu, Chem. Rev. **103,** 553 (2003).

[9] R. Srinivasan, J. Appl. Phys. **73,** 2743 (1993).

CHAPTER IV

DEPOSITION OF POLYIMIDE PRECURSOR BY RESONANT INFRARED LASER VAPORIZATION

N. L. Dygert [1], A. M. Gies [2], K. E. Schriver [3,4] and R. F. Haglund, Jr.[3,4]

1- Interdisciplinary Program in Materials Science

2- Department of Chemistry

3- Department of Physics and Astronomy

4- W. M. Keck Foundation Free-Electron Laser Center

Vanderbilt University, Nashville TN 37235

This manuscript was published in *Applied Physics A* **89** (2007) 481-7

4.1 Overview

We report the successful deposition of a polyimide precursor using resonant infrared laser ablation (RIR-LA). A solution of poly(amic acid) (PAA) dissolved in N-methyl-2-pyrrolidinone (NMP), the melt processable precursor to polyimide, was frozen in liquid nitrogen for use as an ablation target in a high-vacuum chamber. Fourier transform infrared spectroscopy was used to determine that the local chemical structure remained unaltered. Gel permeation chromatography demonstrated that the transferred PAA retained its molecular weight, showing that RIR-LA is able to transfer the polymer intact, with no detectable chain fragmentation. These results are in stark contrast to UV-processing which degrades the polymer. After deposition the PAA may be removed with a suitable solvent; however, once the material has undergone cyclodehydration it forms an impenetrable three-dimensional network associated with thermosetting polymers. The transfer of uncured PAA precursor supports the hypothesis that RIR-LA is intrinsically a low temperature process, because the PAA is transferred without reaching the curing temperature. The RIR-LA also effectively removes the solvent NMP from the PAA, during both the ablation and deposition phases; this is a necessary step in generating PI films.

4.2 Introduction and Motivation

Polyimide (PI) is representative of a large class of polymers that are cross-linked, either thermally or chemically, in order to achieve the desired properties. Since their commercial introduction by DuPont in the 1960s, PI films have been used as wire insulation, substrates for printed circuit boards, and solar panel cells. Polyimide films are

commonly synthesized in a liquid-phase, two-step process, beginning with the application of a polyimide precursor in a suitable solvent on the substrate, followed by drying and then a thermal cure at 250 °C to induce cross-linking.

With the increasing attention paid to micro- and nanoscale devices in which films with these desirable properties might play a role, there is growing interest in vapor phase processes to produce polymer films of all types. With PI, there is a particular interest in the possibility of depositing and patterning the film, using either thermal or optical techniques. However, this would require a low-temperature vaporization process that would neither fragment the polymer nor cure it should the vapor condense between source and growth substrate. UV radiation has been shown to decompose polyimide[1,2], making IR radiation a logical choice for our process.

We have previously demonstrated successful thin film synthesis of numerous thermoplastic polymers by resonant infrared laser ablation (RIR-LA) of neat polymer targets.[3-6] In these experiments, the absence of photofragmentation or other degradation of the polymer films suggested that the RIR-LA process was inherently a low-temperature one. In previous work with PI, we examined the evolution of the ambient ablation plume of PAA through the use of shadowgraphy and conducted some initial vacuum film depositions.[7,8]

In this paper, we present more direct evidence of the low temperature character of the process, by showing that films of polyimide precursor can be deposited by a vibrationally selective infrared laser ablation process, without curing. We also present the first experimental study of the mass distribution of the deposited PAA, indicating that the starting mass distribution remains largely unchanged through the RIR-LA process.

4.3 Polyimide Synthesis

A two-step process (see Fig. 4.1) is commonly used to synthesize PI. In the first step, a dianhydride and a diamine are combined in a polar aprotic solvent to form the polyamic acid precursor (PAA); we used 4,4'-oxidianiline (ODA) and, pyromellitic dianhydride (PMDA) dissolved in the solvent N-methyl-2-pyrrolidinone (NMP). For our experiments, a precursor solution of 15 wt% PAA in NMP was obtained from Sigma Aldrich and used without further purification. The second step requires a thermal cure to induce cyclodehydration. The quality of the PI film formed after curing is affected by the degree of imidization, uniformity of the surface, and the interactions of the PAA with the solvent. Solvent PAA interactions have been studied by several authors.[9,10] The solvent forms a complex through hydrogen bonding of the NMP carbonyl to the hydrogen on the amide and carboxylic groups. The existence of a 4:1 NMP di(amic) I acid complex was shown by Brekner et al. using thermogravimetric analysis.[10] Due to the electronegativity of the oxygen atom, the NMP is more strongly bound to the carboxylic acid group. The carboxylic NMP helps to prevent the reverse reaction that would decompose the PAA chain into the original monomers.[11] Preventing the reverse reaction is especially important in step-growth polycondensation polymerizations, such as PI, as it is critical to have a significantly faster forward reaction in order to achieve high molecular weights. Xu et al. showed that the degree of imidization also depends on the solvent content of the film; specifically, they showed that prior removal of the solvent leads to lower curing temperatures and higher quality films.[12] This effect is also due to the hydrogen bonding of the NMP, which can hinder the removal of water and the closure of the five-member lactam ring in the PAA.

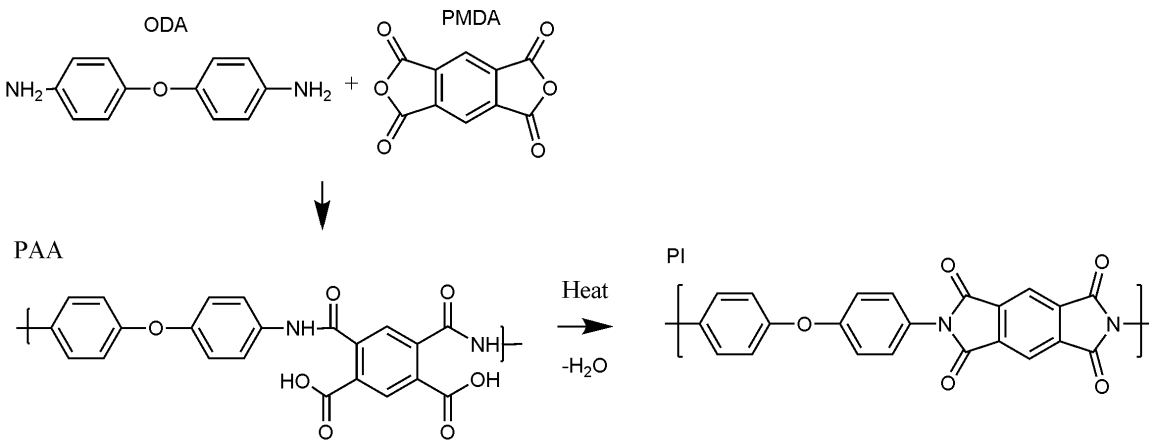

Figure 4.1: Synthetic route to polyimide

In our process the PAA is transferred by laser ablation onto the desired substrate material. Uncured PAA may be removed by a suitable solvent. The substrate could be patterned during the deposition phase using a mask and then thermally cured. Another possibility would be to deposit everywhere, cure the film, and then use a traditional secondary processing technique such as etching with a UV laser.

4.3 Experimental procedure

4.3.1 Free electron laser

The ablation laser used in our experiments is an rf-linac driven free-electron laser (FEL), wavelength tunable from 2 to 10 μm. The accelerator in the FEL is powered by an S-band klystron at 2.865 GHz that produces 4 μs macropulses at a repetition rate of 30 Hz. Within each macropulse, the small acceptance angle of the rf accelerator produces some 10^4 micropulses of approximately 1 ps duration.[13,14] The optical bandwidth of the

pulses is typically 1% of the center frequency (FWHM); the typical micropulse energy is several μJ, yielding a peak irradiance of order 10^9 W/cm^{-2}. The total energy deposited is that of the macropulse; hence, the fluence for the experiments reported here is that of the macropulse.

4.3.2 Vacuum chamber

For vacuum RIR-LA experiments, the FEL was focused by a 50 cm focal length BaF_2 lens, the entrance window to the chamber also had a BaF_2 window. The chamber is evacuated using a turbomolecular pumping system. Base pressures around 10^{-5} mbar were achieved; the pressure during the course of ablation rose to 10^{-4} mbar. Using a pyroelectric joulemeter, we measured the transmission of the lens and entrance window to be 0.8. The beam moved across the target surface with a linear speed of 1 mm/s, and was rotated at a frequency of less than one Hz, to maintain an even track across the target surface. RIR-LA was also performed in air with liquid samples using the same chamber set-up without vacuum. The distance from the target to the substrate was 3.2 cm for both ambient and vacuum depositions. Resonant wavelengths were chosen based on commercial FTIR spectra of the precursor solution. Strong absorption occurs at 3.45, 5.9, 6.67 μm. The deposition rate was measured only under vacuum conditions and was between 10–20 Å/s for a fluence of 2 J/cm^2 at the wavelengths chosen.

4.3.3 Fourier transform infrared spectroscopy

Optical absorption was measured by Fourier transform infrared spectroscopy (FTIR) in transmission using a Bruker IFS 66 vacuum spectrometer. Samples were

analyzed on 13×1mm NaCl discs. The deposited material was examined directly after deposition, after a soft bake at 80 °C for one hour, and after a full cure 250 °C for two hours. Liquid samples were prepared using a vacuum-tight liquid cell with CaF_2 windows and various Teflon spacers (6–250 μm). Polymeric solutions were examined at concentrations of 15, 10, 5, 1, and 0% PAA in NMP.

4.3.4 Gel permeation chromatography

Further analysis of the mass distribution of the starting and as-deposited PI was carried out using gel-permeation (size-selective) chromatography (GPC). ODA-PMDA poly(amic acid) samples and PEG standards were dissolved in DMF (Sigma, 99.9+%, HPLC Grade) (4 mg/mL) and analyzed using an HP series 1100 chromatograph (Hewlett Packard, Palo Alto, CA) and DMF mobile phase. Three mL of filtered sample solution (0.45 μm PTFE Acrodisc, Waters Corp., Milford, Ma) were injected into a 100 μL Rheodyne sampling loop (Rheodyne, Cotati, CA) and pumped (1 mL/min) through a 7.8 × 300 mm Ultrastyragel® 500 Å column (Waters Corp., Milford, MA), with an effective molecular weight range of 100-10,000 Da. Sequential detection was performed though a miniDAWN triple angle laser light scattering (TALLS) detector (Wyatt Technology, Santa Barbara, CA), a WellChrom K-2300 refractive index detector (Knauer, Berlin, Germany), and an HP series 1050 ultraviolet detector (Hewlett Packard, Palo Alto, CA). Peak average molecular weights (M*p*) were then calculated against a calibration of five PEG standards (Polymer Source, Inc.).

4.3.5 Mass spectrometry

The mass distributions for all samples following deposition were measured using a Mariner ESI-TOF MS (Applied Biosystems, Framingham, MA). Mass spectra were obtained in the positive ion mode with the spray tip, nozzle, skimmer, ion guide, and TOF mass analyzer potentials (along with nozzle temperature – 110 ˚C) optimized to achieve the best signal-to-noise ratio. A curtain of nitrogen drying gas was utilized to assist in the ESI process. All spectra were acquired in the reflectron mode of the TOF mass spectrometer (which has a mass range up to 10,000 Da), and had mass resolutions greater than 2500 full width at half maximum (fwhm) in this mass range. External mass calibration was performed using protein standards from a Sequazyme Peptide Mass Standard Kit (Applied Biosystems) and a three-point calibration method using Angiotensin I (m = 1296.69 Da), ACTH (clip 1-17) (m = 2093.09 Da), and ACTH (clip 18-39) (m = 2465.20 Da). Internal mass calibration was subsequently performed using a polyethylene glycol (PEG) standard (Polymer Source, Inc.) to yield monoisotopic masses exhibiting a mass accuracy better than $\Delta m = \pm 0.1$ Da. The instrument was calibrated before every measurement to ensure constant experimental conditions. ODA-PMDA poly(amic acid) samples were dissolved in *N*,*N*-dimethylformamide (DMF) (Sigma, 99.9+%, HPLC grade) (1 mg/mL) before they could be analyzed neat or doped with 0.1% LiBr (for the positive ion mode). PAA solutions were introduced into the ESI interface by a Cole-Parmer syringe pump at a flow-rate of 500 μL/h.

4.4 Experimental results

4.4.1 Kapton® tape

Although there has been some success with deposition of polymers from neat targets, attempts to deposit polyimide by ablating the neat polymer from Kapton® tape using the resonant 5.9 μm carbonyl stretch were unsuccessful.[7,8] The wavelength of 5.9 μm was chosen since it was the strongest absorption in the FTIR spectrum. The target showed significant amounts of thermal damage and did not transfer even damaged polymer fragments at appreciable rates. For comparison, films of vacuum dried 15% PAA supported on glass slides were prepared. Transfer of the uncured PAA was achieved at approximately half of the fluence of Kapton® tape, and the residual uncured PAA target did not show significant thermal damage. This success prompted us to undertake further examination of the precursor material as opposed to continuing experiments with the Kapton® tape.

4.4.2 Deposition morphology

RIR-LA was first attempted on liquid targets in air. The deposited morphology showed a significant number of droplets, most likely containing large amounts of the solvent NMP. Deposition in vacuum showed a contrasting predominance of string-like configurations, perhaps long polymeric chains. Figure 4.2 a and b clearly illustrate the differences in deposition morphologies; films deposited at ambient pressure look wet and appear similar to a spin-coated or drop-cast film while the vacuum transferred films have the unique appearance of small droplets and long string moieties. In both cases the

amount of material transferred was macroscopic, since the deposited material was readily visible to the naked eye. The target material appeared undamaged for both vacuum and ambient pressures; however, if the beam is allowed to dwell in the same spot for multiple macropulses a plasma is observed and the target material forms chunks of hardened PI. Vacuum transfer eliminates the solvent either by the smaller solvent molecules being removed by the vacuum pump or by a lower sticking coefficient for the solvent molecules on the substrate. NMP has an extremely low vapor pressure, only 0.40 mbar at STP; under the same conditions, water has a vapor pressure of 23 mbar, while methanol has a vapor pressure of 130 mbar. The low vapor pressure implies that surface interactions will play a more pivotal role. One might conclude the NMP is not excited at this wavelength; however, it does transfer under atmospheric pressure. The observed morphologies suggest that it is easier for the PAA to de-complex from the NMP under vacuum, producing the desirable reduced solvent films.

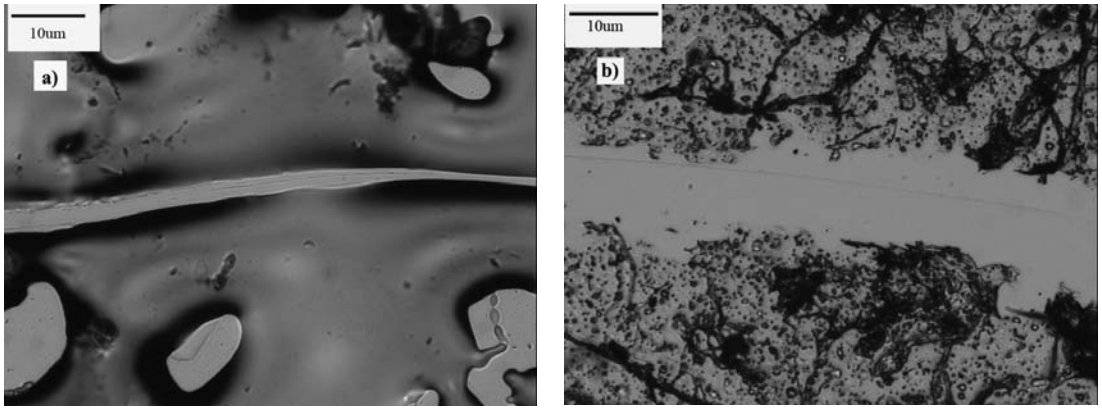

Figure 4.2 a-b: Optical microscope images of the substrate directly after RIR-LA transfer of 15% PAA at 3.45 μm with a fluence of 4 J/cm^2 (**a**) at ambient pressure (**b**) in vacuum ~ 10^{-4} torr

4.4.3 Spectroscopy

Fourier-transform infrared (FTIR) spectroscopy is useful in ascertaining the local electronic structure of the PAA in solution and the pure solvent NMP in the liquid state. The liquid spectra lack some of the resolution of the dried films and are often more ambiguous, showing an increased number of peaks in the fingerprint region, possibly due to water or other impurities. Note the similarities between the PAA spectra and the pure NMP in Fig. 4.3a and b. Since the PAA is dispersed in the NMP, the solvent NMP is responsible for the majority of peaks in the spectra. The peak assignment data for both PAA and NMP are shown in tabular form in Table 4.1. Numerous researchers have previously examined the conversion of PAA to PI. A recent study by Anthamatten and Gies documented the spectral changes during the curing process.[15] While the spectra have not been numerically fit in the same manner as in [15], the general appearance and disappearance of peaks during the imidization process is consistent with previous work. Figure 4a–d shows the as-transferred PAA spectra along with the spectra of the material after undergoing a thermal curing process to transform it into PI. Only the fingerprint region is shown below since it contains the most valuable information. The free OH peak disappears in the RIR-LA transferred material, and the CH and NH stretch peak is very weak (not shown). This is caused by the removal of solvent NMP during the RIR-LA process. The main indication of the conversion to the polyimide is the appearance of the 1375 cm^{-1} imide stretch peak in Fig. 4.4a and b. A secondary indication is the alteration of a broad carbonyl stretch region of 1600–1720 cm^{-1} for the as-transferred PAA, which cleans up to the imide carbonyl stretch at 1724 cm^{-1}. The preservation of the ring structure is shown by the constant 1500 cm^{-1} aromatic ring mode peak present in all four

spectra. The peak assignments are listed in Table 4.2, which shows some variations in the peak locations due to the accuracy of the spectrometer (± 4 cm^{-1}). The enhanced transfer of the 5% PAA may be explained by an increased absorption coefficient due to the cumulative effects of the polymer and solvent absorption.

Table 4.1: FTIR peak assignments for PAA and NMP

Frequency cm^{-1}	Vibrational mode
2924, 2881	C–H stretch
1709	Amic acid C=O stretch
1686	NMP C=O stretch
1661	Amide C=O stretch
1502, 1402	Ring modes
1298	Amide stretch
1294	Ether stretch

Table 4.2: FTIR assignments of RIR-LA PAA

Wavenumber cm^{-1}	Vibrational mode
1724	Imide C=O stretch
1719	Amic acid C=O stretch
1653–4	Amide C=O stretch
1499–1501	Aromatic ring mode
1375–7	Imide stretch
1216, 1238–42	Ether stretch

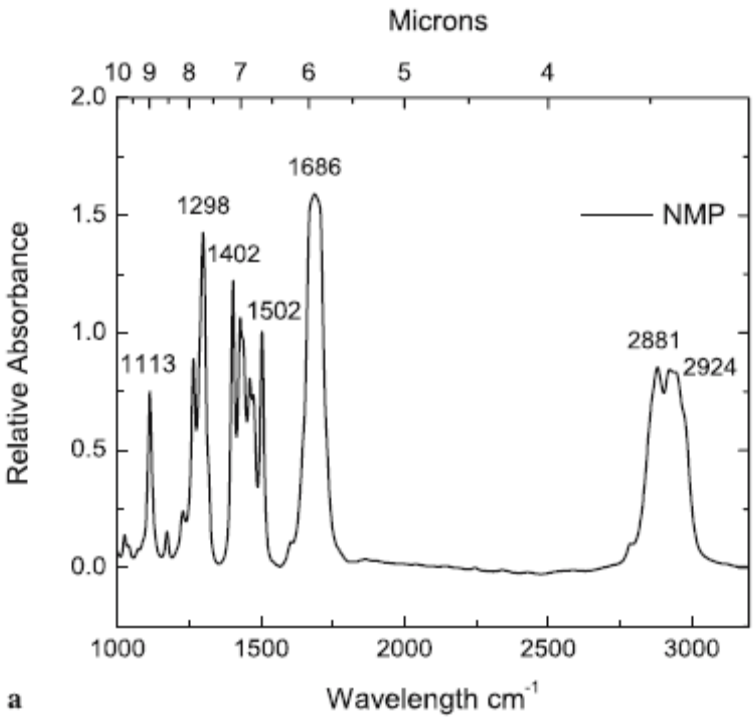

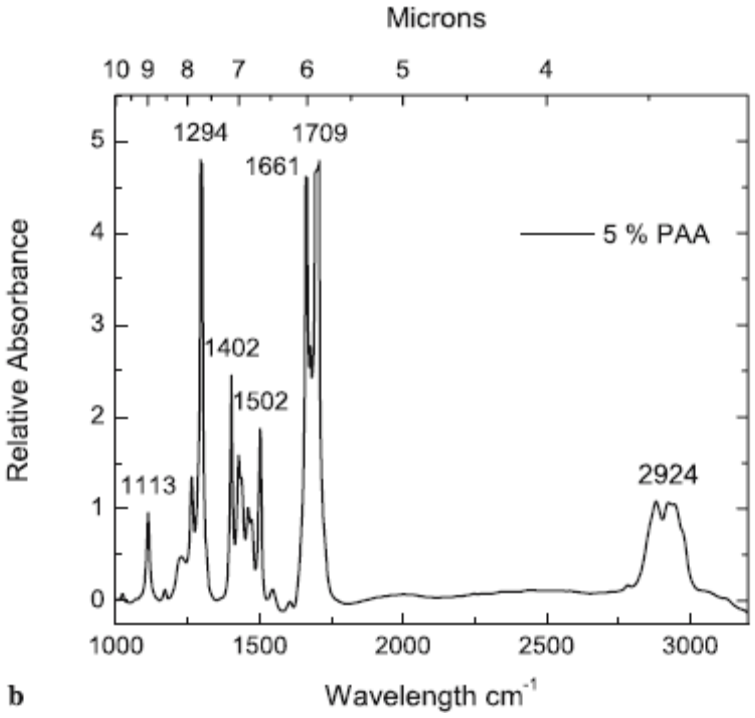

Figure 4.3 a-b: FTIR spectra of a) NMP b) 5% PAA

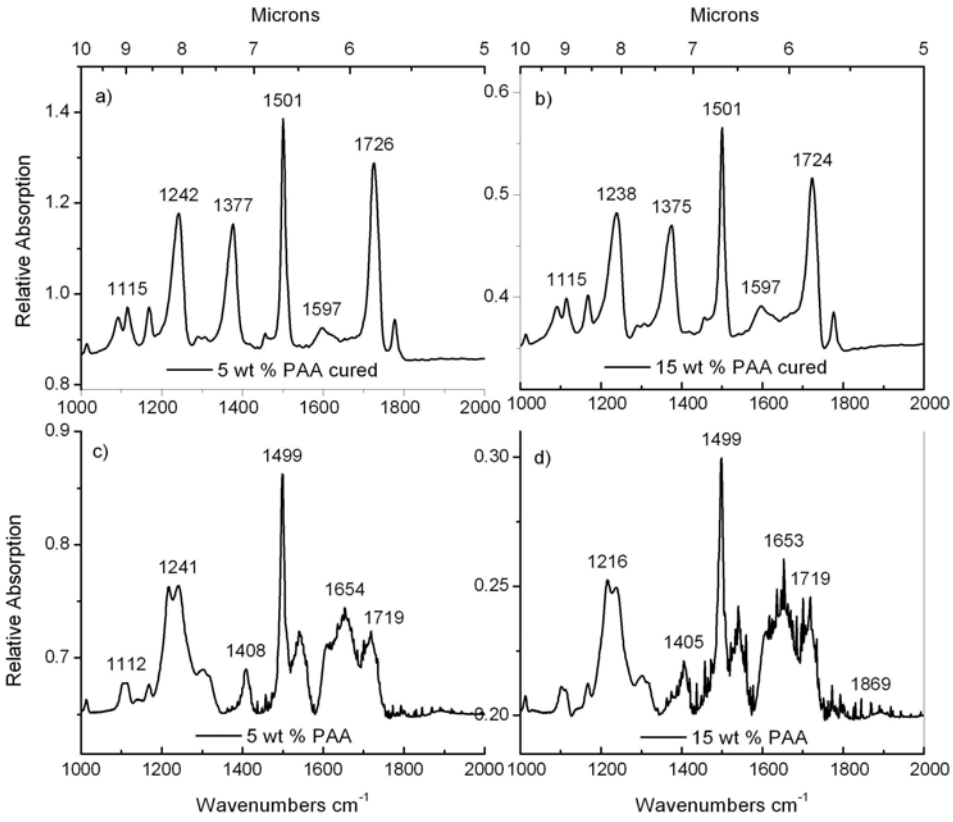

Figure 4.4 a-d: FTIR spectrum of RIR-LA transferred PAA at 3.45 μm and 2 J/cm^2 (**a**) 5wt % PAA after cure (**b**) 15wt.% PAA after cure (**c**) 5wt % PAA (**d**) 15wt % PAA

4.3.4 Mass analysis

Gel permeation chromatography (GPC) was used to ascertain whether or not the polymer chain length was reduced during the laser transfer process. First the starting material, commercially obtained 15%PAA in NMP, was analyzed by the GPC. It showed two major peaks as in Fig. 4.5b. The first, higher molecular-weight peak occurred at an elution time of about six minutes and corresponds to the PAA. The lower molecular-weight peak at eleven minutes corresponds to the solvent NMP along with short-chain

PAA elements complexed with NMP. Analysis of the RIR-LA PAA showed a single high molecular-weight peak centered at six minutes. Coincidence of the first PAA peak demonstrates that RIR-LA is transferring the complete polymer chain. The disappearance of the second peak indicates that the solvent NMP has been removed by the laser transfer process. Using PEG as a standard with the DMF, we have estimated the molecular weight of the polymer. The RIR-LA peak in Fig. 4.5a is centered at six minutes, which corresponds to a molecular weight of 8340 Da. The diluted precursor PAA had an approximate molecular weight of 5360 Da, a difference of 2980 Da. The RIR-LA process appears to have narrowed the molecular weight distribution, retaining the higher molecular weight polymer chains. The commercially obtained PAA showed notable trimming with the increased concentration of DMF. The alteration in distribution is hypothesized to be caused by the addition of another polar aprotic solvent allowing for increased chain extension. This phenomenon could also be contributing to the improved distribution of the laser-deposited material; however, the removal of the lower molecular weight peak shown by the UV/Vis indicates that more than one narrowing mechanism is at work. Difficulties in data interpretation arise due to the disparity in detector response for the RIR-LA vis à vis the as-purchased PAA. This could lead to errors in correctly estimating the distribution of molecular weights. By improving the RIR-LA transfer, these experiments can be repeated with nearly identical concentrations to eliminate any ambiguities. If similar results occur for other polymers and especially those of higher molecular weights, RIR-LA could become an effective way to remove lower molecular-weight moieties and increase the polydispersity index.

The electrospray mass spectrometry data further illuminates the changes in structure. The two spectra show the same two main peaks, but differ in the noise-level of the baseline. The RIR-LA material shows a higher noise level due to a low concentration of material. The mass spectrometry data support the conclusion that the material is unchanged through the RIR-LA process. The major peaks correspond for both the control (as-purchased) 15% PAA sample and the 15% PAA RIR-LA material as seen in Fig. 4.6a and b. The structural assignments are shown in Table 4.3, which illustrates the most common fragmentation patterns of PAA. The PAA1 structure in Table 4.3 is present in both the as-purchased and RIR-LA 15% PAA, while the PAA2 structure is found only in the as-purchased material. The disappearance of the PAA2 fragment in the RIR-LA PAA could potentially indicate that there are a reduced number of fragmentation pathways available due to the removal of the NMP. The current level of noise in the RIR-LA PAA data prevents concrete conclusions. There is also another higher molecular weight section corresponding to 6000–8000 Da (region not shown), illustrating that there are some higher molecular weight species present.

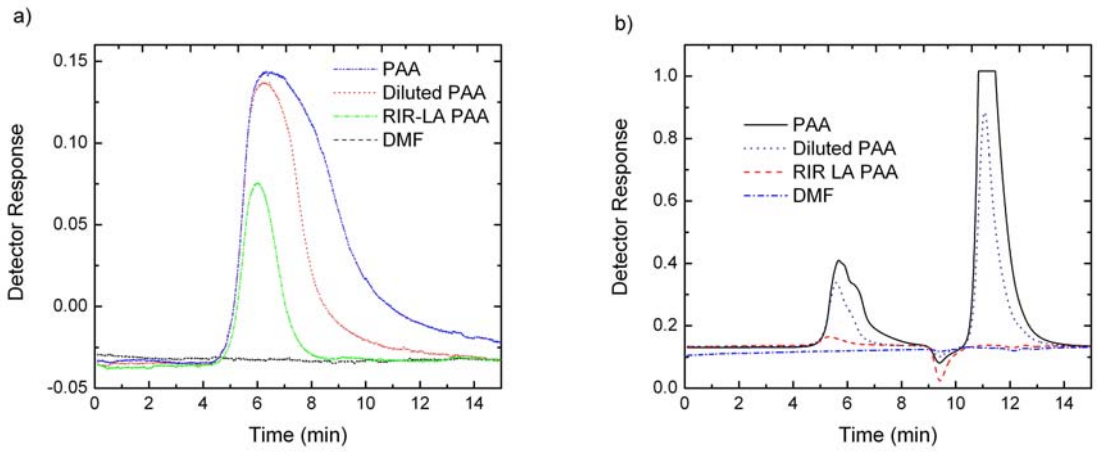

Figure 4.5a-b: GPC results (a) Refractive index detector shows the major PAA peak (b) UV/Vis detector illustrates the PAA peak along with the secondary NMP peak present in the starting material.

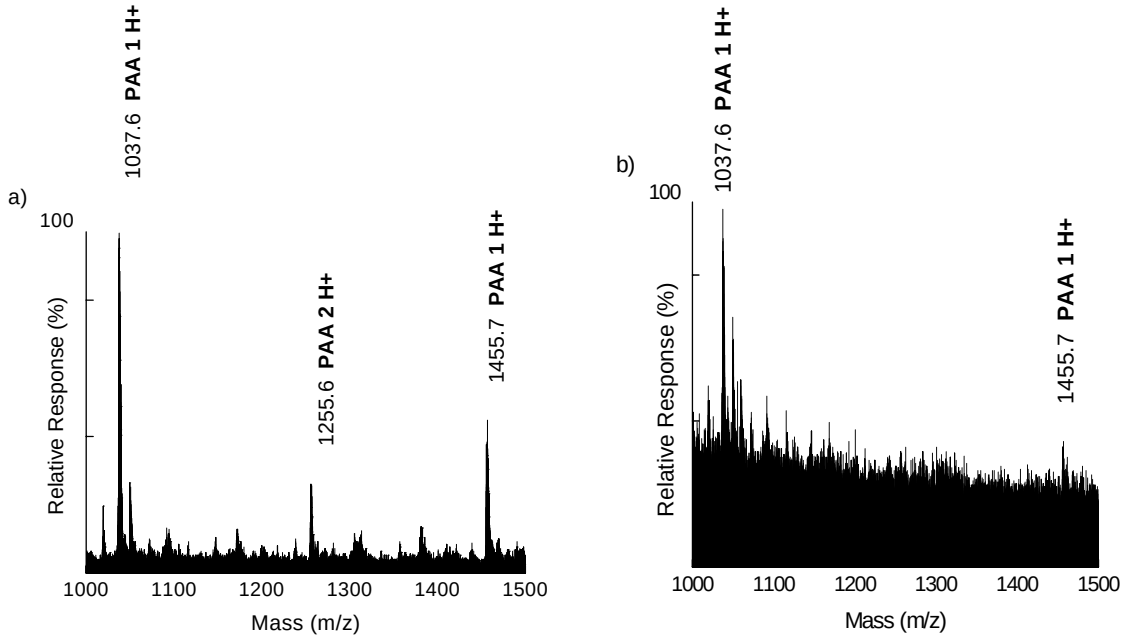

Figure 4.6 a-b : Mass Spectra (a) 15 % PAA (Sigma-Aldrich) (b) RIR-LA transferred 15 % PAA at 3.45 μm 2 J/cm^2

Table 4.3: Structural assignments of ESI data in Figure 4.6 a-b

Species	Structure (M)	$(M+H)^+$ Da
PAA 1	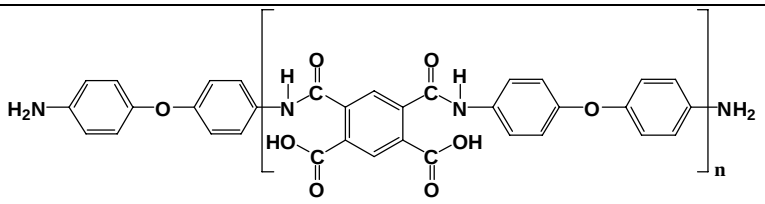	**619.4** (n = 1) **1037.8** (n = 2) **1455.9** (n = 3) **1875.2** (n = 4) **2294.4** (n = 5)
PAA 2	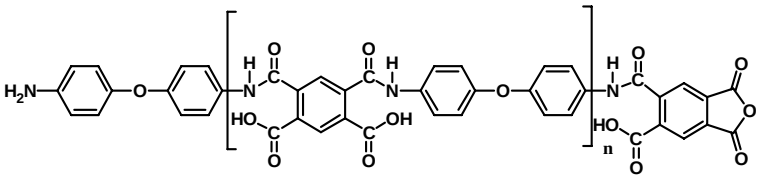	**419.4** (n = 1) **837.4** (n = 2) **1255.9** (n = 3) **1674.9** (n = 4) **2093.8** (n = 5)

4.5 Conclusions

RIR-LA is not the first reduced solvent technique for depositing PAA. Vapor deposition polymerization (VDP) of PIs was spearheaded by Salem in 1986.[16] Numerous others followed suit in the study and manufacture of polymer films by VDP.[17-20] VDP PI tends to be of lower molecular weight than its solution-cast counterparts.[19] The lower molecular weight is an effect of the limited mobility of the monomer units impinging upon the substrate. The solvent NMP, as previously discussed, plays an important role in the chain extension process of building a high molecular-weight polymer. In a recent paper Anthamatten et al. have shown the properties of polybenzoxale films deposited by VDP to be superior to traditional solution cast films.[21] However, VDP is still limited to monomers that have appreciable vapor pressures, in order to attain reasonable deposition rates. RIR-LA offers a potentially complementary thin film deposition technique, which

is not prone to give lower molecular weight polymers and is not limited by the vapor pressure of the monomers. While numerous applications require large areas of PI which are made as solution-cast films, RIR-LA has the potential to make well controlled films in applications where liquid-phase processing is detrimental. Previous studies have suggested that RIR-LA is a gentle process that is able to transfer sizable polymers with intact overall structure.[3] The ablative process transfers visible amounts of material, a snowstorm of polymeric strings under vacuum conditions and a light rain of solvent droplets and polymeric material under ambient pressure. The present study, in which the transferred PAA functions as a molecular thermometer, further implies that RIR-LA is a low-temperature process. The process does not limit the molecular weight as VDP does, although additional experiments will be required to ascertain whether there is an upper limit of the molecular-weight of transferred polymers. The deposited films undergo the imidization process just as if the film had been spin coated or vapor deposited. The process produces the desired result of a film without excess solvent present and is compatible with other vacuum deposition processes common in today's electronics industry. The mechanism of the process is not yet fully understood; however the examination of the FTIR spectra clearly indicates that the solvent plays a critical role. Future experiments will reveal whether other properties such as mechanical strength and permeability are preserved though the ablation process. The preservation of the molecular weight implies that the mechanical properties may be retained as well.

4.6 Acknowledgements

These experiments were partially supported by the Naval Research Laboratory (N00173-05-P-0059); the free-electron laser is supported by the Medical FEL Program of the Department of Defense (F49620-01-1-0429). NLD was supported by a National Science Foundation IGERT fellowship (DMR-0333392). NLD thanks Mr. Stephen Johnson (Vanderbilt University) for many helpful discussions.

4.7 References

1 R. Srinivasan, R. R. Hall, W. D. Loehle, W. D. Wilson, and D. C. Albee, J. Appl. Phys. **78,** 4881 (1995).

2 H. M. Mashuhara, Tomokazu; Takuji Tada, Eiji Nomura, Koji Hatanaka, Hiroshi Fukumura, J. Phys. Chem. A **106,** 2180 (2002).

3 D. M. Bubb, J. S. Horwitz, J. H. Callahan, R. A. McGill, E. J. Houser, D. B. Chrisey, M. R. Papantonakis, R. F. Haglund, M. C. Galicia, and A. Vertes, J. Vac. Sci. Technol. A **19,** 2698 (2001).

4 D. M. Bubb, M. R. Papantonakis, B. Toftmann, J. S. Horwitz, R. A. McGill, D. B. Chrisey, and R. F. Haglund, J. Appl. Phys. **91,** 9809 (2002).

5 D. M. Bubb and R. F. J. Haglund, in *Pulsed Laser Deposition of Thin Films: Applications-Led Growth of Functional Materials*, edited by R. Eason (John Wiley and Sons, New York, 2006), p. 35.

6 M. R. Papantonakis and R. F. Haglund, Jr., Appl. Phys. A **79,** 1687-94 (2004).

7 N. L. Dygert, K. E. Schriver, and R. F. Haglund, Jr., Proc. SPIE **6107,** 212 (2006).

8 N. L. Dygert, K. E. Schriver, and R. F. Haglund, Jr, J. of Physics Conference Series **59,** 651 (2007).

9 Y. Xu, M. Zhan, and K. Wang, J. Polym. Sci. B **42,** 2490 (2004).

10 M. J. Brekner and C. Feger, J. of Poly. Sci A **25,** 2005 (1987).

[11] M. M. Koton, V. V. Kudryatsev, N. A. Adrova, K. K. Kalnin'sh, A. M. Dubnova, and V. M. Svetlichnyi, Polymer Science (USSR) **16,** 2411 (1973).

[12] X. Xu, P. P. Madeira, and E. A. Macedo, Chemical Engineering Science **59,** 1153 (2004).

[13] G. S. Edwards, D. Evertson, W. Gabella, R. Grant, T. L. King, J. Kozub, M. Mendenhall, J. Shen, R. Shores, S. Storms, and R. H. Traeger, IEEE J. Sel. Top. Quantum Electron. **2,** 810 (1996).

[14] G. S. Edwards, S. J. Allen, R. F. Haglund, R. J. Nemanich, B. Redlich, J. D. Simon, and W. C. Yang, Photochemistry And Photobiology **81,** 711 (2005).

[15] M. Anthamatten, S. A. Letts, K. Day, R. C. Cook, A. P. Gies, T. P. Hamilton, and W. K. Nonidez, J. Poly Sci A **42,** 5999 (2004).

[16] J. R. Salem, F. O. Sequeda, J. Duran, W. Y. Lee, and R. M. Yang, J. Vac. Sci. Technol. A **4,** 369 (1986).

[17] M. Iijima, Y. Takahashi, Y. Oishi, M. A. Kakimoto, and Y. Imai, J. Poly. Sci. A **29,** 1717 (1991).

[18] M. Grunze and R. N. Lamb, J. Vac. Sci. Technol. A **5,** 1685 (1987).

[19] R. N. Lamb, J. Baxter, M. Grunze, C. W. Kong, and W. N. Unertl, Langmuir **4,** 249 (1988).

[20] T. Strunskus, M. Grunze, and S. Gnanarajan, ACS Symposium Series **440,** 353 (1990).

[21] X. C. Chen, M. Anthamatten, and D. R. Harding, Macromolecules **39,** 7561 (2006).

CHAPTER V

RESONANT INFRARED LASER ABLATION AND PROFILOMETRY OF POLYAMIDE IMIDE AND POLYETHER IMIDE

Nicole L. Dygert[1], Theo J. Dingemans[2], Richard F. Haglund, Jr.[3,4]

1- Department of Interdisciplinary Materials Science,

Vanderbilt University Nashville, TN 37235

2- Aerospace Engineering, Delft University of Technology, Kluyverweg 1,

2629 HS Delft, The Netherlands

3- Department of Physics and Astronomy

4- W. M. Keck Foundation Free Electron Laser Center

Vanderbilt University, Nashville, TN 37235

5.1 Overview

Prior research has shown the possibility of transferring both thermoplastic and thermoset polymers by resonant infrared laser ablation (RIR-LA). In this paper the technique is expanded to include two high performance thermoplastic polymers polyamide imide (PAI) and polyether imide (PEI). The PAI partially cures at temperatures of 150 °C; this property was used to further investigate the temperature profile of the ablation plume. PAI was obtained in a precipitated powder form which allowed for examination of the RIR-LA process with different matrix solvents as well as a solid target. The PEIs are a homologous series of polymers, where the diamine monomer unit is increased by one ether linkage and one benzene ring from 2 rings in the P0 monomer up to 5 rings in the P3 monomer. The PEI series looked at the effects of the increasing diamine chain length on the RIR-LA process. Fourier transform infrared spectroscopy (FTIR) was used to determine if the RIR-LA process altered the chemical structure of the PAI or PEI. The roughness of the RIR-LA films was characterized by profilometry, while their physical appearance was examined by optical microscopy.

The RIR-LA films deposited from the solid PAI target showed markedly different behavior. The FTIR indicated that the solid PAI film had undergone a thermal transformation, while the matrix based targets showed no indications of a thermal transformation. The results indicate the importance of the matrix solvent in protecting the polymer from thermal damage. The solid PAI produced smooth, thick films for polymer resonant wavelengths, but produced rough, thin films for a non-resonant wavelength. The whole PEI series was transferred without chemical alterations by RIR-LA. The lower the chain lengths of polymer produced smoother films; however the

lower chain lengths also gave thinner films. The PEI illustrated the trade off between thick films and lower roughness. In order to produce the best PEI RIR-LA film a diamine monomer with a moderate chain length should be chosen (P1 or P2).

5.2 Introduction

Thin polymeric films find use in numerous consumer products, such as laptops, cell phones, and scratch resistant coatings to name only a few. Within the large class of high-performance polymers, polyamide imides (PAI) and polyether imides (PEI) find a myriad of uses due to their excellent properties including: high thermal stability, good mechanical properties, and low coefficients of thermal expansion.[1] PAI and PEI offer many of the same properties as polyimide; however they are both melt processable unlike polyimides. For PEI there is a research effort to make liquid crystalline PEI for use in displays.[2-5] PAI has sparked interest as a fluorescent polymer with the addition of fluorine groups.[6,7] By using a Mark III free-electron laser, we were able to investigate the transfer of PAI and PEI at several different infrared resonant wavelengths.

5.2.1 Polyamide imide

Polyamide imides (PAI) offer a positive synergy of properties from both the rugged polyimide group and the more flexible polyamide group. PAIs are not considered as a classic thermosetting polymer since the embedding of some amide groups allows for solubility even after curing. The best known industrial version of PAI is Torlon® manufactured by Solvay Advanced Polymers. By retaining their solubility PAIs may be processed by a number of methods that will not work with polyimides. For example they

may be formed by injection or compression molding and other melt processing techniques. The PAIs do sacrifice a small degree of thermo-oxidative stability allowing for use from cryogenic to around 275 °C. Polyamide imides are most commonly synthesized by combining a trimellitic anhydride and an aromatic diamine.[8] A cure step may be completed before or after forming to the desired shape. The cure temperatures required for PAI are considerably lower than those for polyimides due to the greater chain mobility made possible by the retention of the amide links. Cure temperatures for polyimides are at least 250 °C, while for PAI 150 °C is usually sufficient. The PAI may be precipitated into a powder after curing the polymer melt solution. We worked with a powder of trimellitic anhydride chloride co-4,4'-methylenedianiline that was 50 percent imidized; the structure is shown in figure 5.1.

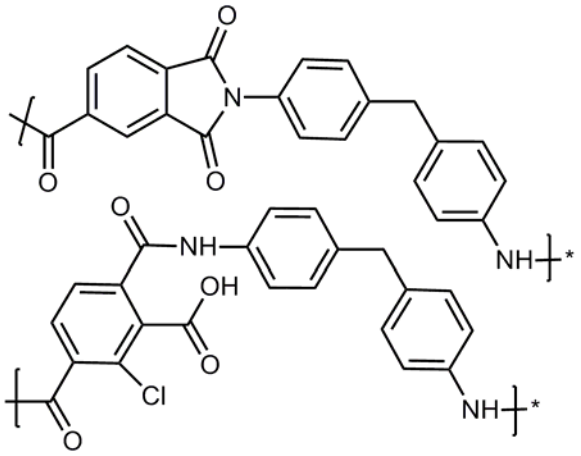

PAI 50% imidized 50% non-imidized

Figure 5.1: Structure of PAI

5.2.2 Polyether imide

Polyether imides are considered a high temperature thermoplastic. PEI offers high tensile strength, flame resistance, low smoke emission, and excellent hydrolytic stability. It may be exposed continuously to temperatures up to 180 °C. The hydrolytic stability is what sets it apart from its PI and PAI counterparts. Both PI and PAI readily absorb water at elevated temperatures even after curing. PEIs made its debut as Ultem® manufactured by General Electric in the early 1970's. PEIs are transparent amber in color (like classic polyimides) due to the interaction between the electron rich diamine and the electron poor dianhydride. The combination of the diamine monomer, P3, shown below in figure 5.2 and 3,3',4,4'-biphenyltetracarboxylic acid dianhydride (BPDA) creates a PEI that can form a liquid crystalline structure.[4] PEI can also give high refractive indices useful for optical coatings.[2] The homologous series of PEIs shown below in figure 5.2 are synthesized by the reaction of a diamine and a dianhydride. The diamines are named P0-P3 and they increase in molecular weight by one aromatic ring and one ether linkage from two rings for P0 up to five rings for P3.

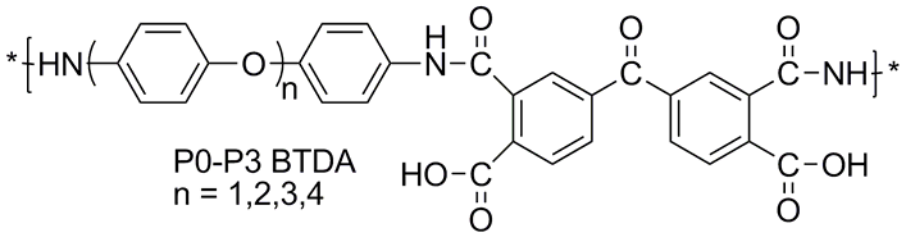

Figure 5.2: Structure of P0-P3-BTDA PEIs

5.2.3 Laser processing

We have previously demonstrated successful thin-film synthesis of numerous thermoplastic polymers by resonant infrared laser ablation (RIR-LA) of neat polymer targets.[9-13] In these experiments, the absence of photofragmentation or other degradation of the polymer films suggested that the RIR-LA process was inherently a low-temperature one. In prior work we examined the evolution of the ambient ablation plume of a polyimide precursor through the use of shadowgraphy and conducted some initial vacuum film depositions of polyimide.[13-16] The present work expands the RIR-LA technique to interesting related polyimides the PAIs and PEIs.

5.3 Experimental Methods

5.3.1 Materials

The PAI was obtained from Sigma-Aldrich in powdered, half imidized form of poly(trimellitic anhydride chloride-*co*-4,4'-methylenedianiline). The first two diamine monomers P0 and P1 were purchased commercially, P0 is 4,4'-oxidianiline from Sigma-Aldrich and P1 is 1,4-bis(4-aminophenoxy)benzene from the Chriskev Co. Inc. The dianhydride, benzophenone-3,3′,4,4′-tetracarboxylic dianhydride (BTDA), was also procured from Sigma-Aldrich. For the solvents, N-methyl-2-pyrrolidinone (NMP) was purchased from Sigma-Aldrich while dimethyl formamide (DMF) was purchased from Fischer Scientific. All commercially purchased chemicals were used without further purification. The P2, bis[4-(4-aminophenoxy)phenyl] ether, and P3, 1,4-bis[4-4-

aminophenoxy)phenoxy]benzene, diamines were synthesized by N. Dygert under the direction of T. Dingemans (for synthesis information see Dingemans in reference [4]).

5.3.2 Free electron laser and ablation chamber

The ablation laser used in our experiments is an rf-linac driven free-electron laser (FEL), wavelength tunable from 2 to 10 μm (additional information in chapter 4 experimental section). The optical bandwidth of the pulses is typically 1% of the center frequency (FWHM); the typical micropulse energy is several μJ, yielding a peak irradiance of order 10^9 W/cm^2. The total energy deposited is that of the macropulse; hence, the fluence for the experiments reported here is that of the macropulse. For vacuum RIR-LA experiments, the FEL was focused by a 50 cm focal length BaF_2 lens; the entrance window to the chamber also had a BaF_2 window. The chamber is evacuated using a turbo-molecular pumping system. The beam moved across the target surface with a linear speed of 1 mm/s, and was rotated at a frequency of less than one Hz, to maintain an even track across the target surface. The distance from the target to the substrate was 3.2 cm for the vacuum depositions. Targets consisted of frozen liquid polymeric precursor solutions and compressed solid pellet targets.

5.3.3 Characterization

Optical absorption was measured by transmission Fourier transform infrared spectroscopy (FTIR) using a Bruker IFS 66 vacuum spectrometer. Samples were analyzed on 13×1mm NaCl discs. A profilometer (Deetak 150, Veeco Instruments, Plainview, NY) was used to measure the roughness parameters of the IR laser transferred

films. A scan length of 3000 μm was used with a time of 10 seconds and a stylus force of 8 mg. Three runs were averaged for each measurement. Data recorded included the average roughness (R_a see eq. 5.1), the root mean square roughness (R_q see eq. 5.2), and the delta average step height (ASH).[17] The RMS roughness is considered the standard when measuring a film's optical quality and the delta average step height is used to find step height when a high amount of roughness or noise is present. Some of the samples measured were deposited with a shadow mask so that there was a spacing of 1 μm between the deposited material and the void area.

$$R_a = \frac{1}{L}\int_{x=0}^{x=L} |y| dx \qquad (5.1)$$

L is the assessment length (scan length) and the y axis is the variation in roughness

$$R_q = \sqrt{\frac{1}{L}\int_0^L y^2(x)dx} \qquad (5.2)$$

corresponding parameter to R_a, root mean square roughness

5.4 Discussion and results

5.4.1 Excitation modes

The FEL has a broad bandwidth especially at the longer wavelengths, which means that nearby resonant modes may be excited as well as the target modes. It can also mean that some of the energy is lost by going into modes that are not resonant with the target. Figure 5.3a-b shows the spectra of PAI and the two pure solvents NMP and DMF along with the FEL modes used. The absorption units of each spectrum have been scaled to one. Figure 5.3a shows how the 6.0 μm FEL mode excites not only the polymer PAI

carbonyl mode stretch mode, but also the carbonyl stretch modes of both solvents NMP and DMF. Often the polymer and solvent have overlapping modes since like dissolves like. The 6.67 μm FEL mode overlaps some of the aromatic ring mode and the C-C stretch modes of the solvents. The shortest wavelength used, 3.45 μm, is contained within the broad C-H stretch peak (see figure 5.3 b). The C-H stretch is only resonant with the solvent. The FEL peak exceeds the effective absorption of the C-H stretch mode, thus the FEL saturates this mode. The PAI spectrum shows a small absorption due to residual NMP contained within the film. Prior to drying imide type polymer films retain some solvent because the solvent is hydrogen bonded to the molecule.[18,19] There is a large difference in the lineshape of the FEL pulse at long and short wavelengths. At the shorter wavelengths the pulse is a single narrow peak, while at the longer wavelengths it is comprised of many smaller peaks.

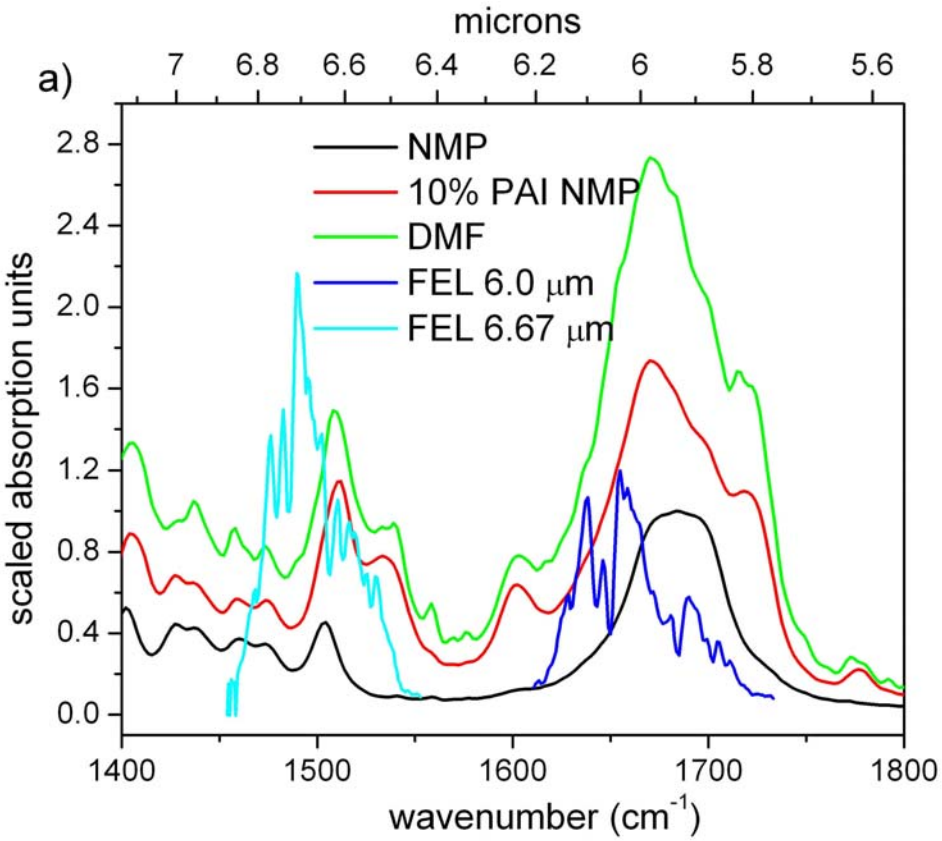
a)
microns
7
6.8
6.6
6.4
6.2
6
5.8
5.6
NMP
10% PAI NMP
DMF
FEL 6.0 μm
FEL 6.67 μm
scaled absorption units
2.8
2.4
2.0
1.6
1.2
0.8
0.4
0.0
1400
1500
1600
1700
1800
wavenumber (cm-1)

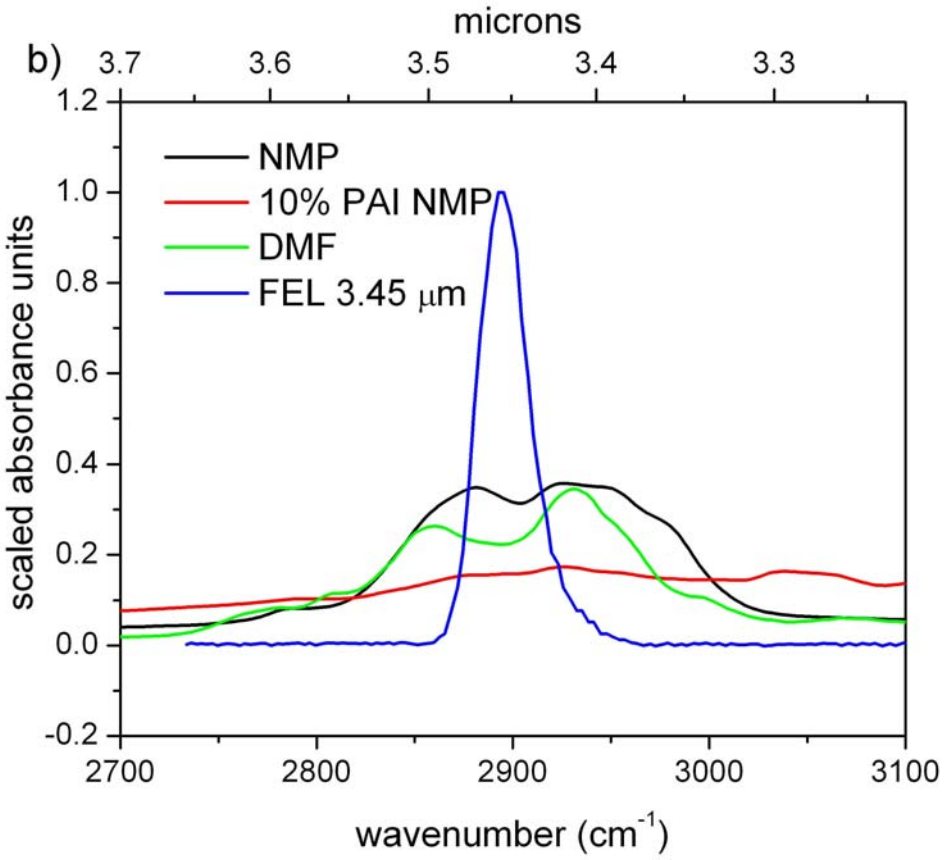

Figure 5.3 a-b: a) FTIR spectra of 10% PAI in NMP and pure solvents DMF and NMP with overlaid FEL wavelengths 6.0 and 6.67 μm b) FTIR spectra of 10% PAI in NMP, pure DMF and NMP, and FEL wavelength 3.45 μm

5.4.2 FTIR behavior of PAI

We investigated the curing behavior of the spincast polymer films to determine if the RIR-LA process causes the polymer to cure in the ablation plume. For PAI, which is already partially imidized, we spincoated a 10% PAI in NMP solution onto a salt plate, allowed the film to dry at room temperature for one day, and then took a transmission FTIR spectrum. Next the film was dried at 70 °C for one hour, followed by an additional two hours at 150 °C causing the film to increase its imidized portion by approximately 25%. The percentage was calculated from the ratio of amide to imide mode absorbance

for the cured versus uncured films. As shown in figure 5.4a the cured spectra shows a 25% increase in both the imide carbonyl stretch and the C-N imide stretch peaks (1720 and 1375 cm^{-1}). Figure 5.4 b-d shows RIR-LA PAI films transferred at various wavelengths. Both of the films made from the solution based targets show spectra similar to the uncured spincast PAI control spectrum. Thus the RIR-LA process prevents the PAI from reaching or sustaining temperatures near 150 °C. In contrast, the film from the solid target shows changes associated with imidization. Figure 5.5 shows the visible damage to the PAI solid pellet target; the inner band of the target where the beam was rastered over the surface is discolored. The results of these experiments illustrate the importance of the solvent in protecting the polymer from the high heat generated by the laser. The resonant infrared wavelength used for the transfer had no apparent effect on the spectra of film for both solid and matrix based targets. The spectra of the previously ablated matrix target solutions were also examined and there were no visible change in the spectra even after multiple uses of the same matrix target solution.

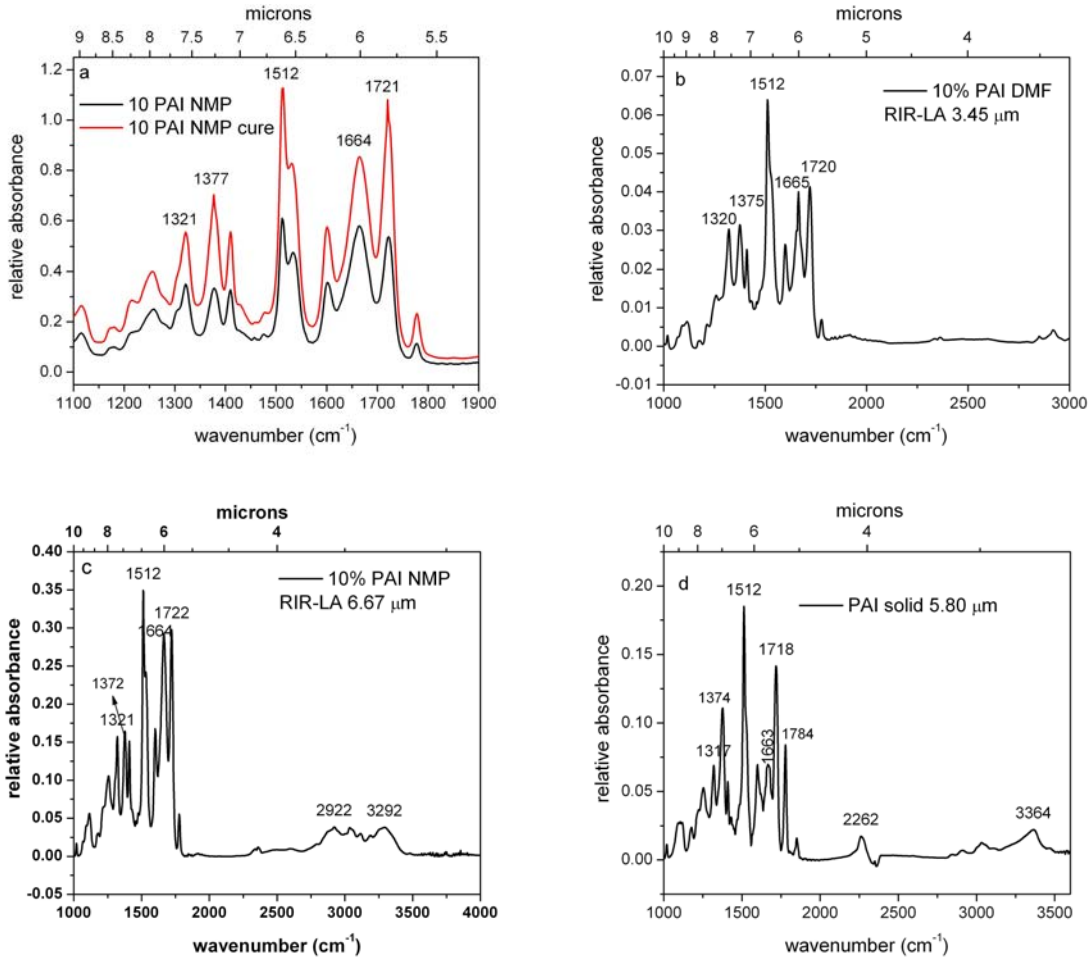

Figure 5.4 a-d: FTIR spectra of a) 10% PAI in NMP spincoated (black line) and cured (red line) b) RIR-LA 10% PAI in DMF at 3.45 μm c) RIR-LA 10% PAI in NMP at 6.67 μm d) RIR-LA from solid PAI at 5.80 μm

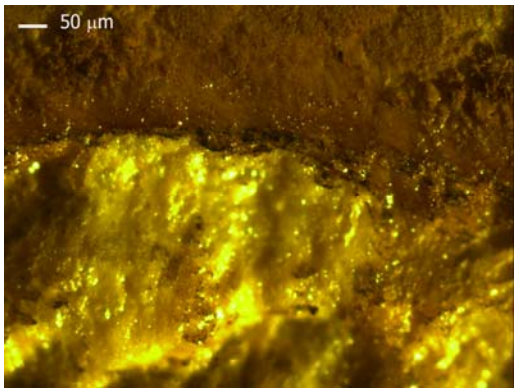

Figure 5.5: Solid PAI target after RIR-LA

5.4.3 FTIR behavior of PEI series

PEI films were spincoated onto salt plates from 10 wt% P0-3 BTDA in NMP solution, the films were allowed to dry for one day at ambient temperatures, and then the initial control spectra were recorded (see figure 5.6). The PEI requires higher cure temperatures than the PAI; the PEI films were cured at 50 °C for one hour, 100 °C for one hour, and then 250 °C for two hours. To allow for clarity in reading the spectra only the comparison of cured versus uncured P3-BTDA is shown, the other solutions gave similar spectra, see figure 5.7 a. The P3-BTDA does not show a clear imide stretch after curing; however the transformation from a broad carbonyl stretch (1600-1700 cm^{-1}) to a narrower imide carbonyl stretch (1720 cm^{-1}) is clear. The other two main peaks shown are the aromatic ring mode at 1487 cm^{-1} and the ether stretch at 1209 cm^{-1}, these two modes are not altered by the curing process. RIR-LA PEI films showed no apparent signs of a curing transformation and the RIR-LA PEI spectra compare well with the control PEI films spectra (see figure 5.7 b-d).

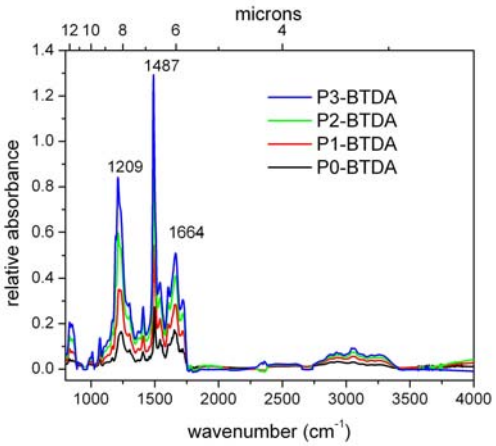

Figure 5.6: FTIR spectra of the PEI series 10% P0-3 BTDA in NMP spincoated onto salt plates

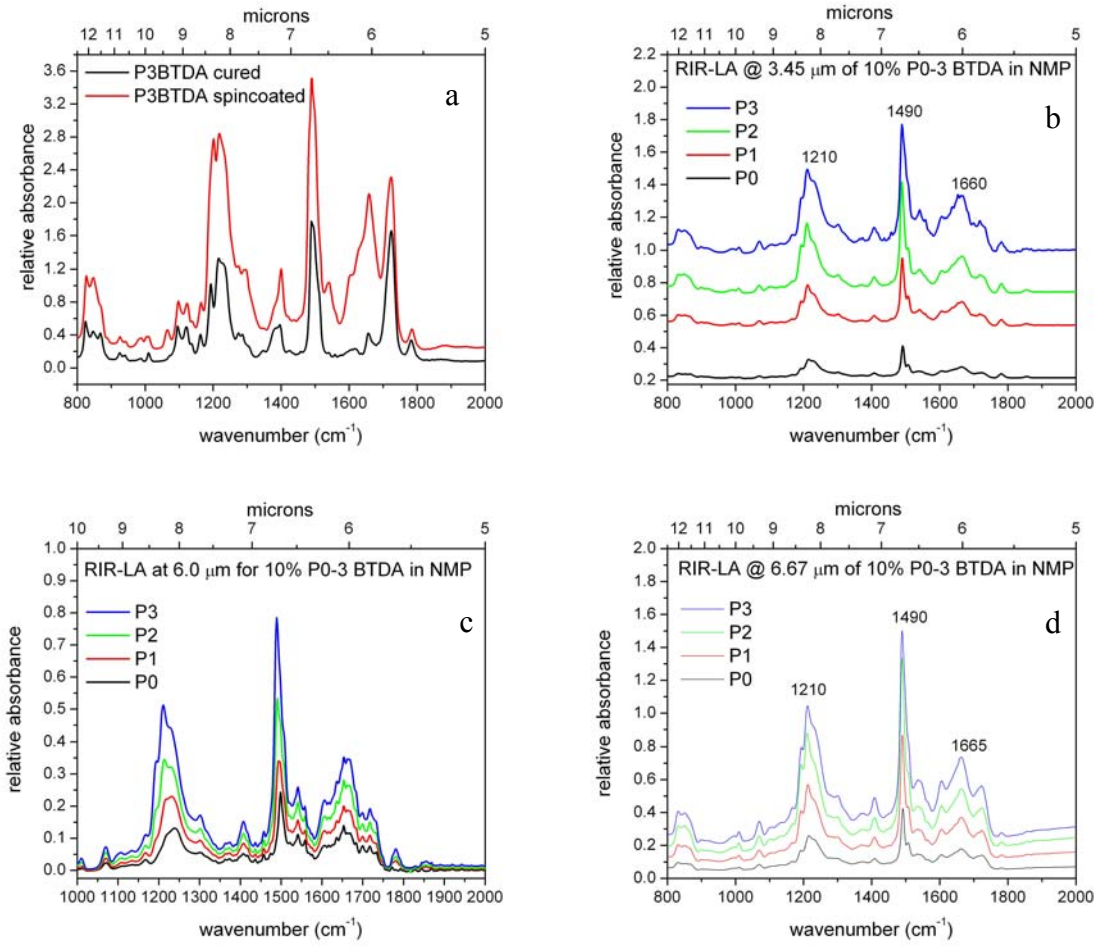

Figure 5.7 a-d: FTIR spectra of a) comparison of spincoated 10% P3BTDA film to one that has been cured b) 10% P0-3 BTDA in NMP RIR-LA at 3.45μm c) 10% P0-3BTDA in NMP RIR-LA at 6.0 μm d) 10% P0-3 BTDA in NMP RIR-LA at 6.67 μm

5.4.4 Characterization of PAI RIR-LA films

PAI films deposited by RIR-LA had lower roughness values compared to prior roughness measurements made on RIR-LA polyimide, PMDA-ODA.[20] Profilometry data for RIR-LA films from various concentrations of PAI in NMP as well as a solid target of PAI are shown in Figure 5.9 a-b. The RIR-LA films from a solid PAI target had markedly different properties depending on the deposition wavelength used. The 3.45

μm wavelength is not resonant with the polymer and for a solid target of PAI it produced a thin, rough film. At 6.67 μm, a polymer resonant wavelength, the solid PAI target produced the thickest and smoothest film. Films from solid targets are significantly smoother since there is no evaporative shrinkage to disrupt the deposition; however, the solid polymer films also show undesirable signs of chemical transformations such as curing. In general increasing the concentration of the PAI gave increased film thickness with increased roughness values. Encouragingly the thickness seems to increase more rapidly than the rms roughness. Figure 5.8 shows the variation of the profilometry data with a constant PAI concentration while changing the ablation laser energy used; as we expected higher laser energies produced thicker, rougher films. The optical micrographs shown below in figure 5.10 a-b show the difference in coloration and coverage between a solvent based RIR-LA film in 5.10a and a solid target film in 5.10b. The solid target has better substrate coverage and a darker amber color associated with the cured polymer, the black spots indicate some carbonization may be taking place as well.

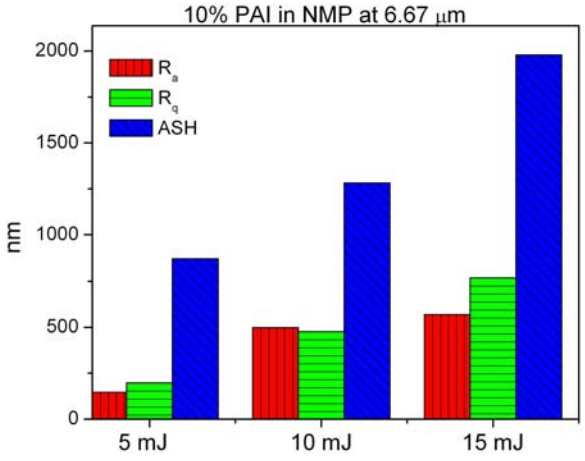

Figure 5.8: Profilometry data for RIR-LA 10% PAI NMP at 6.67 μm, deposition time of 10 minutes for three different energies (5, 10, 15 mJ)

a

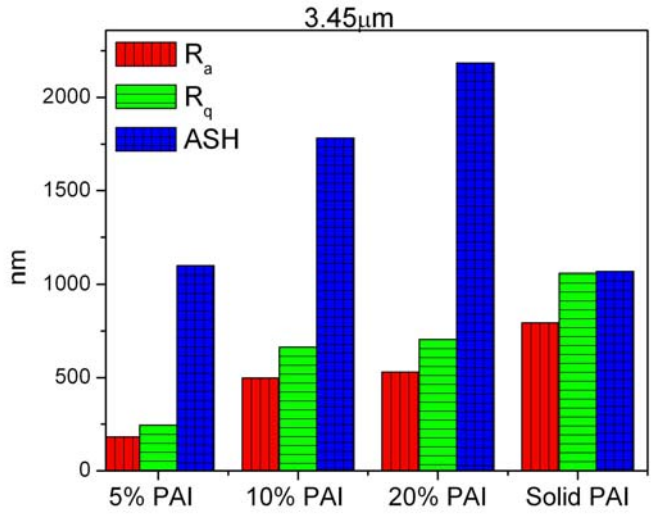

b

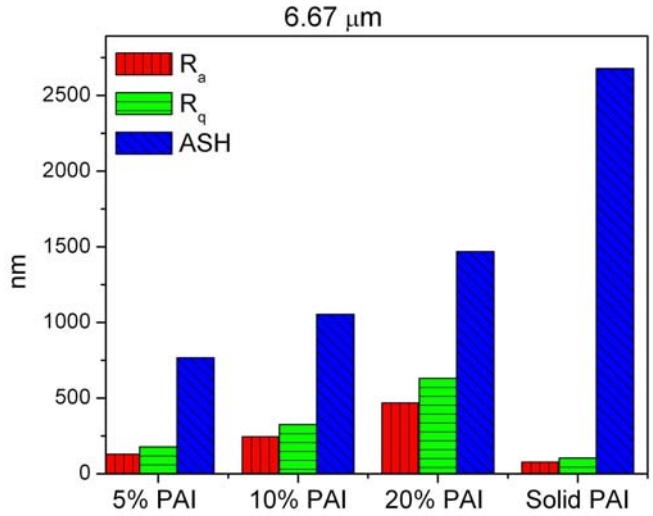

Figure 5.9 a-b: Profilometry data of varying concentrations of PAI in solution and solid PAI targets deposited at RIR-LA wavelength of a) 3.45 μm b) 6.67 μm with a beam energy of 10 mJ and a deposition time of 10 minutes

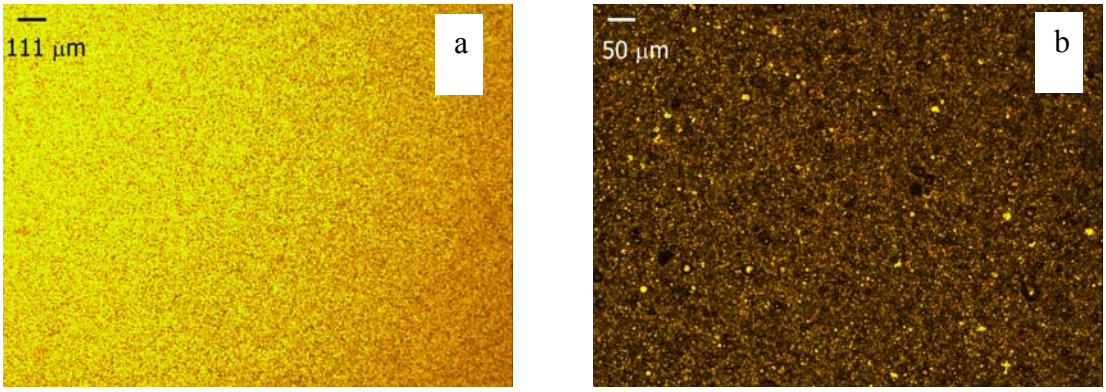

Figure 5.10 a-b: Optical micrographs of RIR-LA films taken with 10 mJ beam energy and deposition times of 10 minutes a) 5% PAI in NMP at 5.80 µm b) Solid PAI at 6.0µm

5.4.5 Characterization of RIR-LA PEI

Measurements of the PEI series revealed that the smaller the polymer the easier it is to deposit relatively smooth films. The RMS roughness and ASH increased for increasing diamine monomer chain length in a fairly linear fashion (see figure 5.12). Optical micrographs of the PEI series RIR-LA films deposited at 6.0 µm are shown in figures 5.11 a-d. The P0-BTDA film is barely discernable from the background, the film may be smooth but the coverage is not adequate. The P2 and P3-BTDA films appear to have good substrate coverage, but they also have a rough, textured appearance.

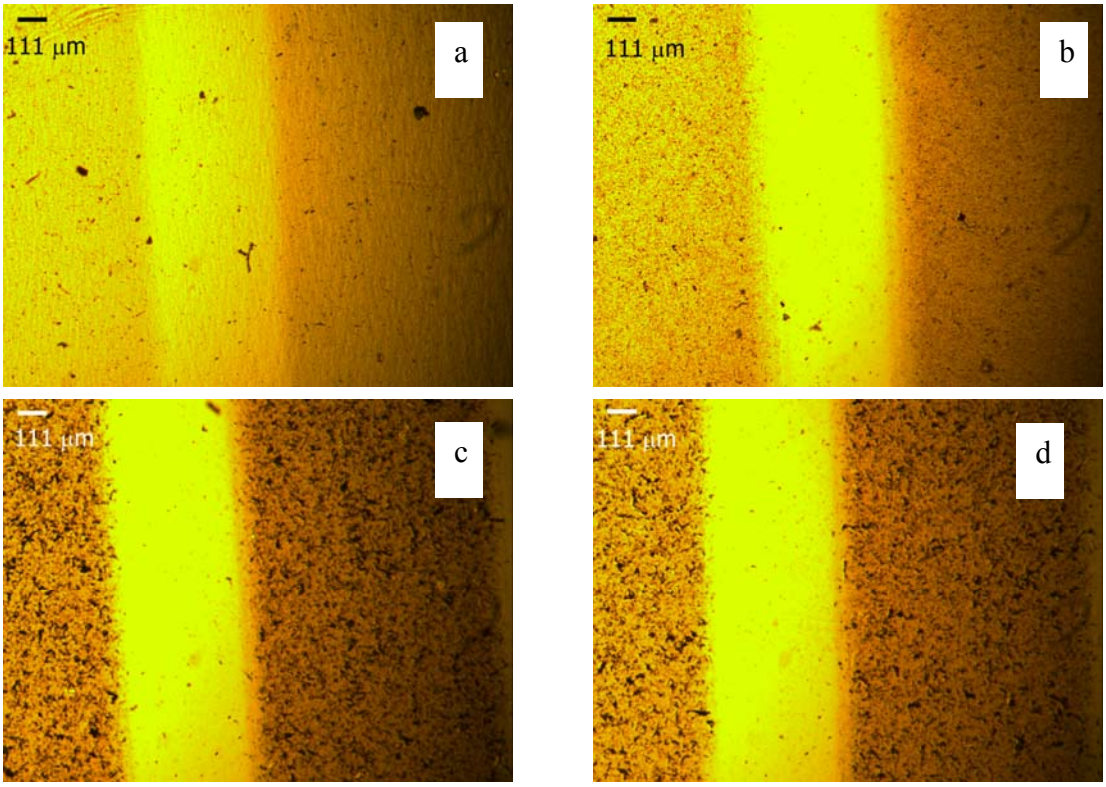

Figure 5.11 a-d: Optical micrographs of 6.0 μm RIR-LA films of a) 10% P0-BTDA b) 10% P1-BTDA c) 10% P2-BTDA d) 10% P3-BTDA in NMP, energy 10 mJ, time 10 minutes

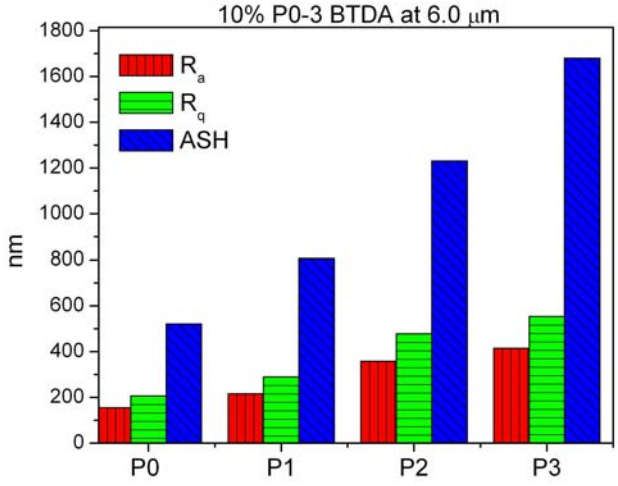

Figure 5.12: Profilometry data for 6.0 μm RIR-LA films of 10% P0-3 BTDA in NMP

5.5 Conclusions

We have demonstrated the ability to transfer chemically intact PAI and PEI thin films using RIR-LA. The FTIR spectra show that there is no difference between control spincast PAI and PEI films, and the RIR-LA films of PAI and PEI from matrix-based targets. Laser ablation is thought of as a high temperature process with calculated temperatures of approximately 3000 K to > 10,000 K.[21-24] The unaltered FTIR spectra illustrate that the RIR-LA process does not cure either the PAI or the PEI and thus must be a "low-temperature" process. The polymer may be shielded from the heat of the plume by the solvent or by slow thermal transport in the viscous polymer solution. The PAI studies have indicated the importance of the solvent in preventing the polymer from being exposed to temperatures high enough to cause curing. The solvent manages to keep the polymer equilibrated below 150 °C for PAI and below 250 °C for PEI, which is significantly lower than the postulated plume temperatures.[21-24] The strong interaction between the solvent and polymer probably helps to preserve the solvation shell as the polymer is transferred by ablation. Our previous work has shown that RIR-LA transfers macroscopic amounts of material.[13,15,16] The macroscopic droplets allows for the creation of a large solvation shell to better shield the polymer from the high heat of the ablation plume. The changes in roughness with target type and diamine monomer chain size help to identify a strategy to create smoother films; smaller polymers transferred from solid targets should give the lowest roughness values, but then some undesired thermal transformations may occur.

5.6 References

[1] D. Wilson, H. D. Stengenberger, P. M. Hergenrother, and Eds., *Polyimides* (Blackie, Glasgow, 1990).

[2] T. J. Dingemans, T. L. StClair, and E. T. Samulski, Chem. Mater. **16,** 966 (2004).

[3] P. M. Hergenrother, High Perform. Polym. **15,** 3 (2003).

[4] T. J. Dingemans, E. Mendes, J. J. Hinkley, E. S. Weiser, and T. L. StClair, Macromolecules **41,** 2474-84 (2008).

[5] M. Ijima, Y. Takahashi, Y. Oishi, M. A. Kakimoto, and Y. Imai, J. Polym. Sci. A **29,** 1717 (1991).

[6] S. Khoee and S. Zamani, Eur. Poly. Jour. **43,** 2096-110 (2007).

[7] A. Banihashemi and A. Abdolmaleki, Eur. Poly. Jour. **40,** 1629 (2004).

[8] Y. Imai, in *Polyimides: Fundamentals and Applications*, edited by M. K. Ghosh and K. L. Mittal (Marcel Dekker Inc., New York, 1996), p. 49-70.

[9] D. M. Bubb, J. S. Horwitz, J. H. Callahan, R. A. McGill, E. J. Houser, D. B. Chrisey, M. R. Papantonakis, R. F. Haglund, M. C. Galicia, and A. Vertes, J. Vac. Sci. Technol. A **19,** 2698-2702 (2001).

[10] D. M. Bubb, M. R. Papantonakis, B. Toftmann, J. S. Horwitz, R. A. McGill, D. B. Chrisey, and R. F. Haglund, J. Appl. Phys. **91,** 9809-9814 (2002).

[11] D. M. Bubb and R. F. J. Haglund, in *Pulsed Laser Deposition of Thin Films: Applications-Led Growth of Functional Materials*, edited by R. Eason (John Wiley and Sons, New York, 2006), p. 35-61.

[12] M. R. Papantonakis and R. F. Haglund, Jr., Appl. Phys. A **79,** 1687-94 (2004).

[13] N. L. Dygert, K. E. Schriver, and R. F. Haglund, Jr, J. of Physics Conference Series **59,** 651-6 (2007).

[14] R. F. Haglund, Jr , R. J. Belmont, D. M. Bubb, N. L. Dygert, S. L. Johnson, Jr, and K. E. Schriver, Proc. SPIE **6261,** 262-70 (2006).

[15] N. L. Dygert, K. E. Schriver, and R. F. Haglund, Jr., Proc. SPIE **6107,** 212-20 (2006).

[16] N. L. Dygert, A. P. Gies, K. E. Schriver, and R. F. Haglund, Jr., Appl. Phys. A **89,** 481-7 (2007).

[17] V. Instruments, (Veeco Instruments, Tuscon, Az, 2007), p. 332.

[18] M. J. Brekner and C. Feger, J. of Poly. Sci A **25,** 2005-20 (1987).

[19] D. W. Zeng, K. C. Yung, and C. S. Xie, Surf. Coat. and Tech. **153,** 210-6 (2002).

[20] N. L. Dygert and R. F. Haglund, Jr, SPIE Photonics West LASE proceedings**,** Accepted for publication Jan 2008 (2008).

[21] D. P. Brunco, M. O. Thompson, C. E. Otis, and P. M. Goodman, J. Appl. Phys. **72,** 4344-50 (1992).

[22] A. A. Oraevsky, S. L. Jacques, and F. K. Tittel, J.Appl. Phys. **78** (1995).

[23] F. H. G. Olmes A, Bansch E, Lubatschowski H, Raible M, Dziuk G and Ertmer W, Appl. Phys. B **65,** 659-666 (1997).

[24] B. Hopp, T. Smausz, E. Tombacz, T. Wittmann, and F. Ignacz, Optics Communications **181,** 337-343 (2000).

CHAPTER VI

ABLATION RATES OF RESONANT INFRARED LASER ABLATED POLYIMIDE, POLYAMIDE IMIDE, AND POLYETHER IMIDE

Nicole L. Dygert [1], Theo J. Dingemans [2], and Richard F. Haglund, Jr. [3,4]

1- Department of Interdisciplinary Materials Science,

Vanderbilt University Nashville, TN 37235

2- Aerospace Engineering, Delft University of Technology, Kluyverweg 1,

2629 HS Delft, The Netherlands

3- Department of Physics and Astronomy

4- W. M. Keck Foundation Free Electron Laser Center

Vanderbilt University, Nashville, TN 37235

6.1 Overview

We have successfully deposited several high performance polymers by resonant infrared laser ablation (RIR-LA). It is important to characterize not only the collected material but also the ablation process. In this paper we examine the resonant infrared deposition rates of three polymeric precursors: polyimide (PMDA-ODA), polyamide imide (PAI), and polyether imide (PEI) using a quartz crystal microbalance (QCM). The high resolution, ± 0.01 Angstroms, makes the QCM an ideal tool to study laser ablation processes. The effect of the resonant ablation wavelength was examined for all three of the aforementioned polymers. The resonant wavelength had a significant effect on the relationship of fluence on deposition rate in all cases. We used varying concentrations (1-20 wt %) of PAI in dimethylformamide (DMF) to determine the dependence of deposition rate on polymer concentration. We anticipated that increasing the polymer concentration would increase the deposition rate proportionally; however, the QCM data show that this is not always true for all polymer and resonant wavelength combinations. A solid pressed pellet target of PAI was ablated and it exhibited rates similar to the highest (20 wt%) concentration of the frozen matrix targets; however the solid target film would be apt to retain more of its deposition weight since it contains no complexed or entangled solvent particles. The relationship between deposition rate and chain size was examined by ablating the homologous series of PEIs (P0-3 BTDA), where the diamine chain length increases by one ether linkage and one benzene ring from two rings in P0 up to five rings in P3. The relationship between the deposition rate and chain length was found to be dependent on the ablation wavelength used: solvent resonant wavelengths produced minimal differences in deposition rates for P0-3 BTDA, dianhydride monomer

resonant wavelengths showed increasing deposition rates for decreasing diamine chain lengths, and diamine resonant wavelengths displayed increasing deposition rates for increasing diamine chain lengths. Deposition rates are shown to have a complex dependence on the resonant wavelength chosen, the target composition, and the size of the polymer.

6.2 Introduction

Laser ablation of thin polymer films is an industrially relevant process that has remained of interest to the research community.[1-5] As new types of lasers and polymers become available it is important to be able to quantify the effects of the ablation process. How is the rate of the process to be determined? With a solid target or free-standing film etch depth measurements can show the amount of material removed from a crater. Kuper et al. measured the ablated depth of a Kapton® films as a function of fluence and showed the curves to be smooth and exponential for λ = 248, 308, 351 nm, but linear for λ = 193 nm.[6] More recently, a logarithmic dependence of ablation depth on fluence has been shown for polyimide in the ultraviolet regime. Lasagni and co-workers detailed both experimental and theoretical results for the ablation of polyimide films at 355 nm, and their results showed a clear logarithmic trend attributed to shielding from the expelled gaseous plume.[5] Dumont et al. measured the loss of mass from quartz crystals coated with cured PMDA-ODA using ultraviolet light at λ = 193, 248, and 308 nm.[7] Dumont's ablation rate curves showed an exponential behavior for the latter two wavelengths with respect to fluence; in contrast, 193nm radiation produced a linear plot with a small curvature at the highest fluences.[7] The rate of material removed provides clues about the

ablation mechanism driving it; however the etch depth curve is not sufficient to determine an ablation model unambiguously.[8]

For frozen liquid targets it is more practical to capture the transferred mass. A sensitive way of measuring the mass transferred is with a quartz crystal microbalance (QCM). The crystal senses the mass by changes in the frequency of the vibration of the quartz crystal. Most of the rate experiments focus on characterizing the ablation as either photothermal[9] or photochemical[10]; however many processes show characteristics of both. There are two main heuristic ablation models, the blow-off model and the steady-state model. If the ablation ejects a large amount of material, it may be compared to blow-off or saturation model where it shows an initial increase in deposited material with fluence and then it levels off at high fluences due to plume shielding.[11] The blow-off model is dependent on the effective absorption coefficient of the polymer, for large absorption coefficients the initial ejection of material is small and then it slowly increases while for a small absorption coefficient there is a steep increase in the removal of material. Contrastingly the steady-state ablation models show a linear relationship between fluence and deposited material over the entire fluence range.[11] The steady-state model is not explicitly dependent on the absorption coefficient it depends only on the ablation enthalpy. An ablation process may also show a combination of the two models having a different behavior for low fluence versus high fluence measurements.

Due to the complex nature of the ablation process there are few theoretical models that can accurately emulate the experimental process. The majority of modeling work has been done with polymers ablated by ultraviolet radiation[8,12-14]; however some of the findings are applicable to infrared radiation. Leveugle and Zhigilei showed the

theoretical material yields using a molecular dynamic model based on a matrix-assisted pulsed laser evaporation (MAPLE) system.[15] Their simulations were for poly(methylmethacrylate) at concentrations of 1,3, and 6 wt% polymer ablated with ultra-violet radiation.[15] They showed that increasing the polymer concentration caused large droplets of matrix and polymer to be ejected. The polymer chains entangle with the solvent and form a network to stabilize large droplets for laser transfer. The total yield of transferred molecules showed a logarithmic dependence, while the yield of polymer molecules alone showed a linear dependence on fluence. Increasing concentrations of polymer were calculated to eventually impede the ablation process requiring increasing energy to give significant material transfer.[15] In contrast, our experiments showed little to no collection of pure solvent molecules even for solvent resonant modes and increased polymer concentrations produced larger deposition yields.

The polymers used in this experiment: the polyamic acid of polyimide (PMDA-ODA), polyamide imide (PAI), and polyether imide series (P0-3BTDA) have been introduced in some detail in the preceding chapters. The structures of the polymers used in the QCM experiments are shown below in figure 6.1 a-c.

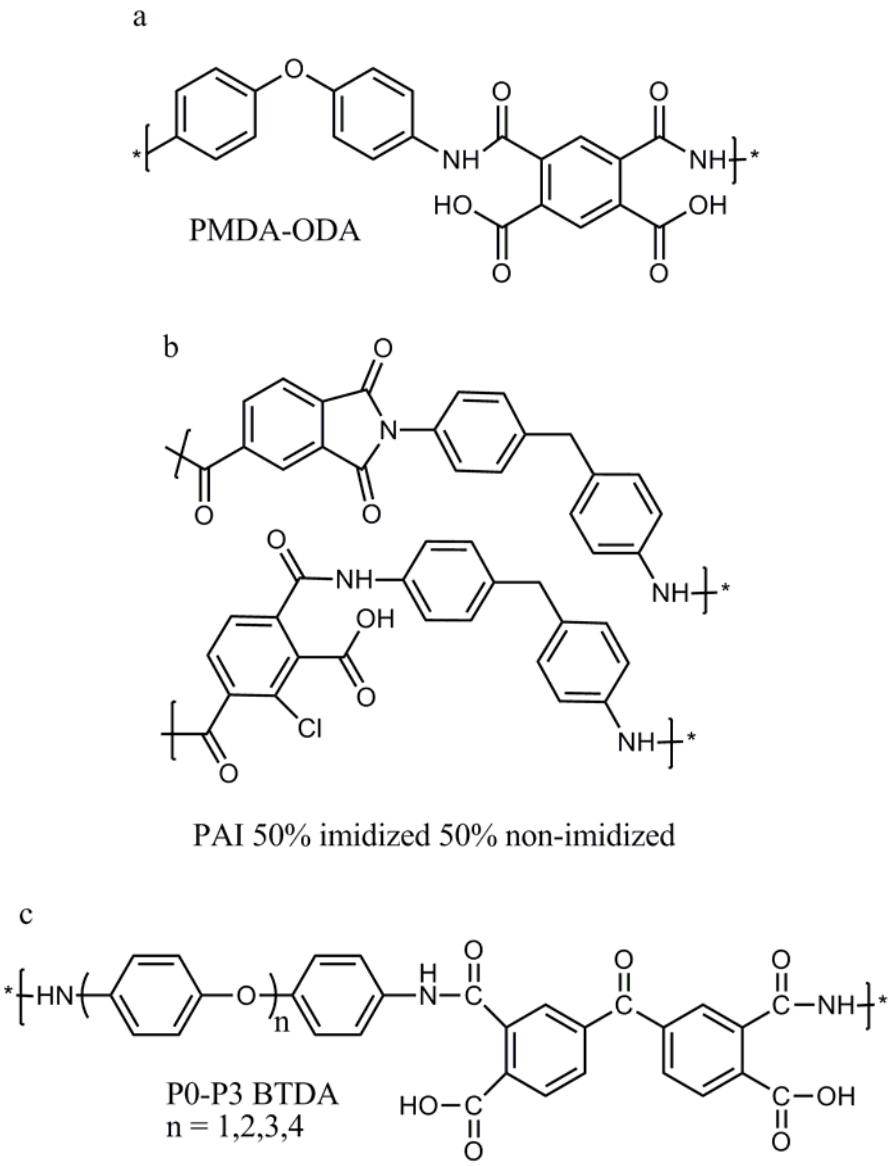

Figure 6.1 a-c: Polymeric structures of a) PMDA-ODA b) PAI c) P0-P3 BTDA

6.3 Experimental methods

6.3.1 Materials and ablation laser

Three different high performance polymers were used for the experiment. A solution of 15 % pyromellitic dianhydride (PMDA) and 4, 4'-oxidianline (ODA) poly (amic acid) was obtained from Sigma-Aldrich (batch #'s 08411PC and 06102CH) and was used without further purification. Poly (trimellitic anhydride chloride-*co*-4, 4'-methylene-dianiline) (PAI) powder was also purchased from Sigma-Aldrich (batch # 02207JD) and used without additional purification. The P2 and P3 diamine monomers were synthesized by N. Dygert under the direction of T. Dingemans at the Technical University of Delft (additional synthesis details may be found elsewhere [16]). Polyether-imides were formed from these by combining with 3, 3', 4, 4'-biphenyltetracarboxylic dianhydride from Aldrich Chemical Co used as received. 1, 4-bis-(4-aminophenoxy) benzene (P1) was purchased from the Chriskev Company Incorporated and used as received. 4, 4'-oxidianiline (P0) was purchased from Sigma Aldrich and also used as received. The ablation laser used in our experiments is a Mark III-type free-electron laser (FEL) at the W.M. Keck Free Electron Laser Center. The FEL is wavelength tunable between approximately 2 to 10 μm. The optical bandwidth of the pulses is typically 1% of the center frequency (FWHM); the typical micropulse energy is several μJ, yielding a peak irradiance of order 10^9 W/cm^2. The total energy deposited is that of the macropulse; hence, the fluence for the experiments reported here is that of the macropulse. Additional details may be found in chapter III experimental section.

6.3.2 Deposition chamber

For vacuum RIR-LA experiments, the FEL was focused by a 50 cm focal length BaF_2 lens through a BaF_2 entrance window into a chamber evacuated using a turbo-molecular pumping system. Base pressures around 10^{-5} mbar were achieved; the pressure during the course of ablation rose to 10^{-4} mbar. Using a pyroelectric joulemeter, we measured the combined transmission of the lens and entrance window to be 0.8. The beam moved across the target surface with a linear speed of 1 mm/s, and was rotated at a frequency of less than one Hz, to maintain an even track across the target surface. The distance from the target to the substrate was 3.2 cm for all QCM measurements. Resonant wavelengths were chosen based on commercial and in-house FTIR spectra of the precursor solutions. Targets consisted of compressed pellets and frozen liquid polymeric precursor solutions. The spot size was optimized for each wavelength using a knife-edge set up to determine the focal point.

6.3.3 Quartz crystal microbalance

A quartz crystal microbalance (QCM) was used to measure the *in situ* deposition rate of the RIR-LA of PI. A tooling factor of 100% was used since the QCM is in the same location as films are normally deposited, directly above the target. The QCM unit was manufactured by Inficon (XTM/2) and has a resolution of 0.01 Angstroms for the thickness measurements. We used gold coated Inficon 6 MHz crystals as the oscillating medium. The density of the target was input for each sample and the Z factor, which is used to incorporate the elasticity of the deposit for thick films, was one for all targets. The Z factor is only necessary for thick depositions which have a dampening effect on

the vibrations of the crystal; the films deposited in this work were sufficiently thin to ignore the Z factor hence its value of one. All targets were "seasoned" (FEL beam was rastered over surface for 5 minutes at a moderate ~ 5 J/cm^2 fluence) before beginning the experiment to provide a more repeatable ablation behavior. For each measurement the beam was "on" for 15 seconds at the desired energy and the thickness deposited on the QCM crystal was recorded once the value was steady. The fluence is ramped from low to high energy for measurements and three separate thickness measurements were taken. The thicknesses were averaged and divided by the ablation time of 15 seconds to give an ablation rate of nanometers per second.

6.4 Results and discussion

6.4.1 PMDA-ODA

We examined the transfer behavior of a 15% PMDA-ODA solution at three different resonant wavelengths 3.45, 5.87, and 6.67 μm to determine the importance of the resonant mode on the deposition rate. For 15% PMDA-ODA the 5.87 μm carbonyl stretch mode shows a linear or steady-state dependence on fluence (see figure 6.2). The steady-state ablation model, discussed in the introduction, should show a linear behavior over the entire range of fluences and the 5.87 μm mode illustrates this behavior. The 6.67 μm, aromatic ring mode, also shows a linear behavior with respect to fluence; however, the deposition rates are lower than those obtained for the other two modes. The 3.45 μm solvent resonant C-H stretch mode shows a different ablation behavior; the ablation rate increases until around 12 J/cm^2 and then it tapers off. The behavior is typical of a blow-

off or saturation model behavior, where the ablation rate increases until plume shielding, bond saturation, or a combination of the two occurs. Bond saturation may occur for the 3.45 μm mode because the FEL bandwidth is narrower at the lower wavelengths. In contrast, at the longer modes the broad bandwidth of the FEL (50-100 nm) excites not only the polymer mode mentioned but it also excites some neighboring resonant solvent modes and non-resonant modes. The additional excitation modes prevent saturation and allow a steady-state behavior for 5.87 and 6.67 μm. The lower transfer rates for the 6.67 μm could be a result of increasing beam size, causing a more laterally expanding plume. The target size of the QCM substrate, positioned directly above the ablation target, remains constant thus a laterally expanded plume would transfer less material in the forward direction resulting in lower perceived ablation rates. The uncollected ablated material ends up coating the vacuum chamber and for all wavelengths tested there was a significant amount of material deposited on the walls of the chamber.

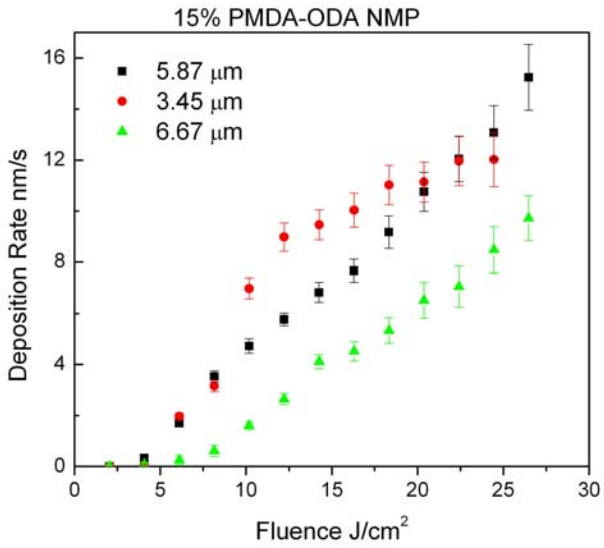

Figure 6.2: QCM graph showing the dependence of the deposition rate of 15% PMDA-ODA at three different wavelengths on fluence.

6.4.2 Polyamide imide

With the PAI matrix based targets, we looked at the effects of changing the polymer concentration on the deposition rate. Polyamide imide solutions were prepared by dissolving the purchased powder in dimethyl formamide (DMF) to produce concentrations by weight of 1, 5, 10, 15, and 20%. According to the calculations of Leveugle it should become increasingly difficult to transfer the higher polymeric concentrations.[15] We did not observe this trend: at equal fluences the highest concentration of polymer always produced the highest deposition rate. The deposition rate at the 5.90 μm, carbonyl stretch, has a logarithmic dependence for concentrations of PAI greater than 1 %, see figure 6.3a. Increasing the concentration from 10 % PAI to 15 % PAI more than doubled the deposition rate for 5.90 μm. For the 5.90 μm mode the relationship of deposition rate and PAI concentration is not proportional. Contrastingly at 6.67 μm, aromatic ring mode, increasing the PAI concentration proportionally increases the deposition rate. Figure 6.3b shows that the two highest polymer concentrations ablated at 6.67 μm have a linear relationship with fluence if last data point is ignored. The lower concentrations at 6.67 μm have a more ambiguous behavior, being almost linear but with multiple outlying data points. Both of the aforementioned modes, 5.90 and 6.67 μm, are polymer and solvent resonant due to the bandwidth of the FEL. The different behaviors of the two modes could be due to the greater number of ring mode sites available for excitation compared to the carbonyl sites. The orientation of the molecule in the target could also play a role. The solvent resonant mode, 3.45 μm, shows an interesting trend at the higher polymer concentrations (15-20%) there is a slope change after a period of rapid increase in deposition rate with little change in fluence (see

figure 6.3c). Perhaps the polymer concentration is increasing at the target surface due to depletion of the matrix causing a saturation behavior.[15] At 3.45 μm a target of the pure solvent DMF was also ablated and it produced no significant mass transfer even at high fluence. This confirms that the polymer is integral in allowing the solvent to reach the substrate.

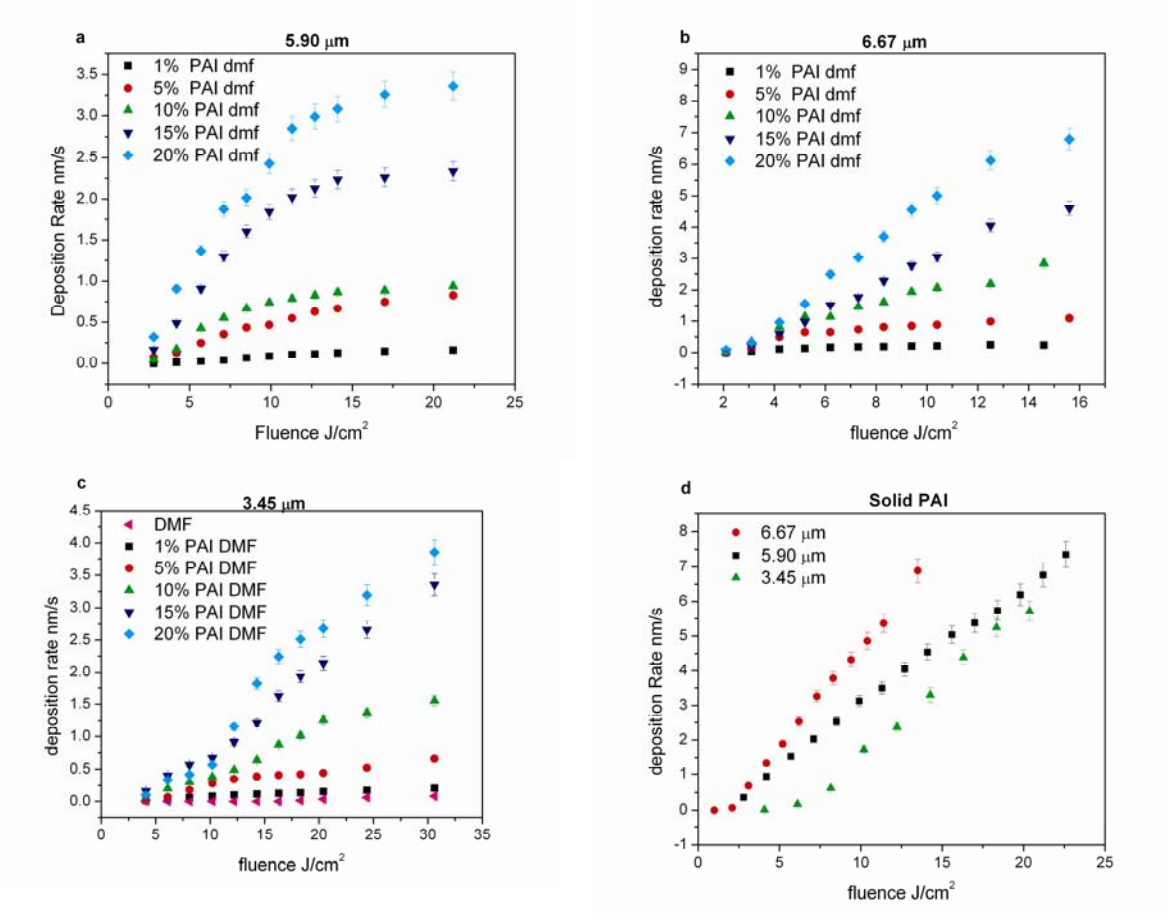

Figure 6.3 a-d: QCM data of deposition rate versus fluence for a) 1-20% PAI in DMF transferred at 5.90 μm b) 1-20% PAI in DMF at 6.67 μm c) 0-20% PAI DMF at 3.45 μm d) Solid PAI target at three different wavelengths

In the previous chapter it was shown that the solid PAI undergoes a thermal transformation and that the target and transferred material showed signs of carburization. For the two polymer resonant wavelengths, 5.90 and 6.67 μm, there was a linear trend for deposition rate with fluence. The 6.67 μm showed a much steeper slope, see figure 6.3d, it appears to be the optimal wavelength to reach high thickness with lower energy input. The plot for the non-resonant 3.45 μm mode initially has an exponential dependence of deposition rate on fluence, at higher fluences (~10 J/cm^2) the dependence became linear. This behavior may be explained by the decomposition and carburization of the polymer allowing for increased deposition rates.

6.4.3 Polyether imide

The PEI series was used to assess the effect of chain length on the ablation rate at various resonant wavelengths. The solvent resonant mode exhibited a linear dependence that hardly varied for P0-P3 BTDA, see Figure 6.4 a. The absorbed laser energy must be more than sufficient to transfer even the longest diamine chain-length polymer P3-BTDA. The carbonyl mode, 5.90 μm, showed a linear behavior with respect to fluence for P0 and P1-BTDA, but P2 and P3-BTDA showed saturation by leveling off at higher fluences. The P3-BTDA curve in Figure 6.4 b has a pronounced S-shape indicating a change in the ablation mechanism after a threshold value of fluence is reached (~ 8 J/cm^2). The carbonyl bond excited at 5.90 μm is present in the dianhydride monomer BTDA, which remains unchanged throughout the P0-P3 BTDA series. As the diamine unit increases in chain-length, the molar mass of the diamine unit is increased; the equivalent weight of dianhydride monomer required for polymerization is reduced. Thus

the P3-BTDA polymer possesses the lowest weight percentage of BTDA explaining why it illustrates saturation. For ablation at 6.67 μm the P0-P3 BTDA series shows two linear slope regions on a plot of deposition rate versus fluence (figure 6.4c), below ~6 J/cm^2 there is a steep slope and for fluences greater than ~6 J/cm^2 there is a much gentler slope. The ablation mechanism must undergo a change; one possible explanation is the surface depletion of the polymer. With a lower concentration of polymer at the surface the ablation process would become less effective leading to lower deposition rate. Another explanation is that increasing the fluence results in an increased penetration depth and thus an increased laser affected volume; the larger volume requires a greater amount of energy to transfer the same amount of material. Figure 6.4d is a plot of the deposition thickness in kilo-angstroms versus the time increment in seconds. The plot is linear until around 30 seconds when the deposition rate begins to increase exponentially. The plot explains why there are discrepancies between the measured film thickness for long ablation times and the thickness estimated from QCM rate data.

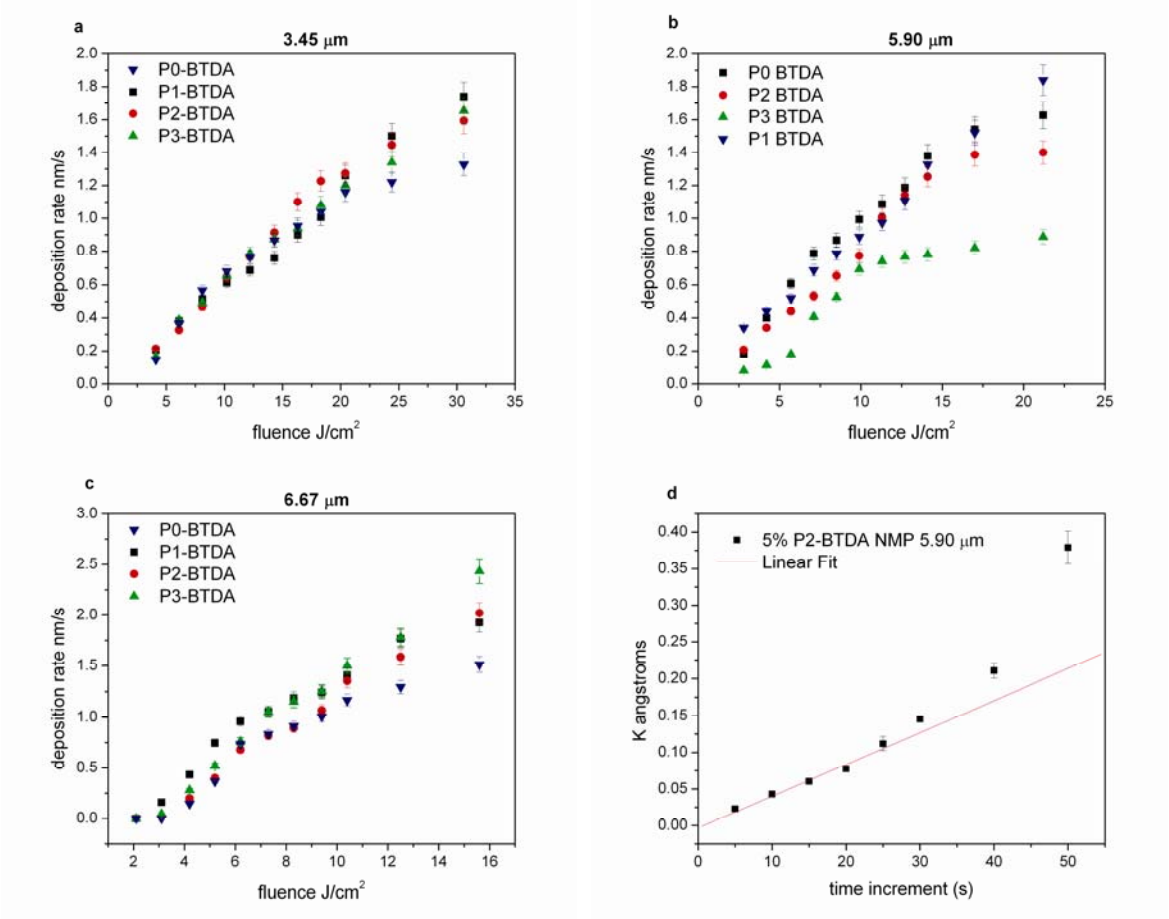

Figure 6.4 a-d: QCM relationship of deposition rate to fluence for 10% P0-P3 BTDA in NMP for a) 3.45 μm b) 5.90 μm c) 6.67 μm d) shows the deposition thickness with respect to laser exposure time for 5% P3-BTDA in NMP at 5.90 μm

6.5 Conclusions

The resonant infrared laser ablation deposition rates are strongly affected by the choice of wavelength. All three polymer discussed displayed some dependence on the wavelength chosen. Modes that reach saturation display plateaus in deposition rate while those that are not fully saturated show a linear, steady-state behavior. Increasing the polymer concentration does increase the deposited thickness; however, it is not always proportional to the increase in polymer concentration. The solvent does not transfer

readily alone; it requires the polymer to bind together the macroscopic droplets. The solvent is enmeshed in the polymer by processes of entanglement and hydrogen bonding. Thus all RIR-LA films contain a portion of entrained solvent molecules. The diamine monomer chain length plays a different role depending on the excitation mode. If ablation is performed with a non-polymer resonant mode, the diamine chain length has no discernible effect on deposition rates. Exciting the unchanging dianhydride side of the polymer caused an increase in diamine monomer chain length to decrease the ultimate deposition rates achieved. Contrastingly, exciting a diamine mode resulted in increasing diamine chain lengths giving increasing polymer deposition yields. The solvent may have an important role to play in protecting the polymer from overheating, but the polymer is what ensures that the RIR-LA mechanism transfers macroscopic amounts of material.

6.6 References

1 O. Y. F. Henry, S. A. Piletsky, and D. C. Cullen, Biosensors and Bioelectronics **23,** 1769-75 (2008).

2 I.-B. Sohn, Y.-C. Noh, S.-C. Choi, D.-K. Ko, J. Lee, and Y.-J. Choi, Appl. Surf. Sci. **254,** 4919-24 (2008).

3 R. K. Gupta, K. Ghosh, P. K. Kahol, J. Yoon, and S. Guha, Appl. Surf. Sci. **In Press** (2008).

4 P. E. Dyer, M. Pervolaraki, C. D. Walton, T. Lippert, M. Kuhnke, and A. Wokaun, Appl. Phys. A **90,** 403-9 (2008).

5 A. Lasagni, M. Cornejo, F. Lasagni, and F. Muecklich, Adv. Eng. Mat. **10,** 488-93 (2008).

6 S. Kuper, J. Brannon, and H. Brannon, Appl. Phys. A **56,** 43 (1993).

7 T. Dumont, R. Bischofberger, T. Lippert, and A. Wokaun, Appl. Surf. Sci. **247,** 115-22 (2005).

[8] N. Bityurin, B. S. Luk'yanchuk, M. H. Hong, and T. C. Chong, Chem. Rev. **103,** 519-22 (2003).

[9] B. Luk'yanchuk, N. Bityurin, M. Himmelbauer, and N. Arnold, Nucl. Instr. Meth. B **122,** 347-55 (1997).

[10] R. Srinivasan, B. Braren, and R. W. Dreyfus, J. Appl. Phys. **61,** 372-6 (1987).

[11] A. Vogel and V. Venugopolen, Chem. Rev. **103,** 577 (2003).

[12] L. V. Zhigilei, E. Leveugle, B. J. Garrison, Y. G. Yingling, and M. I. Zeifman, Chem. Rev. **103,** 321-47 (2003).

[13] E. Leveugle, L. V. Zhigilei, A. Sellinger, and J. M. Fitz-Gerald, J. of Phys: Conf. Series **59,** 126-31 (2007).

[14] S. Georgiou and A. Koubenakis, Chem. Rev. **103,** 349-93 (2003).

[15] E. Leveugle and L. V. Zhigilei, J. Appl. Phys. **102,** 1-19 (2007).

[16] T. J. Dingemans, E. Mendes, J. J. Hinkley, E. S. Weiser, and T. L. StClair, Macromolecules **41,** 2474-84 (2008).

CHAPTER VII

THERMOGRAVIMETRIC AND LIGHT SCATTERING ANALYSIS OF THE POLYIMIDE FAMILY

Nicole L. Dygert [1], Joseph M. Pickel [2], Theo J. Dingemans [3], and

Richard F. Haglund, Jr. [4,5]

1- Department of Interdisciplinary Materials Science,

Vanderbilt University Nashville, TN 37235

2- Oak Ridge National Laboratory Center for Nanophase Material Science,

Oak Ridge TN 37830

3- Aerospace Engineering, Delft University of Technology, Kluyverweg 1,

2629 HS Delft, The Netherlands

4- Department of Physics and Astronomy

5- W. M. Keck Foundation Free Electron Laser Center

Vanderbilt University, Nashville, TN 37235

7.1 Overview

We have previously characterized the deposited RIR-LA films by Fourier transform infrared spectroscopy, profilometry, and gravimetric studies with a quartz crystal microbalance. In this chapter we characterize the films using light scattering to determine molecular weight and thermogravimetric analysis to examine the oxidative decomposition. It is important for the RIR-LA technique to preserve the molecular weight, because the molecular weight is related to many strength and structural properties of the polymer. Multi-angle laser light scattering (MALLS) was used to determine the molecular weight of the precursors to polyimide, polyamide imide, and the polyether imide series. The polyimide precursor compared the molecular weight behavior of the standard to three different resonant wavelength deposited RIR-LA polymer samples. Then the polyamide imide standard and two resonant wavelength deposited RIR-LA samples were compared. The results showed that the weight average molecular weight is slightly reduced for RIR-LA material. Wavelengths that are only resonant with the solvent minimized the loss. The reduction of molecular weight could be from three sources: degradation from the RIR-LA process, reduced solvent amounts lowers chain extension hence molecular weight, and exposure of the thin film to atmospheric water caused degradation. For the polyether imide series, MALLS determined the relationship between the diamine monomer chain length and the molecular weight. The results were surprising, showing an exponential relationship of diamine monomer chain length on molecular weight instead of the expected linear relationship. Thermogravimetric analysis of the three polymers determined the oxidative decomposition temperature (T_o), the point where the polymer film begins to rapidly degrade, and the temperatures at which the film

has lost 5 and 10 % of its mass. Thermogravimetric analysis of the polyimide precursor examined the differences between spincast, cured, and 3.45 μm RIR-LA PMDA-ODA films. Similar oxidative temperatures were found for the three different PMDA-ODA films, but larger difference occurred for the 5 and 10 % weight loss temperatures. To examine the effect of the resonant infrared wavelength used on the thermoxidative stability, two RIR-LA PAI films were compared: one deposited with a solvent resonant wavelength (3.45 μm) and the other at a polymer and solvent resonant wavelength (5.90 μm). The polyether imide series was examined to see if there was a correlation between molecular weight or chain length and the thermoxidative stability. Overall RIR-LA films tended to have minutely lower T_o, but were superior to uncured spincast films in both the 5 and 10 % weight loss temperatures.

7.2 Introduction

The first step in determining if laser transfer of a polymer was successful is to determine if the basic repeat structure of the polymer is still intact. It is equally important that the laser transfer preserves the molecular weight of the polymer, since a number of polymer properties, for example tensile strength, depend on the molecular weight.[1] Volksen et. al. showed the dependence of Young's modulus, elongation, and tensile strength on the molecular weight of polyimide films; increasing molecular weight leads to higher Young's moduli, reduced elongation, and increased tensile strength. Polymers are defined by average molecular weights and the four common molecular weight averages are: weight average (from light-scattering), number average (colligative properties), Z-average (ultracentrifuge measurements), and viscosity average (dilute

viscosity measurements). Gel permeation chromatography (GPC) gives the molecular weight distribution of the material, rather than a single molecular weight average as defined above. GPC is a relative technique, for complex polymers it relies on calibration with curves from standard polymers such as polystyrene or polyethylene glycol. For most random coil polymers this generates an error of less than 30%; however for complex polymer systems the error may be higher.[1] Conversely multi-angle laser light scattering (MALLS) is an absolute technique that requires no calibration curve.

Previous studies of ultraviolet laser ablation have shown that the polymer molecular weights are severely degraded.[2-5] The ultraviolet radiation causes the polymers to unzip and return to their original monomer components or to decompose.[2] The products of UV laser ablation were found to be highly diverse in molecular weight range and composition being dependent on the fluence and UV wavelengths used.[4] Research indicates that transfer using infrared radiation may prevent the decomposition of the polymer molecular weight. Thermoplastic polymers such as polystyrene and polyethylene glycol have been successfully transferred using infrared radiation while retaining the majority of their original molecular weight.[6-8] Thermosetting polymers such as polyimide can not have their molecular weight measured directly because they are insoluble. Instead the molecular weight is estimated by measuring the molecular weight of their soluble precursor polyamic acid (PAA).[9,10] We have previously determined the molecular weight of RIR-LA films of the polyimide precursor by gel permeation chromatography (GPC) and the results showed the 3.45 μm RIR-LA ablated PAA (PMDA-ODA) to have a slightly higher molecular weight, ~ 8000 Da compared to ~6000 Da for standard PAA.[11] Prior studies have given theoretical estimates of the molecular

weight between 7,000 and 100,000 g/mol and experimental molecular weights of 7,100 g/mol to 48,500 g/mol for PAA.[9,10,12] Cotts postulated that GPC may not give the most accurate results due to the dynamic chemistry of the PAA; the intermolecular hydrogen bonding of the amide and acid groups may cause low molecular weight species to behave like higher molecular weight species.[10] Cotts and co-workers showed that the addition of small amounts of low molecular weight PAA drastically affected the average molecular weight.[13] Other unique transfer methods such as vapor deposition polymerization (VDP) have been shown to give lower molecular weights. Gies et al. quoted a molecular weight of ~1,500 Da calculated using matrix assisted laser desorption ionization (MALDI) for a VDP film of polyimide.[14] In this paper we wished to determine the weight average molecular weight of two RIR-LA ablated polymers, polyimide (PI) and polyamide imide (PAI) using MALLS. Additionally we examined the relationship of the diamine monomer chain size to molecular weight using a homologous polyether imide (PEI) series.

High thermoxidative stability is an essential characteristic of high performance polymers, as it is vital to know when the polymer will begin to break down in use. Thermogravimetric analysis (TGA) allows for the determination of the oxidation temperature at which the polymer begins to rapidly decompose. TGA can also show when the polymer first begins to lose mass. TGA can provide a portion of the polymer decomposition scheme; essential information may also be gleaned from examining the evolved gaseous products. Dinetz et al showed that UV laser pyrolysis of polyimide gave evolved gaseous products of CO, CO_2, C_2H_2, H_2NNH_2, CH_4, and HCN; while thermal pyrolysis of polyimide only showed CO and CO_2.[15] These results indicated that UV laser

ablation takes a different decomposition route compared to simple thermal pyrolysis. Ortelli and co-workers provide a proposed mechanism for the decomposition of Kapton® in air: decomposition begins with the imide ring, then the aromatic system, and finally the carbonyl groups.[16] Ortelli identify several intermediate groups including nitriles and alkynes by diffuse reflectance infrared Fourier transform (DRIFT) spectroscopy.[16] We examined the decomposition behavior of both spin-coated and RIR-LA films of polyimide and polyamide imide to determine if there were differences in behavior caused by processing technique. The effects of chain length and molecular weight on the thermoxidative stability were examined for the polyether imide series.

7.3 Experimental Methods

7.3.1 Materials, ablation laser and chamber

The materials used have been described in previous chapters. The ablation laser used in our experiments is a Mark III-type free-electron laser (FEL) at the W.M. Keck Free Electron Laser Center. The FEL is wavelength tunable between approximately 2 to 10 μm. Characteristics of the FEL beam were described previously. The vacuum deposition chambers parameters have also been detailed in previous chapters.

7.3.2 Refractive index detector

The differential change in refractive index with concentration (dn/dc) was determined experimentally using Optilab REX (Wyatt Technologies, Santa Barbara, CA) setup at Oak Ridge National Laboratory's Center for Nanophase Materials Science

(CNMS). To detect the refractive index Optilab REX uses a 658 nm laser. The instrument was run in a continuous manner with a syringe pump operating at a flow rate between 2-5 μL/min. Each sample was filtered three times through at 0.2 μm filter prior to being placed in a disposable syringe. The data was processed using the ASTRA software (version 5.3.2.15).

7.3.3 RIR-LA sample preparation

For the multi-angle laser light scattering (MALLS) experiments known concentrations of RIR-LA polymers were needed. A blank glass slide was cleaned with ethanol and dried with a lint free wipe; then it was weighed on a balance accurate to ±0.01 mg and mounted a few cm above the ablation target. The desired frozen polymer solution target was then ablated at a specific wavelength; the sample slide was removed and weighed again to determine the amount of polymer deposited. Multiple sample slides are needed to give enough material for 3-5 mL aliquots with concentrations between 1-10 g/L. A calculated amount of solvent is weighed and then used to wash the polymer from the slides into a beaker; this solution is collected as the sample for MALLS. The possibility of significant concentration errors exist because there are several chances to lose the transferred material, first if the material adheres to the sample slide and second if it remains in the glass beaker. Every attempt was made to minimize the loss of material, but losses up to 15 % of the sample weight may have occurred. Standard samples were prepared by dissolving desired amounts of the polymers in solution.

For TGA the slides were prepared either by spincoating polymeric precursor solutions onto the slides or by using RIR-LA to deposit thin polymer films. To make the spincoated samples a few drops of polymeric precursor were placed on a clean glass slide, and then the spincoater rapidly rotates the slide whilst holding it in place with vacuum; this generates a thin, even film that dries rapidly. For PMDA-ODA one of the spincoated samples was cured by the following procedure: first, it was dried at ambient conditions overnight, then it was held at 80 °C for one hour, and then 250 °C for two hours. RIR-LA samples were prepared by depositing the chosen frozen polymeric precursor target on clean glass slides. All of the samples had to be cut down to fit in the tiny TGA platinum pan, a glass cutting tool was used to take the center portion of each film.

7.3.4 Multi-angle laser light scattering

The analysis was performed on the DAWN HELEOS (Wyatt Technologies, Santa Barbara, CA) at Oak Ridge National Laboratory's CNMS. The instrument was operated in batch mode and each sample set was run with both quasi-elastic laser light scattering (QELS) and static light scattering (SLS). The laser in the instrument was a 120mW solid state laser with a wavelength of 658 nm. The instrument measures the intensity of scattered light at 18 different angles ranging from approximately 15-160°. The baseline was determined using pure spectroscopic grade toluene that had been triple filtered through a 0.2 μm filter to remove dust and other particulate matter. To normalize the detectors to the solvent, NMP, first a solution of polystyrene standard in NMP was prepared. The polystyrene displays isotropic scattering and has a known molecular

weight and particle size (30,000 g/mol and 3 nm). The coefficients are calculated from the difference between a baseline NMP solvent measurement and the polystyrene standard NMP solution. The calibration and normalization procedure is also discussed in more detail in Chapter II. Each sample was filtered three times through at 0.2 μm filter into a disposable scintillation vial. Whenever possible at least three different concentrations of sample were used for each run, for certain experimental polymers this was not possible. To mitigate the effect of the solvent a few drops of 1% LiBr solution were added to each sample. The light scattering data were processed using ASTRA (version 5.3.2.15). The static light scattering data were analyzed according to two different formalisms Zimm and Debye, both formalisms gave the weight average molecular weight and the second virial coefficient.[17-19] The second virial coefficient is not reported since a large number of concentrations (>5) need to be run in order to obtain accurate number.

7.3.5 Thermogravimetric analysis with mass spectrometry (TGA-MS)

Thermogravimetric analysis was performed on a TA Instruments 2950 with an attached mass spectrometer at Oak Ridge National Laboratory's CNMS. The mass spectrometer was a Pfeiffer Thermostar capable of registering compounds of 300 Da or less. The connection tube between the TGA and the mass spectrometer was maintained at 200 °C to prevent condensation. Analysis was performed on glass supported films of PI, PAI, and PEI. Samples were run in air to allow for the full decomposition of the film and to emulate conditions that would be experienced in an application setting. The samples were first held at 40 °C for 10 minutes to allow the system to reach thermal

equilibrium. The samples were then heated at a rate of 20 °C/ min until reaching 850 °C. The mass spectrometer recorded data after the thermal equilibration period, taking a sample approximately every 2 seconds. After the run the sample was allowed to cool in the chamber and then removed and visually examined.

7.4 Discussion and results

7.4.1 Refractive index

The refractive index detector was used to determine the change in refractive index with a change in concentration (dn/dc) of the three polymers: PMDA-ODA, PAI, and PEI series (see structures in figure 7.1a-c) in the solvent NMP. The dn/dc is necessary for the calculation of molecular weight by both the Debye and Zimm formalisms. The theory of light scattering has been discussed in chapter II. Literature values of dn/dc were found only for PMDA-ODA. Cotts found a value of 0.192 with a differential refractometer at 632 nm.[20] Our measurement gave a larger value of 0.2299 with an 11% error for a laser wavelength of 658 nm. The dn/dc value has a large effect on the calculated molecular weight; for standard PMDA-ODA using our computed value gave a molecular weight that was 5000 g/mol less. All of the molecular weight data have been computed using our measured values. Table 7.1 shows the measured dn/dc values in tabular form. PAI had a lower dn/dc value than PMDA-ODA with a dn/dc of 0.1512 with an error of 2%. The P0-P3 BTDA series had an interesting trend, increasing dn/dc with reducing diamine chain length. For P0-BTDA the calculated dn/dc value was determined to be in error due

to an order of magnitude deviation from the pattern. Instead an estimated value of 0.180 was used based on continuing the trend.

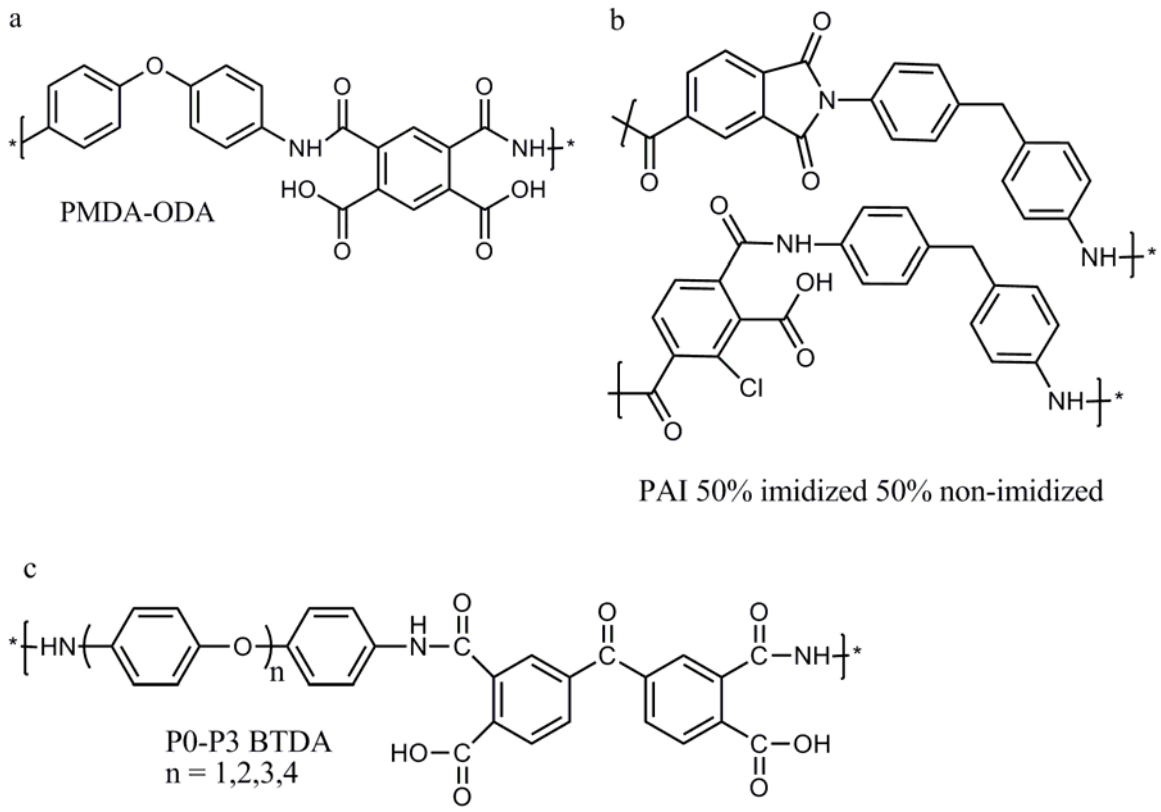

Figure 7.1a-c: Structures of a) PMDA-ODA b) PAI and c) P0-P3 BTDA

Table 7.1: Refractive index determination of dn/dc values

Polymer	*dn/dc (mL/g)*	*Error ± (mL/g)*
PMDA-ODA	0.2299	0.0251
PMDA-ODA	0.192 [a]	unknown
PAI	0.1512	0.0026
P0-BTDA	0.0466 [b]	0.0226
P1-BTDA	0.1717	0.0129
P2-BTDA	0.1590	0.0003
P3-BTDA	0.1359	0.0077

[a] From ref. [20]

[b] Not used, error too high, estimated based on rest of series for MW measurements as 0.180 mL/

7.4.2 Multi angle laser light scattering

For the multi-angle laser light scattering experiments, static light scattering (SLS) in batch mode was recorded and analyzed according to the Zimm and Debye formalisms.[21] The light scattering equation for both formalisms is:

$$\frac{Hc}{R(\theta) - R(solvent)} = \frac{1}{M_w P(\theta)} + 2A_2 c \tag{7.1}$$

where R(θ) is the Rayleigh ratio, c is concentration, H is an optical constant defined in equation 7.2, M_w is the weight average molecular weight, $P(\theta)$ is the scattering form factor, and A_2 is the second virial coefficient.[1] The optical constant H equation is:

$$H = \frac{2\pi_1^2 n_0^2 (dn/dc)^2}{N_A \lambda^4} \tag{7.2}$$

where π_1 represents the constant with a value of 3.1416 and not the osmotic pressure π, n_0 is the refractive index at a wavelength λ, N_A is Avogadro's number, and the dn/dc is the differential change in refractive index with concentration.[1] The Zimm plot combines changes in angle and changes in polymer concentration on a single plot of $R_\theta / H^* c$ vs. $\sin^2(\theta/2)$, that can determine the M_w, A_2, and radius of gyration. The Debye formalism also starts with a plot of $R_\theta / K^* c$ vs. $\sin^2(\theta/2)$ but only for a single concentration with the full range of angles. Second, a polynomial in $\sin^2(\theta/2)$ is fit to the data, and used to obtain the intercept at zero angle, $R_0 / K^* c$, as well as the *slope* at zero angle. For the Debye method the molecular weight is calculated for each concentration, and then the average and standard deviation are computed using all the concentrations. In both the Debye and Zimm data analysis the highest and lowest angle data points were removed to provide an improved fit. Quasi elastic light scattering (QELS) was also run on each sample to

compute the hydrodynamic radius; however the variations in hydrodynamic radii were deemed too large to be meaningful and are not discussed further.

Results for 15% PMDA-ODA are shown below in figure 7.2. For the standard polymer solution the Zimm and Debye formalisms gave similar molecular weights, approximately 15,000 g/mol with less than 10% error. The RIR-LA PMDA-ODA at the solvent resonant wavelength of 3.45 μm had widely differing results for Zimm vs. Debye. The Zimm method gave a molecular weight of ~ 30,000 g/mol for the RIR-LA 3.45 μm PMDA-ODA while the Debye method gave 13,600 g/mol. There is also a large error associated with the Zimm measurement suggesting that the Debye results are probably more accurate. For the RIR-LA PMDA-ODA deposited at the polymer and solvent resonant wavelength of 5.90 μm showed more compatible results between the methods with both estimating the M_w between 8000-9000 g/mol. The value is slightly more than half of the original molecular weight. Finally for the RIR-LA films at the aromatic ring mode of 6.67 μm, both methods estimated a molecular weight between 12,000 and 13,000 g/mol.

In general the RIR-LA seems to cause a modest loss in molecular weight and compared to UV laser ablation the losses are miniscule.[2,4,5] PMDA-ODA like most polyimide precursors is highly sensitive to water readily undergoing hydrolysis with even a tiny amount of water present.[22,23] A strong possibility exists that atmospheric water causes some film degradation when the films are exposed to the ambient air. Water could also condense onto the target during the freezing process with liquid nitrogen and affect the surface layer of the polymer target. The solvent serves an important function as a

chain extender[23]; therefore the loss of large amounts of solvent during the RIR-LA process may lead to lower molecular weights.

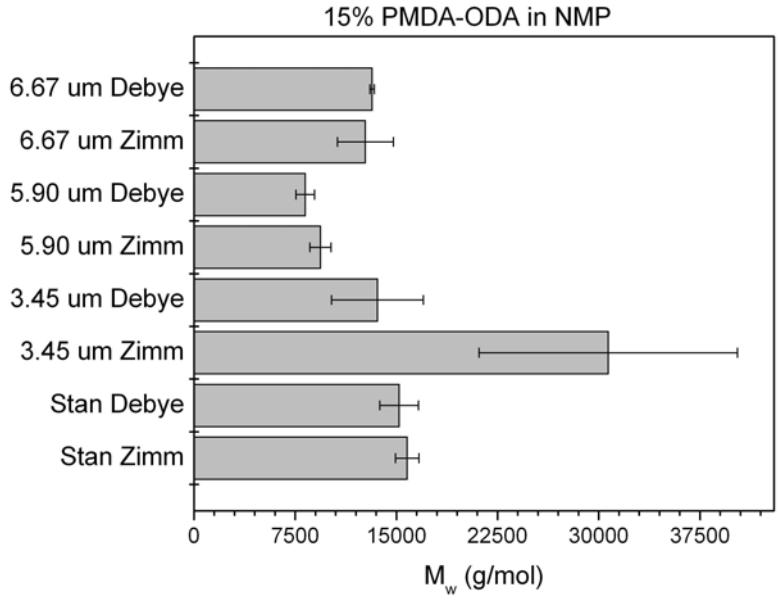

Figure 7.2: Graphical representation of 15% PMDA-ODA MALLS data

For the 20% PAI in NMP standard the Zimm and Debye methods gave similar results, with the Debye method giving a molecular weight of 14,600 g/mol and the Zimm method a molecular weight of 19,000 g/mol. The values are close to those of PMDA-ODA and seem reasonable. One solvent resonant wavelength, and one polymer and solvent resonant wavelength were used to make RIR-LA PAI samples. The 6.67 μm showed a larger drop in molecular weight for both the Zimm and Debye methods, with molecular weights of less than 10,000 g/mol (Zimm 8,100 and Debye 7,200 g/mol). For the 3.45 μm both methods gave molecular weight within the same range, the Debye formalism gave a higher molecular weight ,14,000 g/mol, compared to 9,700 g/mol for

the Zimm formalism. The solvent resonant wavelength, 3.45 μm, preserved a larger portion of the original PAI molecular weight.

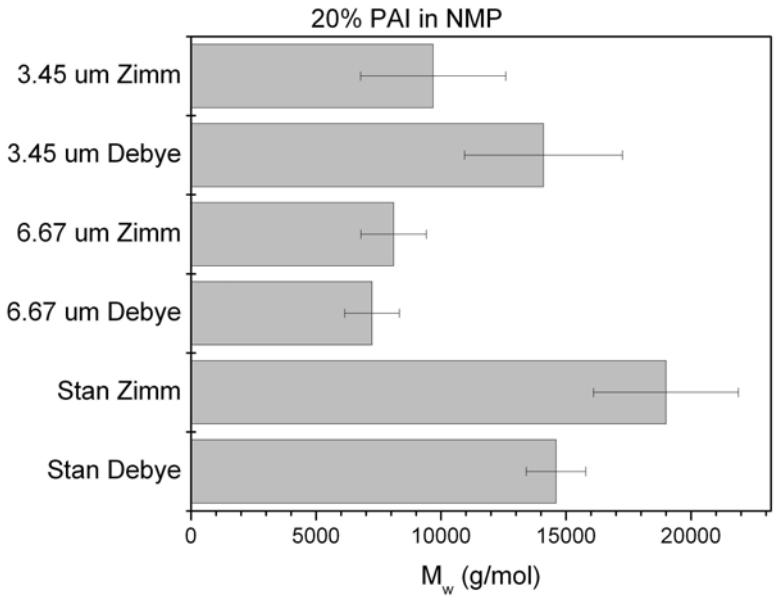

Figure 7.3: 20% PAI in NMP MALLS data in graphical form

The polyether imide series, 10% P0-3 BTDA in NMP, were analyzed to decipher the effect of the diamine unit chain length on the weight average molecular weight. Figure 7.4 shows the slight increase in molecular weight from P0-P2 BTDA. Then P3-BTDA shows a large order of magnitude increase in molecular weight. It was anticipated that the molecular weight would increase monotonically with chain length; however it appears that an exponential take-off occurs at P3 BTDA. The P3 monomer has been shown to have liquid crystalline phases with the diamine (3,3',4,4'-biphenyltetracarboxylic acid dianhydride BPDA); these characteristics may help it order and achieve high molecular weights.[24] It appears that higher molecular weights could be

achieved by further increasing the diamine chain length or possibly the dianhydride chain length; however if the molecular weight becomes too high the material becomes difficult to process.[25]

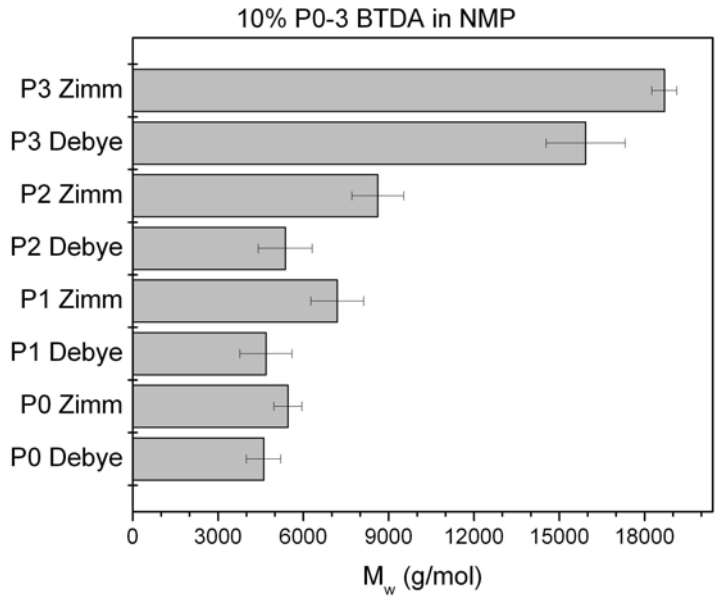

Figure 7.4: Graphical representation of 10% P0-3 BTDA in NMP MALLS data

7.4.3 Thermogravimetric analysis

The TGA results reveal some intriguing trends about the oxidative decomposition behavior of the polymers. The 15% PMDA-ODA polymer film samples were used to examine the effects of curing and RIR-LA on the oxidative stability. A plot relative weight versus temperature is shown for cured, spincast, and 3.45 μm films of 15% PMDA-ODA in figure 7.5a. The RIR-LA ablated film had a much lower starting weight than the spincast films and on the same graph it does not show full weight loss when lined up with the others. The lower weight also generates the higher level of noise seen

in the TGA trace. The data extracted from the TGA plots are shown as bar graphs for ease of comparing the different film properties (figure 7.5b). There are no error bars because each film was run only once, TGA runs typically take 3-5 hours and it would be very time consuming to do multiple runs on a sample. As anticipated the cured film shows the highest T_o. The oxidation temperature, T_o, is the point where the slope of the TGA curve is nearly vertical and the derivative weight loss is at a maximum. The spincast PMDA-ODA films showed lower values for the 5 and 10% weight loss temperatures compared to both the cured PMDA-ODA film and the RIR-LA PMDA-ODA film. The spincast films early weight loss is most likely water and NMP from undergoing curing during the TGA run. The RIR-LA PMDA-ODA film showed temperatures similar to the cured film for 5 and 10% weight loss. The RIR-LA films should mimic the behavior of the spincast film; however, the lower retention of the solvent reduces the early mass loss.

We hoped that the mass spectrometry data would be able to confirm solvent differences between the spincast and RIR-LA films. Unfortunately this was not possible from our data. It appears that the NMP condenses prior to reaching the mass detector since the connection from the TGA to the mass spectrometer was maintained at 200 °C and the boiling point of NMP is 202 °C. The main gases evolved were carbon monoxide, nitrogen, CH_3O, and C_3H_4. Other products such as carbon dioxide, and nitrous oxide were present in smaller amounts. No significant high mass (>100 amu) products were detected.

a

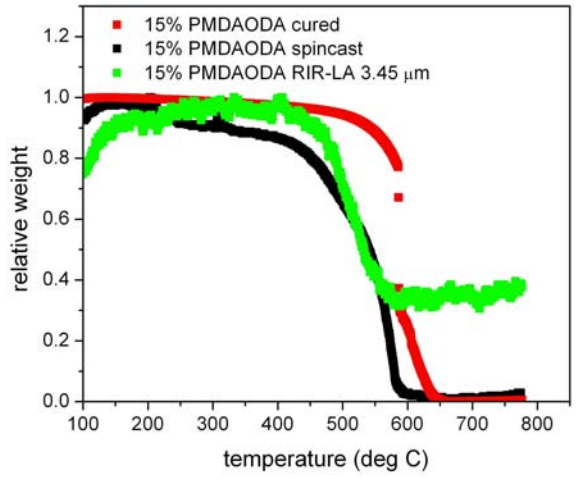

b

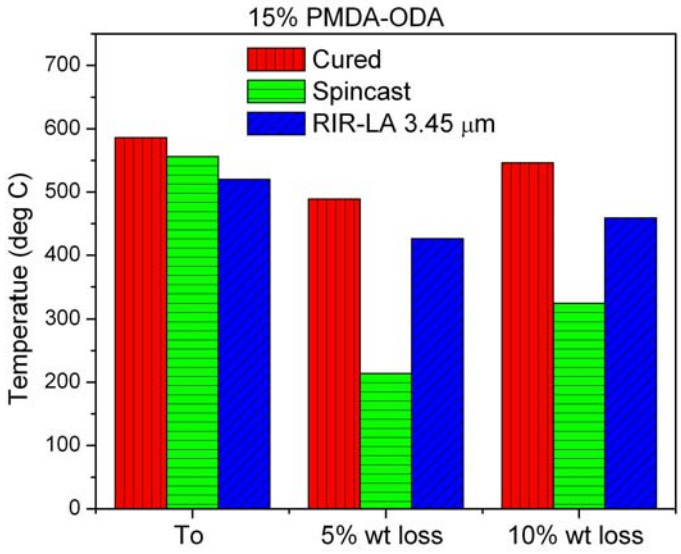

Figure 7.5 a-b: a) TGA scan from 40-800 °C showing the relative weight loss of PMDA-ODA b) Graphical representation of extracted T_o and 5, 10% weight loss temperatures

The oxidative stability of two RIR-LA films deposited at different wavelengths, the solvent resonant, 3.45 μm (C-H stretch) and the solvent and polymer resonant 5.90 μm (C=O stretch), were examined for PAI. The spincast PAI films showed the highest oxidation temperature, but the lowest 5 and 10 % weight loss temperatures (see figure

7.6b). The low weight loss temperatures shown for the spincast PAI are most likely caused by the film undergoing curing releasing water and solvent molecules. The 3.45 μm RIR-LA PAI film showed the second highest T_o and the highest 5, 10 % weight loss temperatures. 5.90 μm RIR-LA PAI had moderately lower values for all categories compared to the 3.45 μm RIR-LA PAI. The results reaffirm that the ablation at a pure solvent excitation mode may be the best way to get the highest thermoxidative stability. Mass spectra of the evolved gaseous products were taken to attempt to determine the concentration of DMF (boiling point of 153 °C). Despite the lower boiling point no solvent peak was detected. PAI showed the same gaseous products as PMDA-ODA.

The diamine series examined the effects of changing diamine chain length and molecular weight on the thermoxidative stability. In figure 7.7a it appears that the P2-BTDA film was significantly thicker than the others, but the film thickness does not significant alter the onset of oxidative decomposition. P2-BTDA had the lowest 5, 10 % weight loss temperatures, but it also had one of the highest oxidation temperatures. The P0-BTDA films had high 5 and 10% weight loss temperatures in addition to a high oxidation temperature. As shown in figure 7.7b there is no apparent relationship between diamine chain length and the oxidative stability of the polymer.

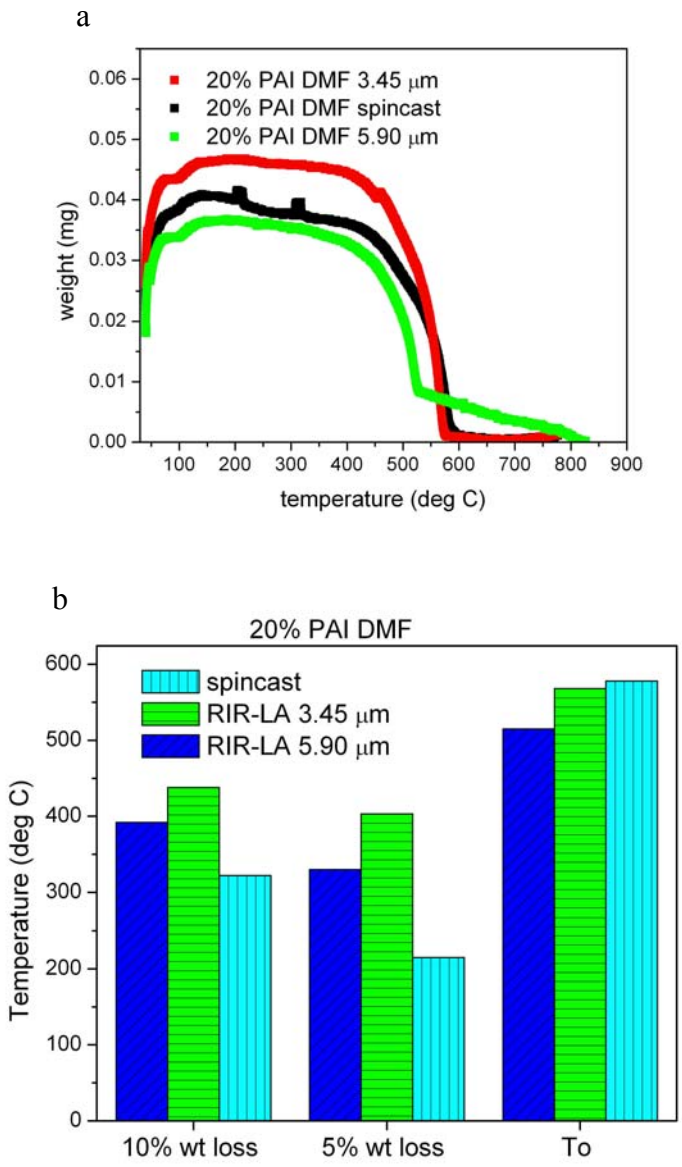

Figure 7.6a-b: a) TGA data for 20% PAI in DMF b) data extracted from TGA

a

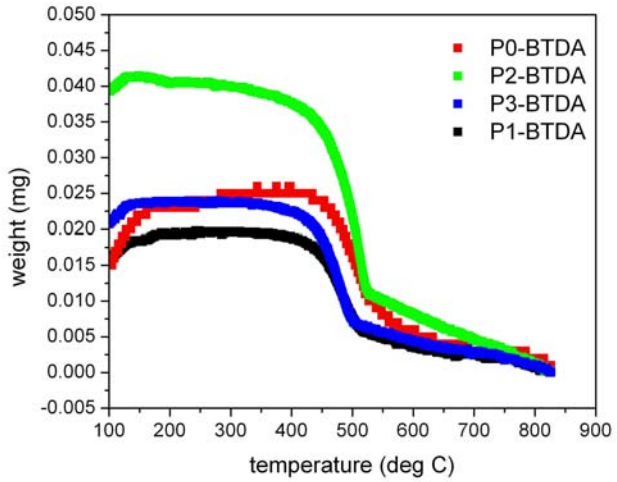

b

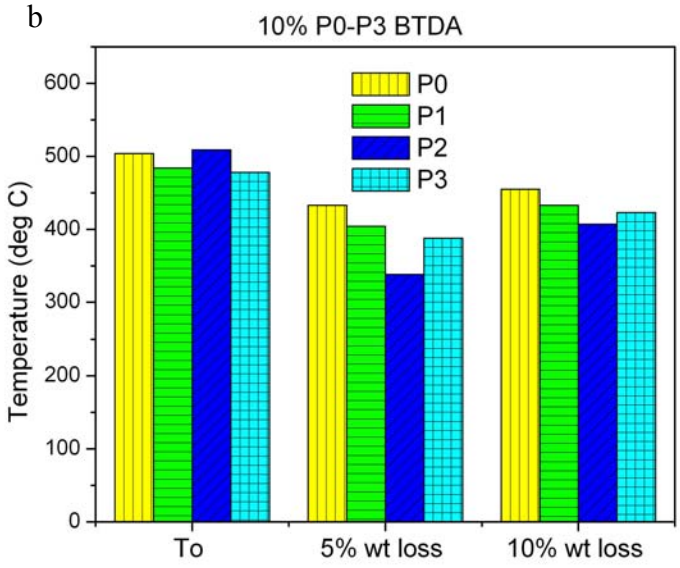

Figure 7.7a-b: a) TGA of 10% P0-3 BTDA b) data extracted from TGA plot

The evolved gases were also measured for the polyether imide series, this time focusing on products less than 100 amu using a trend graph. The previous experiments used bar graphs covering the whole 0-300 amu range of the mass spectrometer. The same evolved gases as before were seen (figure 7.8a). The dominant product by an order

of magnitude was mass 28, identified as either carbon monoxide or nitrogen (see table 7.2). P3-BTDA gave the highest ion signals for masses 14, 28, and 32, while P0-BTDA gave the highest ion signal for mass 40. Since P3-BTDA is the largest molecule it should give the largest ion concentration for all masses. The temperature of the maximum ion current was also determined, this value can help to elucidate when the majority of a product is released. The temperature of the maximum ion current varied for P0-P3 BTDA for masses 14 and 28, but all have similar temperatures for masses 32 and 40. The high temperatures for masses 14 and 28 for P2-BTDA could possibly indicate a different mechanism for the decomposition of P2-BTDA compared to the rest of the series; however the data here are insufficient to postulate a decomposition pathway for any the PEI series.

Table 7.2: Maximum ion current signals for the most prevalent products in the thermoxidative decomposition of P0-P3 BTDA

Mass	*Possible products*	*P0 [A]*	*P1 [A]*	*P2[A]*	*P3[A]*
14	N^+	2.51E-08	2.39E-08	2.19E-08	3.19E-08
28	N_2, CO	4.98E-07	4.60E-07	4.04E-07	6.08E-07
32	O_2, CH_3OH H_2NNH_2	9.94E-08	9.18E-08	7.97E-08	1.22E-07
40	C_3H_4	4.54E-08	2.22E-08	1.81E-08	2.16E-08

a

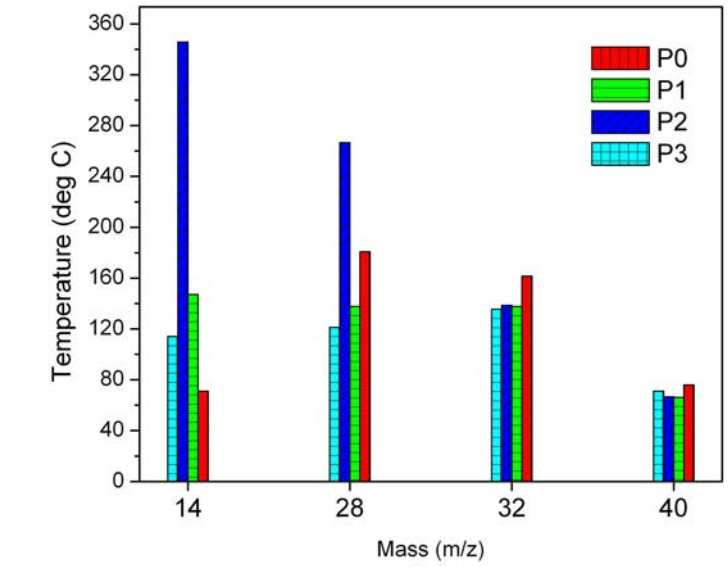

b

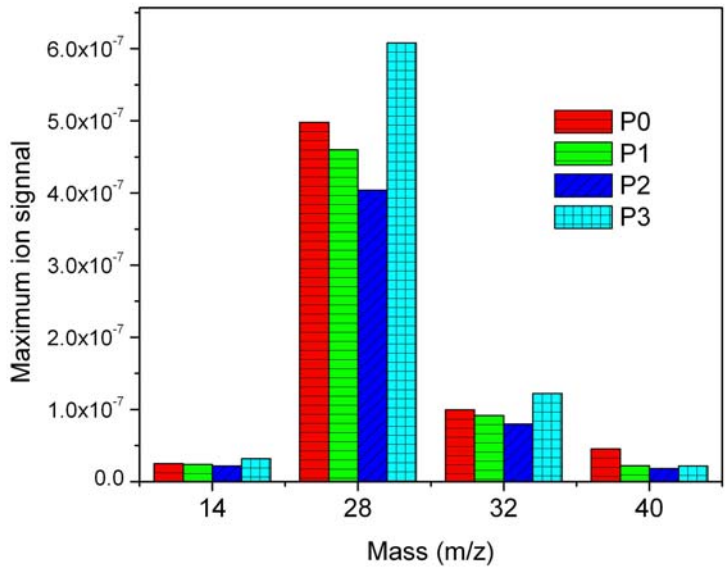

Figure 7.8a-b: a) maximum ion currents for 10% P0-P3 BTDA in NMP b) Temperature at which the maximum ion current occurred for 10% P0-P3 BTDA in NMP

7.5 Conclusions

Good thermoxidative stability and reasonably large molecular weight are essential to having a useful high performance polymer. The large molecular weights are necessary to give high strength, but too large of a molecular weight will limit the processability. For the thermoxidative properties a high T_o and high 5 and 10% weight loss temperatures are desirable to give the largest range of usage temperatures. The data thus far have illustrated that the RIR-LA technique gives polymer films of adequate molecular weight and reasonable thermoxidative stability.

We have shown that the molecular weight may be determined using either the Zimm or the Debye formalism without large molecular weight differences. There are a few instances when the methods gave widely differing results but this is thought to be caused by errors in the experiment. There appears to be a small reduction in the weight average molecular weight with the RIR-LA process; however this could be due in part to solvent loss or moisture exposure. This reduction is still orders of magnitude less than that seen for UV laser ablation processes.[2-5] By exciting resonances that are only active within the solvent the molecular weight loss can be minimized. The polyether imide series showed an exponential relationship between diamine monomer length and molecular weight instead of the anticipated linear one.

The TGA analysis illustrated that curing has only a minimal effect on the oxidative temperature, but has a larger effect on when the polymer first begins to lose mass. RIR-LA films gave slightly lower oxidation temperatures; however they did show increased resistance to initial mass loss most likely due to reduced solvent amounts. Unfortunately we were unable to confirm the reduced solvent content with mass

spectrometer on the evolved gaseous decomposition products. Reduced solvent films are desirable because they limit shrinkage and evaporative solvent distortion.

RIR-LA at solvent resonant wavelengths is viable way to process high performance polymers while preserving the chemical structure, the majority of the molecular weight, and increasing the initial weight loss temperature during oxidative decomposition.

7.6 References

[1] L. H. Sperling, *Introduction to Physical Polymer Science*, 3rd ed. (Wiley-Interscience, New York, 2001).

[2] G. Blanchet, J. Appl. Phys. **80,** 4082-89 (1996).

[3] R. Srinivasan, B. Braren, and R. W. Dreyfus, J. Appl. Phys. **61,** 372-6 (1987).

[4] R. Srinivasan and B. Braren, Chem. Rev. **89,** 1303-16 (1989).

[5] R. Srinivasan, R. R. Hall, W. D. Loehle, W. D. Wilson, and D. C. Albee, J. Appl. Phys. **78,** 4881-7 (1995).

[6] D. M. Bubb, J. S. Horwitz, J. H. Callahan, R. A. McGill, E. J. Houser, D. B. Chrisey, M. R. Papantonakis, R. F. Haglund, M. C. Galicia, and A. Vertes, J. Vac. Sci. Technol. A **19,** 2698-2702 (2001).

[7] D. M. Bubb, M. R. Papantonakis, B. Toftmann, J. S. Horwitz, R. A. McGill, D. B. Chrisey, and R. F. Haglund, J. Appl. Phys. **91,** 9809-9814 (2002).

[8] M. R. Papantonakis and R. F. Haglund, Jr., Appl. Phys. A **79,** 1687-94 (2004).

[9] M. Wallach, J. Polym. Sci., Polym. Phys. Ed. **5,** 653 (1967).

[10] P. M. Cotts, *Polyimides: Synthesis, Characterization, and Applications Volume I* (Plenum Press, New York, 1984).

[11] N. L. Dygert, A. P. Gies, K. E. Schriver, and R. F. Haglund, Jr., Appl. Phys. A **89,** 481-7 (2007).

[12] T. H. Hou and R. G. Bryant, High Perform. Polym. **9,** 437-48 (1997).

[13] P. M. Cotts, W. Volksen, and S. Ferline, J. Poly Sci B **30,** 373-9 (1992).

[14] A. P. Gies, W. K. Nonidez, M. Anthamatten, and R. C. Cook, Macromolecules **37,** 5923-5929 (2004).

[15] S. F. Dinetz, E. J. Bird, R. L. Wagner, and A. W. Fountain, J. of Analy. and Appl. Pyrolysis **63,** 241-9 (2002).

[16] E. E. Ortelli, F. Geiger, T. Lippert, and A. Workaun, Appl. Spect. **55,** 412-9 (2001).

[17] B. Zimm, J. Chem. Phys. **16,** 1093 (1948).

[18] B. Zimm, J. Chem. Phys. **16,** 1099-1116 (1948).

[19] P. Debye, J. Phys. Coll. Chem. **51,** 18 (1947).

[20] P. M. Cotts, J. Poly Sci B. **24,** 923-30 (1986).

[21] W. T. Corporation, (Wyatt Technology Corporation, 2007).

[22] M. J. Brekner and C. Feger, J. of Poly. Sci A **25,** 2005-20 (1987).

[23] J. A. Rogers and K. A. Nelson, J. Poly Sci B **34,** 861-72 (1996).

[24] T. J. Dingemans, E. Mendes, J. J. Hinkley, E. S. Weiser, and T. L. StClair, Macromolecules **41,** 2474-84 (2008).

[25] T. J. Dingemans, T. L. StClair, and E. T. Samulski, Chem. Mater. **16,** 966 (2004).

CHAPTER VIII

CONCLUSIONS

Nicole Leigh Dygert

Interdisciplinary Materials Science

Vanderbilt University

Nashville TN 37235

8.1 Summary

The laser ablation of synthetic polymers has been under investigation since 1982, when Srinivasan began his work on ultraviolet laser ablation.[1] Through the course of the ultra-violet laser ablation work it was determined that high temperatures are reached during the process[2,3]; these temperatures are high enough to decompose the polymer leaving only fragments or a reduced molecular weight polymer.[4,5] Thus, direct UV laser ablation was determined to be unsuitable for the manufacture of thin polymeric films. To obtain undamaged polymeric materials with ultra-violet light the matrix assisted pulsed laser evaporation (MAPLE) technique was pioneered at the Naval Research Laboratory.[6-8] In this technique the polymer is dissolved in small quantities (< 5%) in a suitable, volatile solvent and transferred from a frozen solution under vacuum. Intact transfer of neat thermoplastic polymer films was shown using resonant infrared laser irradiation with a free-electron laser.[9-11] The chapters of this dissertation show the inner workings of a new technique, resonant infrared laser ablation (RIR-LA). In RIR-LA polymers are transferred by exciting vibrational modes as opposed to the electronic modes excited with ultraviolet light. We postulated that we could use RIR-LA to transfer intact thermosetting polymeric precursors without curing and indeed using this technique we have demonstrated the successful transfer of intact polyimide, polyamide imide, and polyether imide polymeric precursors.

Chapter III detailed our initial research efforts, showing the unsuccessful transfer of fully cured polyimide films. Shadowgraphy was used to visually examine the ablation mechanism of the pure solvent vs. the polyimide precursor solution, and there were clear differences between the ablative mechanisms of the pure solvent compared to a viscous

polymer solution. The pure solvent showed the ejection of plumes of liquid, while the polymer showed a largely gaseous plume with a few dark globs of polymeric material. We experimented with ablating the polyimide precursor solution at different wavelengths; trying a solvent resonant and two polymer resonant modes. The solvent resonant wavelength had a longer incubation time for the start of material ejection; it also showed a peak pressure wave velocity that was subsonic (<300 m/s) and lower than the velocities associated with the polymer resonant modes (~ 400 m/s). These results illustrated that the ablation mechanism was dependent on the ablation wavelength chosen.

In Chapter IV the chemical composition of the transferred material was examined via Fourier transform infrared spectroscopy (FTIR). We wished to determine if the RIR-LA process was heating the polymer above the cure temperature, around 250 °C for PMDA-ODA. Curing the polymer produces changes in the FTIR spectrum caused by the rearrangement of the molecules to form the imide. The FTIR spectra showed no differences between the RIR-LA PMDA-ODA films and the control spincast films while there were clear spectral differences between the RIR-LA PMDA-ODA films and the cured spincast films. The FTIR results confirmed that the RIR-LA process does not induce curing for films made from solvent based targets. Some possible explanations of this behavior are: 1. the polymer does not reach the cure temperature because the required temperature is not being reached, 2. the rapid timescale of the process does not allow time for adequate heat transfer to the polymer, 3. the kinetics of the conversion to the imide group are slower than the time scale of the transfer, or 4. the solvent absorbs the majority of the incoming energy shielding the polymer. Ablation mechanism studies have shown that number one is unlikely. There is no information available in the

literature on the kinetics of imidization during a laser ablation process. Laser ablation is considered a non-equilibrium event and thus may not follow the same path as conventional imidization caused by heating or chemical dehydration. In light of the FTIR results from Chapter V illustrating the different behavior of the RIR-LA films from a solid PAI target and a solution based target, I would conclude that the solvent must play an important role in the process. Chapter IV also showed some initial work using gel permeation chromatography (GPC) to determine if the transfer process was reducing the molecular weight. The GPC results illustrated that the molecular weight distribution of the RIR-LA polymer was not reduced; instead the RIR-LA polymer had a narrower molecular weight distribution.

Chapter V expanded the RIR-LA ablation technique to new polymers in the imide family. The spectra of the free-electron laser wavelengths were overlayed with the polymer and solvent FTIR spectra demonstrating that the long wavelength modes activated polymer resonant, solvent resonant, and non-resonant modes simultaneously. The intact transfer of polyamide imide (PAI) and polyether imide (PEI) were confirmed by FTIR studies. The polyamide imide has an even lower cure temperature (150°C) than polyimide and the unaltered FTIR spectrum of RIR-LA PAI deposited from solution based target reaffirmed the findings of the previous chapter that the heat of the ablation process is not registered by the polymer. At identical ablation wavelengths and fluences the film from the solid PAI target showed signs of thermal damage and imidization while the film from the solvent PAI target matched the spincast control spectrum. These results strongly suggest that the solvent is essential in preserving the polymer structure. Though the kinetics and timescale of the ablation process may have an important role, my

personal conclusions from the data I have collected are that shielding and evaporative cooling provided by the solvent are the chief mechanisms involved in the prevention of imidization. The profilometry roughness measurements of the PEI series revealed that the roughness increases with increasing diamine monomer size most likely caused by surface packing effects.

Chapter VI examined the rates of the RIR-LA process for the three polymers using a quartz crystal microbalance (QCM). Investigation of the ablation of PMDA-ODA showed a difference in ablation mode for the solvent resonant wavelength compared to the two solvent and polymer resonant wavelengths. QCM results for different concentrations of PAI showed that the deposition rate always increased with increasing polymer concentration, though not necessarily in a proportional manner. Ablation of the solvent alone barely registered on the QCM, showing the importance of the polymer in facilitating the transfer. Theoretical modeling of the MAPLE process by Leuvegle has shown that polymer entanglement helps to transfer macroscopic quantities of material.[12] The ablation rates of the PEI series examined effects of diamine monomer size, essentially steric hindrance, on the RIR-LA process. The results were shown to be highly wavelength dependent, with solvent resonant wavelengths showing no distinction between the polymers (P0-P3 BTDA). The two polymer and solvent resonant wavelengths had differing results as well, with the 5.90 μm ablation showing drastically reduced rates for the largest diamine monomer in the series P3, while the 6.67 μm ablation showed the highest transfer rates for P3.

Chapter VII further explored the properties of the transferred polymers. Light scattering was used to determine the weight average molecular weight, M_w. The

measurements showed a slight reduction in M_w for RIR-LA polymers. The difference is minimized by using solvent resonant wavelengths. The degradation of molecular weight could be caused by several factors: 1. the RIR-LA process itself, 2. loss of solvent resulting in reduced chain extension, and 3. absorption of water from air or from frozen target leading to hydrolysis. The preservation of the majority of the molecular weight implies that the polymer film should also retain its strength and structural properties. Thermogravimetric studies showed that RIR-LA process increases the temperature when weight loss first begins compared to uncured spincast films. This is a highly desirable trait for polymer thin films used in high temperature applications.

RIR-LA, especially at solvent resonant wavelengths, is a viable way to transfer high performance thermosetting polymers such as polyimide. Through the course of this research we have shown the following:

1. RIR-LA transfers the polymers with the basic repeat unit structure intact as shown by FTIR.
2. The polymer does not reach the temperatures required for curing due to solvent shielding, slow heat transfer, or insufficient time for chemical rearrangement.
3. Both the RIR-LA process and the resulting film properties show a dependence on the resonant wavelength selected.
4. The majority of the original molecular weight is preserved through the process in stark contrast to ultraviolet laser processing.
5. The loss of the solvent during RIR-LA increases the temperature at which the film begins to lose mass during thermoxidative degradation.

8.2 Future experiments

The work of this dissertation represents a significant contribution to the field of laser induced polymer deposition; however, there are still many opportunities for continuing experiments. Imaging of the ablation plume under vacuum would help elucidate the process, since there could be significant difference between atmospheric and vacuum ablation as implied by their product films. This experiment was attempted by the author; however the use of a small ablation chamber limited the view of the process. There is no pressure wave under vacuum and it was impossible to track individual particles as each picture in our set up represents a different laser pulse. Thus a new experimental setup would be required in which the ablation event is recorded continuously with a fast camera. *In situ* examination of the gaseous plume would give information about any degradation occurring in the process. This could be accomplished using mass spectrometry or gas chromatography. It would be important for the instrument to have a large mass range to resolve both the polymer (up to 20,000 Da) and the solvent (~ 100 Da) molecules. Additional experiments with mass spectrometry or other quantitative surface analysis techniques could determine the amount of residual solvent remaining in the RIR-LA films. The behaviors observed in the collected manuscripts imply that the RIR-LA reduces the amount of solvent present, but it would be helpful to confirm quantitatively.

8.3 References

[1] R. Srinivasan and W. Mayne-Banton, Appl. Phys. Lett. **41,** 576 (1982).

[2] P. E. Dyer and R. Srinivasan, Appl. Phys. Lett. **48,** 445 (1986).

[3] D. P. Brunco, M. O. Thompson, C. E. Otis, and P. M. Goodman, J. Appl. Phys. **72,** 4344 (1992).

[4] G. Blanchet, J. Appl. Phys. **80,** 4082 (1996).

[5] R. Srinivasan and B. Braren, Chem. Rev. **89,** 1303 (1989).

[6] D. M. Bubb, B. R. Ringeisen, J. H. Callahan, M. Galicia, A. Vertes, J. S. Horwitz, R. A. McGill, E. J. Houser, P. K. Wu, A. Pique, and D. B. Chrisey, Appl. Phys. A **73,** 121 (2001).

[7] P. K. Wu, B. R. Ringeisen, J. Callahan, M. Brooks, D. M. Bubb, H. D. Wu, A. Pique, B. Spargo, R. A. McGill, and D. B. Chrisey, Thin Solid Films **398,** 607 (2001).

[8] D. B. Chrisey, A. Pique, R. A. McGill, J. S. Horwitz, B. R. Ringeisen, D. M. Bubb, and P. K. Wu, Chem. Rev. **103,** 553 (2003).

[9] D. M. Bubb, J. S. Horwitz, J. H. Callahan, R. A. McGill, E. J. Houser, D. B. Chrisey, M. R. Papantonakis, R. F. Haglund, M. C. Galicia, and A. Vertes, J. Vac. Sci. Technol. A **19,** 2698 (2001).

[10] D. M. Bubb, M. R. Papantonakis, B. Toftmann, J. S. Horwitz, R. A. McGill, D. B. Chrisey, and R. F. Haglund, J. Appl. Phys. **91,** 9809 (2002).

[11] M. R. Papantonakis and R. F. Haglund, Jr., Appl. Phys. A **79,** 1687 (2004).

[12] E. Leveugle and L. V. Zhigilei, J. Appl. Phys. **102,** 1 (2007).